Energy Efficiency Maximisation in Large-Scale MIMO Systems

A thesis submitted for the degree of Doctor of Philosophy

by

Vaina Malar Panneer Selvan

Department of Electronic and Computer Engineering
College of Engineering, Design, and Physical Sciences
Brunel University London

Supervised By: Professor Hamed Al-Raweshidy

March 2017

Dedicated to:

My great late Father,

My caring Mother,

moreover,

My supportive sister

Acknowledgements

Above all, my sincere and earnest appreciation to my supervisor, Professor Hamed Al-Raweshidy, for his guidance and mentorship. I feel fortunate to have thought-provoking discussions that resulted in inspiration. I have benefited immensely from his insight and wisdom. Mere words cannot show how much I appreciate his invaluable help. Furthermore, I would like to thank my second supervisor Dr Maysam Abbod for his support.

Secondly, I would like to convey my greatest gratitude to my sponsor Ministry of Higher Education Malaysia, for giving me an opportunity to further my study and to enhance my knowledge and profession likewise. It would be beyond my reach to envision and accomplished my study without the financial support. Also, I would like to acknowledge all the support given by my colleagues at the Wireless Networks and Communications Centre and staffs at PGR Programmes at the College of Engineering, Design, and Physical Sciences, Brunel University London.

Last but not a least, I would like to thank my mother and sister in Malaysia for continuously giving their unconditional love and support throughout my PhD journey. I cannot imagine life without their moral and emotional support. This thesis is my dedication to their love and support, and I am always indebted to them.

Abstract

The power usage of the communication technology industry and the consistent energy-related pollution are becoming major societal and economic concerns. These concern stimulated academia and industry to an intense activity in the new research area of green cellular networks. Bandwidth Efficiency (BE) is one of the most important metrics to select candidate technologies for next-generation wireless communications systems. Nevertheless, the important goal is to design new innovative network architecture and technologies needed to encounter the explosive development in cellular data demand without increasing the power consumption. As a result, Energy Efficiently (EE) has become another significant metric for evaluating the performance of wireless communications systems. MIMO technology has drawn lots of attention in wireless communication, as it gives substantial increases in link range and throughput without an additional increase in bandwidth or transmits power. Multi-user MIMO (MU-MIMO) regarded when evolved Base Station equipped with multiple antennas communicates with several User Terminal (UEs) at the same time. MU-MIMO is capable of improving either the reliability or the BE by improving either the multiplexing gains or diversity gains. A proposed new idea in MU-MIMO refers to the system that uses hundreds of antennas to serve dozens of UEs simultaneously. This so-called, Large Scale-MIMO (LS MIMO) regarded as a candidate technique for future wireless communication systems.

An analysis is conducted to investigate the performance of the proposed uplink and downlink of LS MIMO systems with different linear processing techniques at the base station. The most common precoding and receive combining are considered: minimum mean squared error (MMSE), maximum ratio transmission/combining (MRT/MRC), and zero-forcing (ZF)processing. The fundamental problems answered on how to select the number of (BS) antennas M, number of active (UEs) K, and the transmit power to cover a given area with maximal EE. The EE is defined as the number of bits transferred per Joule of energy.

A new power consumption model is proposed to emphasise that the real power scales faster with M and K than scaling linearly. The new power consumption model is utilised for deriving closed-form EE maximising values of the number of BS antennas, number of active UEs and transmit power under the assumption that ZF processing is deployed in the uplink and downlink transmissions for analytic convenience. This analysis is then extended to the imperfect CSI case and to symmetric multi-cell scenarios. These expressions provide valuable design understandings on the interaction between systems parameters, propagation environment, and different components of the power consumption model. Analytical results are assumed only for ZF with perfect channel state information (CSI) to compute closed-form expression for the optimal number of UEs, number of BS antennas, and transmit power. Numerical results are provided (a) for all the investigated schemes with perfect CSI and in a single-cell scenario; (b) for ZF with imperfect CSI, and in a multi-cell scenario.

The simulation results show that (a) an LS MIMO with 100 – 200 BS antennas are the correct number of antennas for energy efficiency maximisation; (b) these number of BS antennas should serve number of active UEs of the same size; (c) since the circuit power increases the transmit power should increase with number of BS antennas; (d) the radiated power antenna is in the range of 10-100 mW and decreases with number of BS antennas; (e) ZF processing provides the highest EE in all the scenarios due to active interference-suppression at affordable complexity. Therefore, these are highly relevant results that prove LS MIMO is the technique to achieve high EE in future cellular networks.

Table of Contents

Dedication……i
Acknowledgement……ii
Abstract……iii
Table of Content……iv
List of Figure……viii
List of Table……ix
List of Abbreviation……x
List of Symbols……xii

Chapter 1: Thesis Introduction……1
1.1 Introduction……1
1.2 Background……1
1.3 Research Motivation……3
1.4 Aim and Objectives……5
1.5 Main Contributions……6
1.6 Research Methodology……7
1.7 Thesis Structure……8
1.8 Summary……9

Chapter 2: Large-Scale MIMO Systems – An Overview……10
2.1 Introduction……10
2.1.1 Evolution of Cellular Network……11
2.2 The Wireless Channel……12
2.2.1 Rayleigh Channel Fading……15
2.2.2 Rician Channel Fading……16
2.2.3 Channel Model……16
2.3 Multi-user MIMO……18
2.3.1 Spatial Multiplexing……19
2.3.2 Shannon Capacity……20
2.3.3 Energy Efficiency……21
2.3.4 Channel Estimation……22
2.4 Large-Scale MIMO……23
2.4.1 Antenna Configuration……26
2.4.2 Channel Measurement……27
2.4.3 Channel Model……28
2.4.4 Data Transmission Protocol in Large -Scale MIMO……30
2.4.4.1 Channel Estimation……31

2.4.4.2 Uplink Data Transmission.....31
2.4.4.3 Downlink Data Transmission.....31
2.4.5 Linear Processing in Large-Scale MIMO.....32
2.4.6 Challenges in Large-Scale MIMO.....33
2.4.6.1 Pilot Contamination.....34
2.4.6.2 Unfavourable Propagation.....34
2.4.6.3 New Standards and Designs.....35
2.5 Summary.....35

Chapter 3: Energy Efficiency in Large-Scale MIMO Systems.....36
3.1 Introduction.....36
3.2 Energy Efficiency in Large Scale MIMO System.....37
3.2.1 Power Consumption in Large Scale MIMO.....38
3.2.1.1 Power Consumption Model in LS MIMO.....39
3.2.1.2 Systems Parameters in LS MIMO.....40
3.2.1.3 Power Amplifier Power Consumption.....40
3.2.2 Detection in Uplink LS MIMO.....41
3.2.3 Channel Estimation in Downlink LS MIMO.....42
3.3 Large Scale MIMO System and Signal Model.....43
3.3.1 Channel Model and Linear Processing LS MIMO System.....45
3.3.2 Uplink in LS MIMO System.....46
3.3.3 Downlink in LS MIMO System.....48
3.4 Existing Power Consumption Model in LS MIMO System.....50
3.5 Large Scale MIMO System and Signal Model.....51
3.6 Summary.....52

Chapter 4: Energy Efficiency Maximisation in Large-Scale MIMO Systems – Analytical Framework.....53
4.1 Introduction.....53
4.2 Total Power Consumption Model EE in LS MIMO System.....53
4.3 Realistic Circuit Power Consumption Model in LS MIMO System.....54
4.3.1 Transceiver Circuit Power.....55
4.3.2 Channel Estimation Circuit Power.....55
4.3.3 Coding and Decoding Circuit Power.....56
4.3.4 Backhaul Circuit Power.....56
4.3.5 Linear Processing Circuit Power.....57
4.4 Energy Efficiency Maximisation with ZF Processing in LS MIMO Systems.....58
4.4.1 Optimal Number of Users for Energy Efficiency Maximisation.....61

4.4.2 Optimal Number of BS Antennas for Energy Efficiency Maximisation……64
4.4.3 Optimal Transmit Power for Energy Efficiency Maximisation……65
4.4.4 Alternating Optimisation……67
4.5 Imperfect CSI and Multi-Cell Deployment……68
4.6 Total Power Requirement in Single-Cell and Multi-Cell scenario with Perfect and Imperfect CSI……71
4.7 Summary……74

Chapter 5: Simulation and Numerical Results……75
5.1 Introduction……75
5.2 Simulation Setting……75
5.3 Simulation Method……79
5.4 Optimal Energy Efficiency in Single Cell with Existing Power Consumption Model with Analytical ZF processing……80
5.4.1 Comparison of EE Optimal for Existing Energy Model and Realistic Power Model with Analytical ZF processing……81
5.5 Optimal Energy Efficiency in Single Deployment for ZF Processing Scheme With Monte Carlo Simulation……83
5.5.1 Comparison of EE Optimal obtained under Analytical ZF processing and ZF Processing under Monte Carlo Simulation……84
5.6 Total Power Requirement in Single-Cell and Multi-Cell scenario with Perfect and Imperfect CSI with Analytical ZF Processing……85
5.7 Single-Cell Deployment……87
5.8 Multi-Cell Deployment……94
5.9 Summary……98

Chapter 6: Conclusion and Future Research……99
6.1 Conclusion……99
6.2 Future Research……100

Appendix
A.1 Proof of Lemma 1 and Lemma 2……102
B.1 Proof of Lemma 3……104
B.2 Proof of Theorem 1……106
B.3 Proof of Corollary 1……107
B.4 Proof of Theorem 2……107

B.5 Proof of Corollary 4……107
B.6 Proof of Corollary 5……108
B.7 Proof of Theorem 3……108
B.8 Proof of Corollary 8……108
B.9 Proof of Lemma 5……107
B.10 Proof of Lemma 6……109

Bibliography……110

List of Publications
A. Published Paper……127

List of Figures

Figure 2.1: Radio Signal Propagation……12
Figure 2.2: MU-MIMO System……..19
Figure 2.3: Example of a Massive MIMO system……25
Figure 2.4: Various antenna configuration……27
Figure 3.1: Illustration of the TDD protocol……43
Figure 3.2: Illustration of a generic Multiuser MIMO……44
Figure 5.1: Energy Efficiency in Single-cell for analytical ZF with Existing Power Consumption Model……81
Figure 5.2: Comparison of Energy Efficiency in the Single-Cell with Perfect CSI for ZF with Existing Power Model and Realistic Power Model……82
Figure 5.3: Energy Efficiency in the Single-cell for ZF with Monte Carlo Simulation……83
Figure 5.4: Comparison of Energy Efficiency in the Single-Cell with Perfect CSI for ZF with Analytical Simulation and Monte Carlo Simulation……84
Figure 5.5: Total Power Consumption in the Single-cell under Analytical ZF for Perfect and Imperfect CSI……85
Figure 5.6: Total Power Consumption in the Multi-cell under Analytical ZF with pilot reuse 1,2, and 4 for Imperfect CSI……86
Figure 5.7: Energy Efficiency under Analytical ZF Simulation in the Single-cell scenario with perfect CSI……88
Figure 5.8: Energy Efficiency under Monte Carlo MMSE Simulation in the Single-cell scenario with perfect CSI……89
Figure 5.9: Energy Efficiency under Monte Carlo MRT/MRC Simulation in the Single-cell scenario with perfect CSI……90

Figure 5.10: Energy Efficiency under Analytical ZF Simulation in the Single-cell the scenario with Imperfect CSI……..90
Figure 5.11: Maximum Energy Efficiency of BS antenna for different processing schemes in the Single-cell scenario at EE optimal number of user scenario……..92
Figure 5.12: Total PA Power of BS antennas and radiated power per BS for different processing schemes in the Single-cell scenario at EE optimal number of user……..93
Figure 5.13: Area throughput of BS antennas for different processing schemes in the Single-cell at EE optimal number of user……94
Figure 5.14: Multi-cell scenario with 25 identical clustered cells for different pilot reuse factor……..95
Figure 5.15: Maximum Energy Efficiency for different BS antennas and different pilot reuse factors in the Multi-cell scenario at EE optimal number of user……96
Figure 5.16: Total PA for different BS antennas and different pilot reuse factors in the Multi-cell scenario at EE optimal number of user……96
Figure 5.17: Area Throughput for different BS antennas and different pilot reuse factors in the Multi-cell scenario at EE optimal number of user……97
Figure 5.18: Energy efficiency with ZF processing in the Multi-cell scenario with pilot reuse 4……98

List of Tables

Table 1 Circuit Power Coefficients for ZF Processing……60

Table 2 Simulation Parameters……78

List of Abbreviations

3GPP	3rd Generation Partnership Project
AA	Antenna Array
AEs	Antenna Elements
AoAs	Angle of Arrivals
AoD	Angle of Departure
APS	Angular power spectrum
AWGN	Additive White Gaussian Noise
BBU	Baseband unit
BE	Bandwidth efficiency
BER	Bit Error Ratio
BS	Base Station
CIRs	Channel impulse responses
CSI	Channel state information
CSIT	CSI at the transmitter
DoF	Degrees of Freedom
DPC	Dirty Paper Coding
DL	Downlink
EE	Energy Efficiency
FDD	Frequency Division Duplex
FIR	Finite Impulse Response
ICI	Inter-cell interference
i.i.d.	Independent identically distributed
IUI	Inter-user interference
LOS	Line of Sight
LS	Large Scale
LS MIMO	Large-scale Multiple-input and multiple-output
MF	Matched filter

MIMO	Multiple-input and multiple-output
ML	Maximum-likelihood
MMSE	Minimum Mean square error
MRC	Maximum ratio combining
MRT	Maximum ratio transmission
MSE	Mean square error
MU-MIMO	Multi-user MIMO
NLoS	Non-line of sight
PA	Power Amplifier
RRU	Remote radio unit
SDM	Spatial division multiplexing
SDMA	Spatial division multiple access
SINR	Signal-to-interference-plus-noise ratio
SNR	Signal-to-noise ratio
TD	Time-domain
TDD	Time division duplex
Tx	Transmitter
UEs	User terminals
UL	Uplink
Uma	Urban Macro Model
VP	Vector Perturbation
VRM	Virtual ray model
ZF	Zero-forcing

List of Symbols

f_c	Carrier Frequency
ul	uplink
dl	downlink
$\tau^{(\mathrm{ul})}$	Uplink pilot
$\tau^{(\mathrm{dl})}$	Downlink pilot
$\zeta^{(\mathrm{ul})}$	the fraction of uthe plink transmission
$\zeta^{(\mathrm{dl})}$	the fraction of downlink transmission
$\eta^{(\mathrm{ul})}$	Power Amplifier efficiency at the Base Station
$\eta^{(\mathrm{dl})}$	Power Amplifier efficiency at the User Equipments
$l(x)$	Large-scale fading
$l(x_k)$	Average channel attenuation
f (x)	User Distribution
$\bar{R}$	uniform gross rate
$\zeta^{\mathrm{ul}}\bar{R}$	uplink rate
$\zeta^{\mathrm{dl}}\bar{R}$	downlink rate
S_x	Propagation environment
d_{min}	minimum distance
d_{max}	maximum distance
ρ	optimization variable
B	Bandwidth
B_{C}	Coherence Bandwidth
T_{C}	Channel Coherence
U	Channel Block
M	Base station antenna
K	user equipment
H	user channel
G	Uplink linear receive combine matrix
V	Linear precoding matrix

Chapter 1

Thesis Introduction

1.1 Introduction

This chapter concisely presents the background of research gaps investigated, the motivation of the study, and aim and objectives of the studies. Additionally, the main contributions and methodology to conduct the research are explained respectively in this chapter. Finally, this chapter outlines and describes the thesis structure to provide access to readers with the current state of the art.

1.2 Background

With the development of smart terminals and their application, the need for multimedia services rapidly increases recently [1]. The increment of the capacity of wireless networks guaranteed the Quality of Service (QoS) requirements of mobile applications [2]. In the meantime, telecommunication manufacturers and operators have also predicted that a load of wireless communication networks is growing exponentially [2]. Hence, it is necessary to introduce new technologies to meet the demands of explosive traffic for next-generation wireless communications networks.

The most vital metrics to choose candidate technologies for next-generation wireless communication systems is usually Bandwidth Efficiency (BE). In the meantime, with extreme power consumption in wireless communications networks, both carbon emission and operator expenses surge yearly [3], [4].

Thus, Energy Efficiency (EE) has become another important metric for evaluating the performances of wireless communications systems with some given BE limitations [5] - [7].

Multiple-Input and Multiple-Output (MIMO) technology have attracted much attention in wireless communication, as it offers substantial rises in data throughput and link range without an additional increase in bandwidth or transmits power. A MIMO approach and the corresponding patent proposed and issued in 1993 and 1994, where numerous transmit antennas jointly located at one transmitter with the objective of improving possible link throughput [8]. Then, the initial laboratory prototype of spatial multiplexing was deployed to demonstrate the practical feasibility of MIMO technology [9]. Currently, MIMO is recognised as one of the leading technologies in the Fourth Generation (4G) wireless communications systems. When an advanced Node B (eNB) equipped with several antennas communicates with several User Terminals (UEs) over the same time-frequency resources, it is known Multi-User MIMO (MU-MIMO). MU-MIMO is capable of improving either the BE or the reliability by improving either the multiplexing gains or diversity gains [10].

To scale up these achievements, the Large-Scale MIMO (LS MIMO) concept, which is likewise known as massive MIMO scheme, was proposed by Marzetta in [11]. Both theoretical and measurement results indicate that an LS MIMO is capable of significantly improving the BE, which simultaneously reducing the transmit power [12], [13]. Therefore, as a candidate technique for next-generation wireless communications systems, an LS MIMO is considered for improving both their BE and EE.

As the down tilt of an Antennas Array (AA) is fixed, traditional MIMO technology can merely adjust the signal transmission in a horizontal dimension. In order to exploit the vertical dimension of signal propagation, AAs such as rectangular, spherical, and cylindrical, were studied by the 3rd Generation Partnership Project (3GPP) [14] – [16]. MIMO with these arrays can adjust both

azimuth and elevation angles, and propagate signals in Three-Dimensional (3D) space, thus termed 3D MIMO. To further increase capacity, 3D MIMO deploys more antennas to achieve larger multiplexing gains. Meanwhile, LS MIMO adopts rectangular, spherical and cylindrical AAs in practical systems by considering the space of AAs. Thus, 3D MIMO with large scale antennas can be as a practical deployment means of LS-MIMO. However, possibilities of this topic not discussed in this thesis, as it is focussed on LS MIMO.

LS MIMO can improve BE since it can achieve significant multiplexing gain when serving tens of UEs simultaneously [11], [17]. The substantial increase in EE is due to the use of more antennas where it helps to focus energy to located UEs with a highly narrow beam on small regions [18]. Due to the excessive Degrees of Freedom (DoF), an LS MIMO can enhance transmission reliability [19]. Alleviation of Inter-User Interference (IUI) is because of the extremely narrow beam [12]. Similarly, approximating the performance achieved by optimal methods, such as Maximum-Likelihood (ML) multiuser detection and Dirty Paper Coding (DPC) is capable of simple low-complexity signal processing algorithms [13].

1.3 Research Motivations

Mobile broadband for cellular networks is continuously being evolved to meet the future demands for higher data rates, improved coverage and capacity. The enormous success of Smart Phones boosts mobile broadband date requirements for 4G or Long-Term Evolution (LTE) is commercial for five years back and is being evolved by 3GPP. LTE brings radio features such as advanced uplink and downlink multi-antenna solutions (MIMO) and larger bandwidths from aggregating multiple carriers. These and other features will bring peak rates of 1 GB/s but also improves other characteristics such as coverage, delay and flexibility. One candidate feature for the evolution of LTE and/or a 5G radio standard is LS MIMO. Multiple-input-multiple-output (MIMO) techniques provide the possibility

of serving multiple users simultaneously with the same resources by proper precoding of the spatially separated streams.

In LS MIMO, the base station is equipped with hundreds of antennas, new possibilities to do beamforming and spatial multiplexing arises, extending coverage and capacity in the system serving more users with higher bitrates. With this new functionality, new cellular network deployments become possible to reduce the networks' energy consumption and lower the deployment costs.

This research is deployed in LS MIMO Systems environments to find the optimal number of base station antennas, and active user to accommodate the ever-increasing number of users who require ubiquitous access to high volumes of wireless data without increasing the power consumption. While throughput optimisation is a well-studied area (in [20] and references therein), the focus here is limited to energy-efficient system design, which has been a key consideration in system-level analyses of LS MIMO [21]–[25]. Energy Efficiency is often characterised by the ratio of achievable data rate (bit/s) and the total power consumption (Watt) [26].

An accurate modelling of the total power consumption is the fundamental importance to obtain a reliable guideline for EE maximisation of some (BS) antennas M and na umber of active (UEs) K for LS MIMO systems [27]. A common assumption in related literature that the total power consumption is computed as the sums of the radiated transmit power and a constant quantity accounting for the circuit power consumption [28]. This model might be very misleading although widely used and can lead to an unbounded EE if utilised to design systems wherein M can be very large because the user rates grow unboundedly as $M \to \infty$ [29].

Attaining infinite EE is evidently impossible as the model does not consider the power consumed by digital signal processing and analogue circuits (for radio-frequency (RF) and baseband processing) grows with M and K. Meaning to say, the circuit power consumption contributions can be taken as a constant only in multi-user MIMO systems where M and K take relatively small values. Instead, the circuit power consumption variability plays a key role in the so-called LS MIMO (or

massive MIMO) systems in which $M, K \gg 1$ and all the BS antennas are processed coherently [13],[17],[18]. The original massive MIMO definition in [11] also assumed $\frac{M}{K} \gg 1$, while with the more general definition from [17],[18], $\frac{M}{K}$ can be a small constant.

1.4 Aim and Objectives

The main aim of the research presented in this thesis is to cooperatively design the uplink and downlink of LS MIMO system from scratch to provide vital solution on how the number of (BS) antennas M, number of active (UEs) K, and the transmit power chosen to uniformly cover a given area with maximal Energy efficiency (EE) for LS MIMO systems to uniformly cover a given area with maximal EE.

The EE is defined as the number of bits transferred per Joule of energy and it is affected by many factors a such as network architecture, transmission protocol, bandwidth efficiency, radiated transmit power, and circuit power consumption [27], [28], [36]-[38].

The research objectives which are briefly explained and summarised as below:

1. To compare the performance of the proposed uplink and downlink of LS MIMO systems for ZF, MRT/MRC, and MMSE processing schemes at BS.
2. To implement a new refined model of the total power consumption for LS MIMO system.
3. To derive closed-form EE-maximal values of the number of (BS) antennas M, na umber of active (UEs) K, and the transmit power ρ using ZF processing and new refined model of the total power consumption in single-cell and multi-cell scenario with perfect and imperfect CSI.

4. To evaluate analytic results for ZF processing scheme with perfect CSI.
5. To implement standard alternating optimisation algorithm to maximise the number of (BS) antennas M, a number of active (UEs) K, and the transmit power ρ separately when the other two are fixed.
6. To measure numerical results for ZF, MRT/MRC, and MMSE processing schemes with perfect CSI in a single-cell scenario.
7. To measure numerical results for ZF processing schemes with imperfect CSI, in a multi-cell scenario.

1.4 Main Contributions

This thesis has contributions to knowledge in three research issues for LS MIMO system, which are the new refined circuit power consumption model, energy efficiency maximisation with ZF processing scheme, and deployment of imperfect CSI case and symmetric multi-cell scenario. Those main contributions of this thesis are summarised and elaborated more detail as follows:

1. The circuit power consumption is the sum of the power consumed by different analogue components and digital signal processing. The new refined model of the total power explicitly described how the total power consumption depends non-linearly on some number of UEs, the number of BS antennas, and transmit power.
2. The closed-form EE expression under the assumption of ZF processing scheme is employed in the uplink and downlink for the optimal number of UEs, the number of BS antennas, and transmit power for a single-cell scenario with perfect CSI. Analytic convenience and numerical results likewise, driven this option by which are close to optimal.

3. Analysis of imperfect CSI case and symmetric multi-cell scenarios deployment are extended using the same method above. A New possible rate derived from symmetric multi-cell scenarios with ZF processing.

1.5 Research Methodology

In the first stage of the research, a literature review of past and current works on the area of MIMO, MU-MIMO, and LS MIMO are extensively conducted to broaden the perspective on such areas of study. Furthermore, state of the art related to those addressed issues is intensely researched and intensively explored during this period.

Following the literature review phase, implementation starts with formulating the EE maximisation problem. Proposal of new refined circuit power consumption model executed. All this then used to compute closed-form expression under the assumption of ZF processing scheme for the optimal number of UEs, the number of BS antennas, and transmit power.

The testing stage starts with simulation. All the simulations were performed based on using analytical Zero Forcing processing scheme and Monte Carlo simulation techniques in MATLAB. Monte Carlo simulation can handle very complex and realistic scenarios. The analytical ZF processing scheme is executed for ZF with perfect CSI and imperfect CSI in single-cell and multi-cell. Nevertheless, the Monte Carlo simulation is executed for all the investigated schemes with perfect CSI in the single-cell scenario, and for ZF with imperfect CSI, and in multi-cell scenarios.

In the validation stage, numerical results from ZF processing analytical technique and simulation technique are used to validate the optimal analytical expression and to make a comparison amongst different processing schemes. Finally, the obtained results are deeply analysed and discussed by giving referred argumentations.

1.6 Thesis Structure

There are six chapters, and the chapters are inter-related to each other in this thesis. Thus, to comprehend the contributions presented in this thesis, readers are suggested to read all the chapter.

Chapter 1 Introduction: This chapter starts with background and then followed by motivations, research objective, main contribution, methodology, and this thesis outline.

Chapter 2 LS MIMO-An Overview: This chapter presents an overview of the LS MIMO concept.

Chapter 3 Literature Review- Energy Efficiency Maximisation in LS MIMO: This chapter gives the outline of the investigated topic, provides a context for the investigation and develops an understanding of existing theories and methods.

Chapter 4 Techniques to Maximise Energy Efficiency: This chapter explains about techniques which have been carried out in this thesis. It also provides details of a justification of the techniques employed.

Chapter 5 Simulation Setup and Numerical Results: This chapter describes description and evaluation for this investigation. The simulation procedures explained in this chapter. Also, presents the data, the graph generated from the simulation during testing and analysis of the result.

Chapter 6 Conclusion & Further Work: This chapter involves interpretation of the findings and comparing the findings with previous findings, discussing the implications and concludes the results of the implementations, and recommendation of developing revised Energy Efficient power consumption model for LS MIMO systems.

1.7 Summary

This chapter describes the background to Large-Scale MIMO systems and the study of Energy Efficiency in Large Scale MIMO systems, but the focus is on how to maximise Energy Efficiency by examining the interplay between Energy Efficiency and differing key system parameters such as the number of Base Station antennas, the number of users and the choice of the transmit power in LS MIMO systems. With this motivation, the effect of the existing total power consumption model will be examined to find the scalable power consumption model which varies with system parameters for Energy Efficient Large-Scale MIMO. Numerical results in Chapter 5 suggests also that it is energy efficient to operate in Large-Scale MIMO systems. This chapter also provides the contributions of the thesis, the aim and the objectives of the research, the research methodology and finally the thesis structure.

Chapter 2

Large-Scale MIMO Systems– An Overview

2.1 Introduction

Internet services such as web browsing, email, video streaming, have become urgent needs for the people's daily life, not only on the traditional wired networks but also on the wireless networks, particularly cellular systems [39]. Wireless communication uses electromagnetic spectrum to carry the modulated information data to the receiver. First generations of cellular systems are mainly designed for only voice and text services. With the advancement of smartphone technology, the devices are nowadays equipped with sophisticated capabilities, thus, new demands for multimedia and high data rate applications are generated [40]. While high data rates services can be reliably provided on wired networks, providing such services on the wireless networks, however, is not a trivial matter to accomplish due to the limited resources and the unpredictable nature of the wireless channel. Besides, the number of subscribers all around the world is still increasing, making provisioning of high data rate services over the cellular systems very challenging problem for both manufacturers and operators. Consequently, the main issue becomes the problem of how to provide high data rate services over limited wireless resources such that the quality of service (QoS) is satisfied. Thus, wireless communication requires very different approaches than that of wired networks.

2.1.1 Evolution of Cellular network

The first generations of wireless mobile networks were voice-oriented, providing low data rate services such as voice. With the dramatic evolution of wireless mobile systems over the last decades, wireless systems have become multimedia oriented mobile networks, and hence raising the expectations for higher data rates. The first generation (1G) was based on analogue technology, deployed in the USA and Europe in the early 1980's, followed by the digital technology-based second generation (2G) deployed in 1991 in Europe. In 2001, third generation (3G) system based on the code division multiple access (CDMA) technology was first operated. The dramatic enhancement of the mobile systems occurred in high-speed downlink packet access (HSDPA) supporting a speed of up to 21 Mbps. Then, it is evolved to HSPA+ with speed reaching up to 42 Mbps.

Later, long-term evolution (LTE) is introduced by the third-generation partnership (3GPP) to provide high data rate up to 160 Mbps within 20 MHz channel bandwidth. LTE is based on orthogonal frequency division multiple access (OFDMA technique for resources sharing among users, and incorporates advanced technologies such as MIMO, adaptive modulation, and link adaptation [41].

In 2008, the technical requirement of the fourth generation (4G) has been identified in the international mobile Telecommunication-Advanced (IMT-A) [42]. In this direction, 3GPP targeted the candidate for cellular technologies that are meeting the IMT-A requirements and proposed LTE-advanced
(LTE-A) [43]. The key technologies that make LTE-A superior over LTE and 3G are carrier aggregation, OFDMA, CoMP technique for interference management, and deploying the heterogeneous networks to improve spectral efficiency and provide uniform coverage [43].

Nowadays, researchers all over the world have been targeting 5G cellular, which is expected to be a ground-breaking technology, overcoming the limitation faced by the previous cellular generations. 5G is envisioned to include massive bandwidth with high frequencies, dense BSs deployment, a massive number of antennas, heterogeneous network deployment, cognitive radio, highly adaptive multicell coordination strategies, and energy efficient technology, not to mention others [44].

2.2 The Wireless Channel

Wireless channel is the air medium which wireless transmission is performed via electromagnetic waves. Since the wave is not restricted to take the single path, it suffers reflection, diffraction, scattering by buildings, hills, bodies, and other objects when travelling from the transmitter to receiver, hence multiple copies of the signal arrive at the receiver as shown in Figure 2.1.

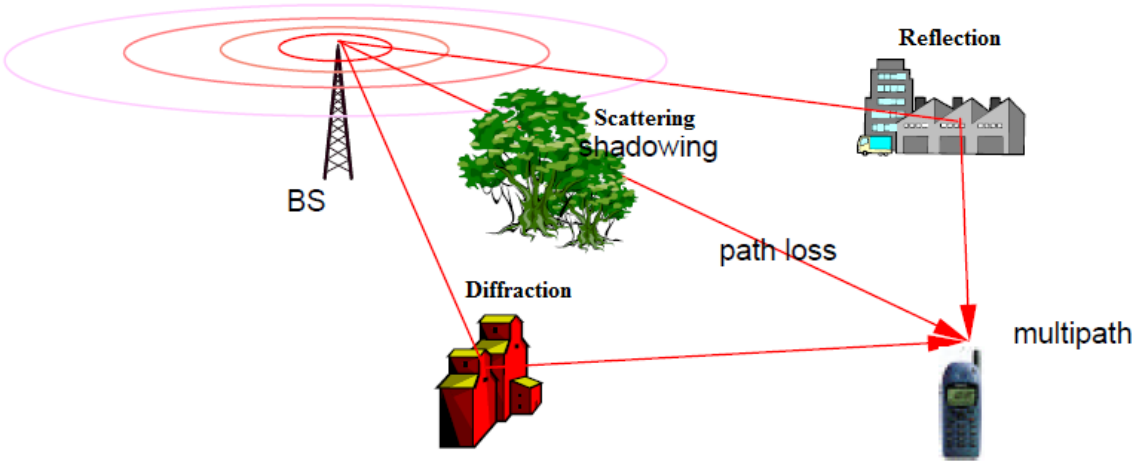

Figure 2.1: Radio Signal Propagation [45].

Each copy of the signal has a different delay, phase, and gain, and thus they interfere constructively or destructively. This is referred as a multipath phenomenon. To fully characterise the random time-varying properties of the multipath channel, statistical models have been developed [46]. In general, the wireless channel is affected by three main factors; path-loss, shadowing, and small-scale fading [46].

Path-loss refers to signal power dissipation in proportion to the distance between transmitter and receiver. In the free space, path-loss is given be

$$L = \frac{\varepsilon G_t G_r}{(4\pi d)^2} \tag{2.1}$$

where ε is the wavelength, G_t is the transmitter antenna gain, G_r is the receive antenna gain, d is the distance between the transmitter and receiver. This model is only valid providto e that there is only one single path between two points, i.e. line-of-sight (LoS), or few multipath component. In cellular communication, the signal propagates through different paths between transmitter and receiver, for which the path-loss is commonly modelled as

$$L = \varsigma d^{-\alpha} \tag{2.2}$$

where ς represents a constant that captures the antenna characteristics and channel attenuation, and α is the path-loss exponent that varies from 2 to 6 depending on the communication environment [46].

Shadowing is a random variation experienced by signal power due to obstacles between transmitter and receiver that attenuate the signal through scattering, reflection, and diffraction [46], [47]. Statistical methods are usually used to model shadowing where log-normal shadowing model is the most accurately validated model [46].

The probability density function (PDF) of a log-normal random variable y is given as

$$f(y) = \frac{1}{y\sigma\sqrt{2\pi}} e^{\frac{\ln y - \mu}{(2\sigma)^2}}, y > 0. \quad (2.3)$$

where μ and σ represent the mean and the standard deviation of y given in dB.

Small-scale fading refers to the microscopic channel variations due to the constructive and destructive addition of multipath signal replicas. Since each replica experiences different attenuation, delay, and phase, the superposition of all components results in a destructive and constructive addition, thus attenuating and amplifying the received signal, respectively [46], [47]. When the drop of the signal is severe, it is referred to as deep fade, and usually results in temporary outage in communication.

Fading variations and its impact on frequency domain can be characterised by the notion of coherence bandwidth W_c. This parameter measures the range of frequencies over which the channel is highly correlated, in other word the channel does not change over the entire signal bandwidth (or flat). Coherence bandwidth is connected to the delay spread arising from multipath phenomenon as $W_c \approx \frac{1}{T_d}$, where T_d is defined as the difference between delays spread associated with the most significant multipath component and the latest component.

If the signal bandwidth w is smaller than the coherence bandwidth, the exhibits a constant gain transfer function over the entire signal bandwidth. However, when the coherence bandwidth is larger than the signal bandwidth, the channel response exhibits frequency-selective behaviour, in other words, different parts of signal bandwidth experience uncorrelated fading, rising the signal distortion or so-called inter-symbol interference (ISI).

To overcome this problem, sophisticated equalisation needs to be utilised at the detection side, which is costly in implementation. The other widely adopted solution is recent advanced wireless technologies using low rate multi-carrier transmission such as orthogonal frequency division multiplexing (OFDM), whereby each subcarrier has the smaller bandwidth to ensure that the channel is flat over each subcarrier bandwidth [46], [47].

On the other hand, fading variations in the time domain are characterised by the notion of coherence time T_c, which refers to time duration at which the channel remains correlated. Coherence time is related to the Doppler spread parameter f_d as $T_c \approx \frac{1}{f_d}$, which is the broadening in the signal bandwidth caused by relativethe mobility of the transmitter and receiver. Channel with larger Doppler spread changes faster, thereby having shorter coherence time [46]. The rate at which the variation in the signal takes place determines how fast the fading is; fast fading occurs with multipath phenomenon as it takes place over very small-time scale (in the order of milliseconds), while slow fading occurs with path-loss and shadowing as it happens over relatively larger time scale (in the order of tens of seconds).

To model small-scale fading, several statistical models have been proposed and utilised. The two most common models are Rayleigh and Rician model.

2.2.1 Rayleigh Channel Fading

This channel fading assumes that there is no line-of-site component between transmitter and receiver, and there are many independent signal paths. Per Central Limit Theorem (CLT), when there are many random variables, the limiting distribution will approximate Gaussian distribution. Thus, the fading channel modelled as a zero-mean complex-valued Gaussian random variable, $x \sim \mathcal{CN}(0, \sigma^2)$ with channel envelope $y = |x|$ and PDF given by

$$p(y) = \frac{y}{\sigma^2} e^{\frac{y^2}{2\sigma^2}}, y > 0 \quad (2.4)$$

where σ^2 is, the average received power.

2.2.2 Rician Channel Fading

When there is line-of-site component between transmitter and receiver, the signal will be composed of a vast number of independent paths plus line-of-site components. The signal envelope is modelled by Rician distribution given by

$$p(y) = \frac{y}{\sigma^2} e^{-K-\frac{(K+1)y^2}{\sigma^2}} I_0\left(2y\sqrt{\frac{K(K+1)}{\sigma^2}}\right) \quad (2.5)$$

where *K denotes* the ratio of the power of the line-of-site component to the power of other multipath components, and $I_0$is the modified Bessel function of the 0th order given by

$$I_0(y) = \sum_{k=0}^{\infty} \frac{\left(\frac{1}{4}y^2\right)^k}{(k!)^2} \quad (2.6)$$

2.2.3 Channel Model

Actual wireless channels are complex and challenging to represent accurately. For simulation studies, empirical models have been developed based on extensive measurements that approximate the most common communication scenarios. As described previously, a complex random variable that models path loss, shadowing and small-scale fading effects modelled the channel coefficient between a transmit and receive antenna. The instantaneous magnitude and phase of the channel coefficient represent the amplitude and phase of channel's frequency response respectively.

The international telecommunication union (ITU) and the 3rd generation partnership project (3GPP) developed spatial channels models (SCM) that model various urban and rural propagation scenarios for simulation studies. The ITU-R IMT-Advanced channel model is a stochastic model based on the scenario geometry. The model includes information about the angle of arrival (AoA) as well as the angle of departure (AoD), the so-called double-directional channel model. It specifies the directions, amplitudes and phases for several rays (plane-waves) instead of the spatial location of the scatterers.

The instantaneous parameters are determined stochastically based on statistical distributions extracted from actual channel measurements for several well-known scenarios. A specific scenario of the simulation study decides the location, geometry and pattern of antennas. The effects of delay, power, and angular parameters are evaluated to obtain the channel coefficients at several instants in time while the rays superimposed at the location of antennas in the simulation setup. Moreover, the superposition of rays produces the effects of correlation between antenna elements, temporal fading and Doppler spectrum at the transmitter as well as at the receiver.

The urban macro model (UMa) targets coverage for pedestrian and vehicular users, with non-line of sight (NLoS) as the dominant mode of propagation. The dominant scatterers such as buildings which are usually assumed placed in a Manhattan grid layout. While the BS elevated to a height greater than the buildings in the vicinity, the mobile terminal is located outdoors at ground level.

2.3 Multi-user MIMO

In the first three generation of cellular technology, the BS served multiple terminals by separating them in time, frequency or code. Each terminal was assigned a different fraction of spectrum resources for communication over the forward-and-reverse links, to minimise intra-cell interference. A multi-antenna BS opens the spatial dimension that allows it to discriminate the signal to/from each terminal based on its location, known as MU-MIMO. The spatial dimension enables each terminal to use all available spectrum resources, improving the throughput without the need for additional (expensive) resources. The hardware cost involved with MU-MIMO is the need to place additional BS antennas at the locations that to transmit/receive the signal. Thus, the available spatial degrees of freedom at the BS is limited by the number of antennas.

A multi-antenna transmitter can precode the signal with a complex weight vector such that the radiated energy from each antenna adds constructively or destructively in desired directions. This approach, called transmit beamforming, can be used to maximise the signal power at the receiver or place nulls in the direction of interferers. The optimal beamforming weights depend on the instantaneous amplitude and phase of the channel. Analogously, a multi-antenna receiver may exploit channel knowledge for receive beamforming to maximise signal power and minimise the interference power.

The MU-MIMO setup of interest consists of a BS with M antennas serving K single-antenna terminals ($K \leq M$), over the same time-frequency resources. The BS exploits channel knowledge for transmitting and receive beamforming to create a spatially separate data stream for each terminal. The data streams function as independent Single-Input Single-Output (SISO) links as under favourable channel conditions are shown in Figure 2.2, and can linearly increase the spectral efficiency with the number of terminals served. However, the benefits of this spatial multiplexing regarding spectral efficiency critically depend on the array size and the accuracy of channel estimates at the BS.

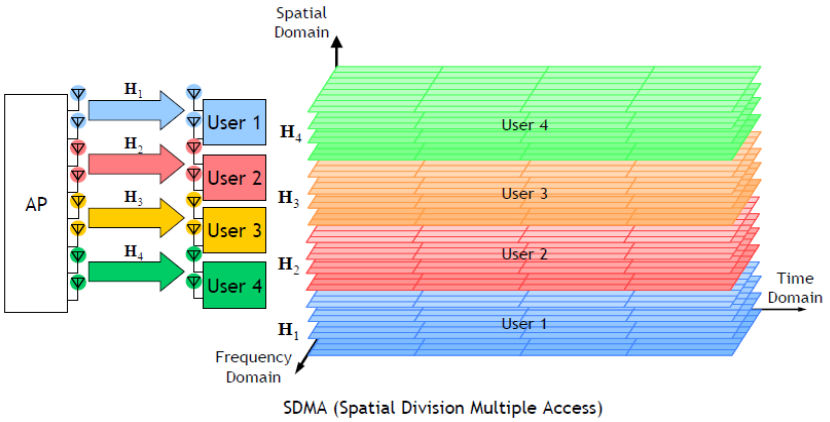

Figure 2.2: MU-MIMO System [48].

2.3.1 Spatial Multiplexing

Spatial multiplexing aims at increasing achievable data rate. The data stream is divided into multiple independent substreams to increase data rates; the sub-streams are transmitted simultaneously through spatial channels. At the receiver, appropriate techniques can be used to separate these sub-streams. The spatial multiplexing gain defined as

$$d_{Mul} = \lim_{\gamma \to \infty} \frac{R}{\log \gamma} \tag{2.7}$$

where *R* denotes the rate measured in (bits/s/Hz) and is a function of the SNR, i.e., *R* = f (SNR). The maximum spatial multiplexing gain achieved by MIMO channel **H** is

$$(d_{Mul})_{max} = min(N_T, N_R) \tag{2.8}$$

which means, the minimum of N_t and N_R . d_{Mul} is also known as the number of degrees of freedom that can be available by MIMO system with channel H.

2.3.2 Shannon Capacity

In his pioneering work on the information theory, Shannon introduced the notion of channel capacity, which means the achievable data rate that transmitted over the channel with arbitrarily small error probability. Capacity has become an important metric for analysing the performance of wireless networks; it possessed even high importance for future mobile networks that are expected to provide high data rate applications. In an additive white Gaussian noise (AWGN) channel, Shannon capacity defined as

$$C = W \log_2 \left(1 + \frac{P}{N_0 W}\right), \text{[bits/sec]} \tag{2.9}$$

where W is signal bandwidth in Hz, N_0 id the noise spectral density in Watt/Hz, and P is the transmit power. The term $\frac{P}{N_0 W}$ is commonly referred to a signal-to-noise ratio (SNR). Shannon capacity gives an upper bound limit on the achievable rate, it could be achieved by advanced signal processing and coding techniques.

It can be observed from the above formula that the two factors fundamentally limiting the capacity are power and bandwidth, which represent the main wireless resources. Two extreme regimes can be deduced from Shannon formula; when SNR gets very large, the capacity becomes logarithmic in power and linear in bandwidth, i.e. $C = W \log_2\left(\frac{P}{N_0 W}\right)$, this is referred to as bandwidth-limited regime.

On the other hand, when SNR get very small, capacity becomes insensitive to bandwidth, i.e. $C = \left(\frac{P}{N_0}\right) \log_2 e$,where e is the base of the natural logarithm. In the first regime, it is more advantageous to increase bandwidth for capacity increase, whereas in the second regime, increasing power is the best strategy.

2.3.3 Energy Efficiency

Energy efficiency has attracted significant attention nowadays since increasing spectral efficiency typically results in more energy consumption. The energy consumption increase in wireless communication systems results in an increase of CO_2 emission, which represents a significant threat to the environment. Thus, there is a consensus on the necessity of protecting the environment from the dangers of modern technology. Moreover, the radio access part of cellular systems consumes about 70% of the electric power bills as reported by mobile systems operators, which means high operational cost from an economic point of view.

Additionally, for uplink radio access it is very reasonable to reduce energy consumption for mobile devices to save the battery power.

For these reasons, reducing energy consumption motivates research circles to investigate new energy efficient techniques in wireless networks technology. There is an inherent conflict in enhancing spectral efficiency and decreasing energy consumption at the same time; reducing energy consumption leads to decrease in spectral efficiency and vice versa.

Consequently, there always exists a trade-off between spectral and energy efficiencies. Thus, the spectral-energy efficiency trade-off can be set off as a milestone for the research to investigate the problem of how much energy consumption for a given spectral efficiency, or how much spectral efficiency can obtain for a given energy consumption.

Two different definitions are used to define the energy efficiency. The first definition is to take the ratio of transmission bit rate (or spectral efficiency) to the transmitted power, measured in bit/Joule. This definition has used in literature. The other definition of energy efficiency (Joule/bit) is to take the ratio of consumed power over bit rate or spectral efficiency . In this thesis, the first definition of energy efficiency used as it implies the energy consumption.

2.3.4 Channel Estimation

Although MU-MIMO is a promising technique to enhance spectral efficiency, nevertheless it is quite challenging in practical implementation. To achieve full multiplexing gain of MU-MIMO, the system requires an acquisition of instantaneous perfect CSI. The BS and the UEs are assumed to have perfect CSI. However, in practice, this CSI must be estimated. The system can acquire the CSI through two different ways depending on the duplex scheme adopted. Depending on the system duplexing mode, the channel estimation schemes are very different.

In time division duplex (TDD), both transmitter and receiver utilise the same frequency band and reception, spacing them apart by multiplexing the downlink and uplink signals on different time slots. A user transmits specific pilot symbol training signal and the BS can learn the CSI through channel reciprocity. This necessitates that the time coherence should be long enough to span the interval of both uplink signalling and downlink transmission [49]. On the other hand, in frequency division duplex (FDD), where the downlink and uplink use different frequency bands, the user can feedback the necessary information to the BS through dedicated low rate uplink channel [49].

2.4 Large-Scale MIMO

Wireless communication is one of the most successful technologies is one of the most successful technologies in recent years, for knowing Copper's Law where an exponential growth rate in wireless traffic sustained for over a century. This trend is driven by new innovative; for example, augmented reality and internet-of-things [50].

Large-Scale MIMO which is also known as Massive MIMO is a Multi-user MIMO technology where an array of M active antenna elements is deployed at each base station (BS) and utilises these to communicate with K single- antenna terminal-over the same time and frequency band. The general multi-user MIMO concept has been around for decades, but the vision of deploying BSs with more than a handful of service antennas is relatively [11]. By coherent processing of the signals over the array, transmit precoding can be used in the downlink to focus each signal at its desired terminal and receive combining can be used in the uplink to discriminate between signals sent from different terminals. The more antennas that are used, the finer the spatial focusing can be [51]. An illustration of these concepts is give in Figure 2.3.

The canonical LS MIMO system operates in a time-division duplex (TDD) mode, where the uplink and downlink transmissions occur in the same frequency resource but different in time. The physical propagation channels are reciprocal, meaning that the channel responses are the same in both directions, which utilised in TDD operation. In particular, LS MIMO systems exploit the reciprocity to estimate the channel responses on the uplink and at that point utilise the acquired channel state information (CSI) for uplink the receive combining and downlink transmit precoding of payload data. Since the transceiver hardware is not reciprocal, calibration is needed to exploit the channel reciprocity; calibration is required to operate the channel reciprocity in practice [51].

Fortunately, the uplink-downlink hardware discrepancies only change by a few degrees over a one-hour period and can be mitigated by simple relative calibration methods, even without additional reference transceiver and by only relying on the mutual coupling between antennas in the array [52]. There are several good reasons to operate in TDD mode. Firstly, only the BS needs to know the channels to process the antennas coherently. Secondly, the uplink estimation overhead is proportional to the number of terminals but independent of M thus making the protocol fully scalable on some service antennas. Furthermore, basic estimation theory tells that the estimation quality recovers with M if there is a known correlation structure between the channel responses over the array the estimation quality (per antenna) but not reduced by adding more antennas at the BS in fact; [53].

Since fading makes the channel responses vary over time and frequency, the estimation and payload transmission must fit into a time/frequency block where the channels are approximately static. The coherence bandwidth B_c Hz and the coherence time T_c, which fit $\tau = B_c T_c$ transmission symbols essentially give the dimensions of this block. Massive MIMO can be implemented either using single-carrier or multi-carrier modulation.

Multi-carrier OFDM modulation is considered here for simplicity because the coherence interval has a neat interpretation: it spans several subcarriers over which the channel frequency response is constant, and several OFDM symbols over which the channel is constant; see Figure 2.3. The channel coherency depends on the propagation environment, user mobility, and the carrier frequency.

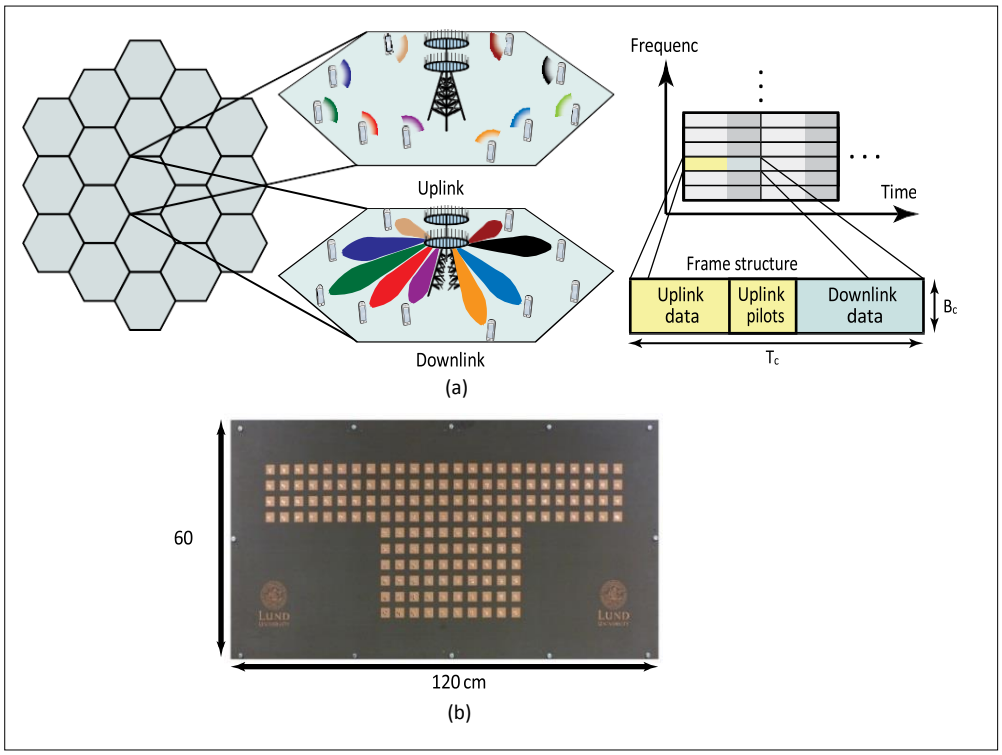

Figure 2.3: Example of a Massive MIMO system. (a) Illustration of the uplink and downlink in line-of-sight propagation, where each BS is equipped with M antennas and serves K terminals. The TDD transmission frame consists of $\tau = B_c T_c$ symbols. (b) Photo of the antenna array consists of 160 dual-polarised patch antennas [53].

2.4.1 Antenna Configuration

In a traditional passive AAs Radio-Frequency (RF) is usually connected to its physical antennas through an RF cable. Recently, Remote Radio Unit (RRU) in conjunction with a Baseband Unit (BBU) has become a preferred configuration recently to reduce the loss imposed by the RF cable and to save the costs of installation and maintenance [54]. The BBU generated baseband digital signal sent to RRUs through an optical fibre. The RF circuit is placed as close as possible to the physical AA. Furthermore, active AAs operating without RF cables are now available commercially, where the careful configuration is required for deploying in the LS MIMO systems [55]. A significant milestone in the development of AA is the integration of the RF circuit and the AA into a single circuit board in an active AA.

The linear AA, spherical AA, cylindrical AA, rectangular AA are some standard LS AAs illustrated in Figure 2.2 [12]. The family of 3D AAs are the spherical AA, cylindrical AA and rectangular AAs belong to, whereas the linear AA is an example of Two-Dimensional (2D) AAs. The spherical, cylindrical and rectangular are practical realistic due to the space limitations at both the eNBs and UEs. The linear AA is mostly supposed in theoretical analysis and practical measurements, whereas the distributed AA is mostly used either inside buildings or for outdoor cooperation.

Moreover, due to the associated aspects of aesthetics and potential health issues, commercial deployment of LS AAs has been partially opposed both by the public and the organisations. LS AAs can be rendered virtually invisible by integrating the AEs into the environment. As shown in Figure 2.2, an aesthetically attractive method is to deploy LS AA as part of the building's façade or signage in an irregular fashion [56], e.g. the black AEs of a rectangular. Instead, to reduce the side lobes of the irregular AA, advanced algorithms relying on subarrays [57], on orthogonal placement [58], or on parasitic AAs [59] can be introduced for improving the beamforming performance of these irregular AAs.

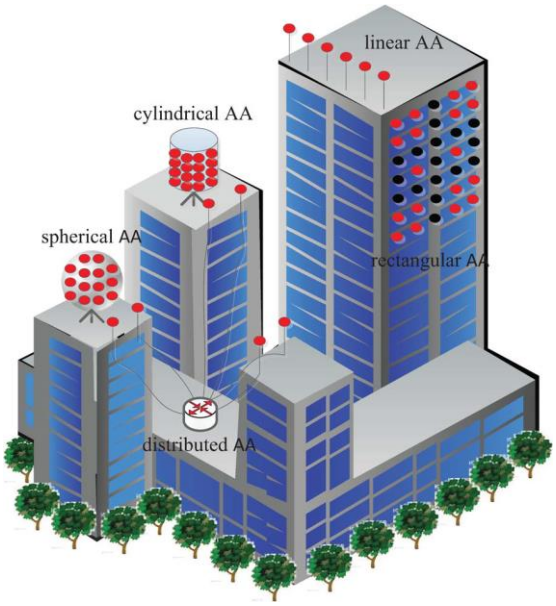

Figure 2.4: Various antenna configuration [1].

2.4.2 Channel Measurement

Realistic channel measurements were conducted in [60], [61] to identify the key features of LS MIMO channels. The outdoor measurements in [60] emphasis primarily on the impact of the number of antennas enforced on the small-scale fading characteristics. When a linear AA employed at the eNB, both the non-stationary nature of the fading and the near-field AA effects have been explored to capture the main properties of a realistic channel model [61]. Though, it requires further investigations to ascertain whether these properties are valid for both spherical as well as cylindrical and rectangular arrays. The main results of these measurements elaborated below.

Since different Antenna Elements (AEs) of the AA at the eNB may encounter different multipath clusters and the AA is frequently subjected to shadow fading, the accurate modelling of LS MIMO systems in practical non-stationary propagation scenarios continues to a large degree an open challenge [60].

The Channel Impulse Responses (CIRs) handled by UEs become more decorrelated from each other in the case of large AAs, since having more AEs allows one to more accurately distinguish both their CIRs and their angles of arrival [62], [63]. Moreover, having additional AEs at the eNB is capable of attaining better-quality orthogonality amongst different UEs in contrast to their conventional small-scale MIMO equivalents. It is particularly important in Spatial Division Multiplexing (SDM) or Spatial Division Multiple Access (SDMA) systems, where the individual and user-specific CIRs used for distinguishing the UEs and the transmission streams.

The linear AA devices have the better angular resolution in azimuth than the cylindrical array. Nevertheless, the latter is capable of achieving a beneficial resolution in both azimuth and elevation, which may be more useful in high urban environments [61].

2.4.3 Channel Model

The Correlation-Based Stochastic Model (CBSM), the Parametric Stochastic Model (PSM) and the Geometry- Based Stochastic Model (GBSM) are three types of channel models devised for evaluating the performance of wireless communications systems, in [61], [62]. The difficulty of the CBSM is low hence primarily used for assessing the theoretical performance of MIMO systems. However, it is somewhat simplistic and hereafter inaccurate for a practical MIMO system. Therefore, it is not directly applicable to the modelling of wireless channels, when encountering a spherical wavefront. By comparison, the GBSM model is capable of accurately describing the realistic channel properties, and hence it is more suitable for LS MIMO channels, although with an increased computational complexity.

The complex nature of the PSM is higher than the CBSM, while the accuracy of the PSM is lower than the GBSM, which results in a lack of studies on the PSM in LS MIMO systems. Therefore, the CBSM is elaborated in this section as it is within the scope of this thesis.

The non-dispersive correlated channel model, the non-dispersive independent identically distributed (i.i.d.) Rayleigh fading model and the dispersive multipath channel model are three kinds of simplified CBSMs, where each tap modelled as either a correlated or uncorrelated fading process.

Non-dispersive i.i.d. Rayleigh channel model is when an i.i.d. Rayleigh fading channel supposed for LS MIMO systems; no correlation occurs between the transmit and receive antennas. Thus, the elements of the fast fading matrix are i.i.d. Gaussian variables. Non-dispersive correlated Rayleigh channel model is to characterise the Doppler-induced received signal correlation, the correlated channel model considered for characterising the possible implementation of LS MIMO systems [17]. The fast fading matrix of the correlated channel model developed by the product of the standard complex-valued Gaussian matrix and the correlation matrix. At the transmitter and receiver of the AEs, the correlation matrix quantifies the long-term correlation, attained through measurements. By comparison, the complex-valued Gaussian matrix describes the i.i.d. Rayleigh fading channel.

The dispersive multipath channel model is different distributions of the Angle of Arrivals (AoAs) from different UEs comprised in the dispersive multipath channel model of LS MIMO systems [66]. Each UE's CIR constituted by multiple independent paths arriving from different directions, in this model. The steering vector of an AoA multiplies a path attenuation to characterise each independent path. The UEs can be separated according to their AoAs when they located at different angular positions. Therefore, this model is useful in analysing the performances of the IUI or Inter-Cell Interference (ICI) schemes.

The characteristics of an LS MIMO channel directly affected by the antenna configuration. The linear AA rises both to non-stationary channel characteristics and to near-field effects, whereas the cylindrical AAs, rectangular, and spherical are capable of accurately directing the beam propagation in the 3D space. Hence, the choice of the configuration of an AA conceived for scenarios requires further investigations.

Currently, the CBSMs primarily devised for analysing the theoretical performance of LS MIMO systems attributed to its simplicity. Measurements conducted for validating the accuracy of this model. The non-stationary LS MIMO channel and the spherical wave propagation effects regarded as the inbuilt properties of the linear AA. The channel model is reflecting both the non-stationary LS MIMO propagation phenomenon and the spherical wave effect propagation effects established for the linear AA, which relies on a cluster-based model. Furthermore, an improved 3D channel model has been specified by the 3GPP. However, characterising the non-stationary propagation of the spherical, cylindrical and rectangular arrays requires further measurements. In conclusion, how to accurately model the channel of LS MIMOs remains an open problem.

2.4.4 Data Transmission Protocol in Large-Scale MIMO

In very Large-Scale MIMO, TDD operation is the desired data transmission protocol. In a coherence interval, there are three operations: channel estimation (with the uplink training and the downlink training), uplink data transmission, and downlink data transmission.

2.4.4.1 Channel Estimation

The BS needs CSI to detect signals transmitted from the users in the uplink, and to precode the signals in the downlink. This CSI is obtained through the uplink training. Each user is assigned an orthogonal pilot, sequences transmitted from all users, and then estimates the channels based on the received pilot signals.

Furthermore, each user may need partial knowledge of CSI to coherently detect the signals transmitted from the BS. This information can be acquired through downlink training or some blind channel estimation algorithm. Since the BS uses linear precoding techniques to beamform the signals to the users, the user needs only the effective channel gain, which is a scalar constant to detect its desired signals. Therefore, the BS can spend a short time to beamform pilots in the downlink for CSI acquisition at the users.

2.4.4.2 Uplink Data Transmission

In the coherence interval, a part of it is used for the uplink data transmission. In the uplink, all K users transmit their data to the BS in the same time-frequency resource. The BS then uses the channel estimates together with linear combining techniques to detect a signal transmitted from all users.

2.4.4.3 Downlink Data Transmission

In the downlink, the BS transmits signals to all K users in the same time-frequency resource. More specifically, the BS uses its channels estimates in combination with the symbols intended for the K users to create M precoded signals which are then fed to M antennas.

2.4.5 Linear Processing in Large-Scale MIMO

Linear processing at the BS is fundamental for the payload transmission in LS MIMO. In the uplink, the BS has a M observation of the multiple access channels from the K terminals. The BS applies linear receive combining to discriminate the signal transmitted by each terminal from the interfering signals. The simplest choice is the maximum ratio (MR) combining that uses the channel estimate of a terminal to maximise the strength of that terminal's signal, by adding the signal components coherently. This result signal amplification proportional to M, which is known as an array gain. Alternative choices are zero-forcing (ZF) combining, which suppresses inter-cell interference at the cost of reducing the array gain to $M - K + 1$, and minimum mean squared error (MMSE) combining that balances between amplifying signals and suppressing interference.

The receive combining creates one effective scalar channel per terminal where the intended signal is amplified and/or the interference suppressed. Any judicious receive combining will improve by adding more BS antennas since there are more channel observations to utilise. The remaining interference usually treated as extra additive noise; thus conventional single-user detection algorithm applied. Another benefit from the combining is that small-scale fading averages out over the array, in the sense that its variance decreases with$M$. This is known as channel hardening and is consequences of the law of large numbers.

There is a strong connection between receive combining in the uplink and the transmit precoding in downlink [56]. This is known as uplink-downlink duality since the uplink and downlink channels are reciprocal in TDD systems. Linear precoding based on MR, ZF, or MMSE principles can be applied to focus each signal at its desired terminal (and possibly mitigate interference towards other terminals).

Many convenient closed-form expressions for the possible uplink or downlink spectral efficiency (per cell) found in the literature; see and references therein. An example for i.i.d. Rayleigh fading channels with MR processing provided, just to show how beautifully simple these expressions are:

$$K\left(1-\frac{K}{\tau}\right).log_2\left(1+\frac{C_{CSI}\,.\,M.\,SNR_{u/d}}{K\,.\,SNR_{u/d}+1}\right) \quad \text{[Bit/sec/Hz/cell]} \qquad (2.6)$$

where K is the number of the terminal, $\left(1-\frac{K}{\tau}\right)$ is the loss from pilot signalling, and $SNR_{u/d}$ equals the uplink signal-to-noise ratio (SNR), SNR_u , when Eq. (2.1) is used to compute the uplink performance. Similarly, $SNR_{u/d}$ is noted as the downlink SNR, SNR_d, when Eq. (1) is used to measure the downlink performance. In both cases, $C_{CSI}=\left(1+\frac{1}{K\,.\,SNR_u}\right)^{-1}$ is the quality of the estimated CSI, proportional to the mean squared power of the MMSE channel estimate (where $c_{CSI}=1$ represents perfect CSI). Notice how the numerator inside the logarithm increases proportionally to M due to the array gain and that the denominator represents the interference plus noise. While canonical LS MIMO systems operate with single-antenna terminals, the technology also handles N-antenna terminals. In this case, K denotes the number of simultaneous data streams and (2.6) describes the spectral efficiency per stream. These streams can be divided over anything from K/N to K terminals, but in this research $N=1$ is selected.

2.4.6 Challenges in Large-Scale MIMO

Despite huge advantages on LS MIMO, many issues need to be tackled. The main challenges of LS MIMO are explained below;

2.4.6.1 Pilot Contamination

In the previous sections, merely single-cell with perfect CSI scenarios are discussed. However, in practice, the cellular network consists of many cells. Due to the limited availability of frequency spectrum, many cells have to share the same time-frequency resources. Thus, single -cell with imperfect CSI scenario and multi-cell systems scenarios are considered. In multi-cell systems, the orthogonal pilot can't be assigned to all the users in all the cells, due to the limitation of channel coherence interval. The orthogonal pilot sequences have to be reused from cell to cell. Therefore, the channel estimate obtained in a given cell will be contaminated by pilots transmitted by users in other cells. This effect, called "pilot contamination", reduces the system performance [67]. The effect of pilot contamination is a major inherent limitation of LS MIMO. Pilot Contamination does not vanish even when the number of BS antennas grows without bound. Thus, considerable efforts have been made to reduce this effect. The eigenvalue-decomposition based channel estimation, pilot decontamination, as well as pilot contamination precoding schemes are proposed in [68]–[71]. In [71], the authors had shown that, under certain conditions of the channel covariance, by using a covariance aware pilot assignment scheme among the cells, pilot contamination can efficiently mitigate. There are continuing researches on this topic.

2.4.6.2 Unfavourable Propagation

Basically, LS MIMO deployed under favourable propagation environments. However, in practice, there may be propagation environments where the channels are not favourable.

For example, in propagation environments where the numbers of scatterers are small compared to the numbers of users, or the channels from different users to the BS share some common scatterers, the channel is not favourable [72]. Distributing BS antennas over a large area is one possibility to tackle the problem.

2.4.6.3 New Standards and Designs

Cellular Networks will be more efficient if LS MIMO is deployed in current systems such as LTE. However, LTE standard only allows up to 8 antennas at the BS [73]. Moreover, LTE uses channel information based on assumption. For example, one option of the downlink in LTE where the BS transmits the reference signals through several fixed beams. Subsequently, the users report back to the BS the strongest beam and BS uses this beam for the downlink transmission. In contrast, LS MIMO uses estimated channel information. Thus, to incorporate LS MIMO into practice, new standards are required. Additionally, with LS MIMO, a costly 40 Watt transceiver can be replaced by large numbers of low-power and inexpensive antennas. Likewise, related hardware designs should be considered, where this requires huge efforts from both academia and industry.

2.5 Summary

Large-Scale MIMO is MU- MIMO cellular system where the number of BS antennas and the number users are large. In LS MIMO, hundred or thousand of BS antennas simultaneously serve tens or hundreds of users in the same time-frequency resource. This chapter describes, the background information such as wireless channel properties, MU-MIMO channel model and system properties, LS MIMO channel model, Transmission and Processing schemes, and finally the main challenges in LS MIMO systems.

Chapter 3

Energy Efficiency in Large-Scale MIMO Systems - Literature Review

3.1 Introduction

The cellular networks of today provide good coverage and service in many countries, in both urban and rural areas. The key challenge for the industry is the rapid proliferation of smartphones, laptops, and tablet PCs with built-in cellular access that is rapidly driving the demand for increased capacity. Forecasts range from a hundred-fold to a thousand-fold increase in traffic volume before 2020. In addition, increasing access to telecommunication services in rural parts of the world has the potential to alleviate the digital divide felt by the people of these regions. Recently, both public and private sector entities have shown more interest in tackling this problem on a global scale. Deployment of connectivity solutions in rural communities, however, faces many practical challenges. Lack of availability and access to reliable electricity sources is one of the major hindrances for rural connectivity, particularly in under-developed countries. As such, wireless connectivity solutions for such applications must focus on low-power hardware operation and high energy efficiency (EE).

EE is an important factor in the design of next-generation (i.e., 5G) urban wireless network. The underlying motivations for energy-efficiency designs in urban networks, however, may be different from their rural counterparts because urban populations often have adequate access to powers sources.

Urban networks are, instead, expected to serve an unprecedented number of

devices through what is called *network densification* (i.e., small cells), with the goal of providing 1,000 times more capacity compared to the current generation of network. Economic and environmental concerns, however, constrain the practical realisation of densified urban networks to power consumption level comparable to (or even lower than) current (i.e., legacy) networks [74]. for example, it is estimated, it is estimated that network operators spend almost half of their operating expenses on energy costs and that the telecommunication industry is responsible for 2% of total carbon dioxide emissions worldwide [75]. As a result, an alternative view of network design has emerged, referred to collectively as *green communication*, which adopts an end-to-end perspective on Energy Efficiency [76].

Regardless of rural or urban setting, focussing on energy optimisation translates into designs in which radio resources are tuned to maximise the amount of reliable information transmitted per watt of total expended power. A traditional approach to EE might include only the transmit power in total expended power. An end-to-end system perspective, however, includes additional digital hardware and perhaps even the consumption due to cooling and networking backhaul.

3.2 Energy Efficiency in Large Scale MIMO System

Many novel approaches have been taken to increase EE in wireless networks. The Large-scale MIMO architecture in [11] has shown promise in this regard. The building block of a Large-scale MIMO is a multi-antenna base station (BS) concurrently serving many single-antenna users, where the number of BS antennas is typically much larger than a number of users. With imperfect CSI at the transmitter, it has been shown that for a fixed rate, a single-cell LS MIMO transmitter can reduce its radiated power by a factor proportional to the square root of the number of deployed BS antennas [18]. The work in [29] extends this result to account for the aggregate impact of various hardware impairments on

massive MIMO systems, concluding that high EE can still be obtained under realistic hardware configurations. Such results suggest that LS MIMO systems may not only be attractive from an EE point-of-view likewise can yield more cost-effective implementations because conventional arrays with only a few antennas fed by expensive high-power amplifiers can be replaced by hundreds of antennas fed by low-cost low-power amplifiers and circuitry [74].

3.2.1 Power Consumption in Large-Scale MIMO

Recently, industry and academia have expressed significant interest in implementing LS MIMO in both single and multi-cell environments [33], [32],[77], [78], [30]. The use of additional antennas at the BS has been shown to improve power efficiency both uplink [33] and for the downlink [77],[78]. LS MIMO is a system where a BS equipped with a hundred or more antennas simultaneously serves several users in the same frequency band by exploiting the degrees-of-freedom (DoF) in the spatial domain [11], [30]-[33],[78]-[82]. Providentially, when the number of antennas at the BS is large enough, from the law of large numbers, the random and mutually independent channel vectors between the BS and the users become pairwise orthogonal [83]. Spatial-division multiplexing for LS MIMO can enhance the reliability and throughput of the system because more distinct paths are established between the BS and the users [84], [85]. Notably, the additional DoF provided a massive number of antennas at the BS can reduce the transmit power for the users on the uplink. This is very efficient when multimedia services are increasing and the design of battery with long time use is a major challenge for manufacturers [86]. Undoubtedly, the electrical power supply to the BS will be higher which is consumed by the rectifier, baseband digital signal processing circuit, power amplifier, feeder, and cooling system on the downlink. Henceforth, solutions to reduce the emission of RF power would help in reducing the power consumption of the BS [87].

3.2.1.1 Power Consumption Model in LS MIMO

An accurate modelling of the total power consumption is the fundamental importance to obtain a reliable guideline for EE maximisation of some (BS) antennas M and a number of active (UEs) K for LS MIMO systems [27]. A common assumption in related literature that the total power consumption is computed as the sums of the radiated transmit power and a constant quantity accounting for the circuit power consumption [28]. This model might be very misleading although widely used and can lead to an unbounded EE if utilised to design systems wherein M can be very large because the user rates grow unboundedly as $M \to \infty$ [29]. Attaining infinite EE is evidently impossible as the model does not consider the power consumed by digital signal processing and analogue circuits (for radio-frequency (RF) and baseband processing) grows with M and K. Meaning to say, its contributions can be taken as a constant only in multi-user MIMO systems where M and K take relatively small values. Instead, its variability plays a key role in the so-called *massive MIMO* (or large-scale MIMO) systems in which $M, K \gg 1$ and all the BS antennas are processed coherently [29-33]. The original massive MIMO definition in [30] also assumed $\frac{M}{K} \gg 1$, while the more general definition from [31] - [32] where $\frac{M}{K}$ is also assumed to be a small constant.

3.2.1.2 System Parameters in LS MIMO

The impact on the EE by the number of antennas M has been recently investigated in [34] – [39]. Power allocation problem focused in the uplink of multi-user MIMO systems and showed that the EE is maximized when specific UEs are switched off [34]. Likewise, in [35] the uplink was studied, where the EE was shown To be a concave function of *M* and the UE rates. In [36] - [38] the downlink was studied, whereby [36] and [37] showed that EE is a concave function of M while a similar result was shown for K in [38]. However, the system parameters were optimized by useful simulations which do not provide a complete picture of how the EE is affected by the context of the different system. The coexisting work [39] derives the optimal M and K for a given uplink sum rate, nevertheless the ,necessary overhead signalling for channel acquisition is ignored thus leading to unrealistic results where it is beneficial to let *K* grow very large, or even go to infinity.

3.2.1.3 Power Amplifier power consumption

As discussed in [93], the base station is divided into three parts. These are pre-transceiver block, transceiver block, and power amplifier (PA) part. The power consumption of these blocks are influenced by traffic load and required transmit power. As the power consumption due to PA is very large, it had been taken as a separate entity. The power of the PA is proportionated to the transmit power of the base station.

One of the reasons for power losses power losses in the BS is PA linearity. Linearity is an important aspect in PAs since the system performance and efficiency are highly dependent on it. The power consumption of PA depends on the peak to average power ratio (PAPR) and PA efficiency.

The non-constant envelope modulation schemes like OFDM exhibit a high PAPR, resulting in a need for a highly linear Radio Frequency PA.

However, this can be mitigated by proper choice of PAPR reduction schemes and PA efficiency can be improved by the advanced PA technologies like Doherty PAs which exhibits high input back off.

Doherty PA (DPA) is designed using the combination of a carrier PA and a peak PA. The Peak amplifier will be active only the carrier amplifier saturates. Otherwise only the carrier amplifier will be in the active region. The DPA will provide high efficiency even at a large Back of Point (BOP) [94]. The BOP with peak efficiency can be achieved by the conventional 2-stage DPA is around 6dB and it can be further increased with the increased in a number of peak PAs [95].

3.2.2 Detection in Uplink LS MIMO

In Multi-user MIMO systems, it is known that a multi-user detection technique called successive interference cancellation (SIC) can achieve maximum rate in the uplink channel [91]. However, the SIC is difficult to be implemented in practice due to its high computational complexity. Thus, other detection methods that are based on linear detectors, including ZF, MRC, MMSE have been developed [32], [30], [78], [84] and [90]. Among them, [11] derived the asymptotic analysis for the signal-to-interference-pulse-noise ratio (SINR) for the uplink by using MRC and the SINR for the downlink by using MRT. An exact performance analysis for the uplink was provided in [84] with arbitrary antennas at the BS. All these results have shown that a linear receiver can exploit the advantages of LS MIMO arrays at the BS with low implementation complexity. A ZF receiver can cancel intracell interference, and therefore it generally outperforms an MRC receiver. This implies that a ZF receiver can reduce the number of BS antennas necessarily, relative to the number needed for MRC, whilst obtain the same system performance.

In general, the performance of the ZF receiver is worse than the MMSE receiver. However, if the SINR is high enough, the performance of the ZF receiver and MMSE are equivalent [33], [91]. Furthermore, an MMSE receiver requires additional knowledge on the SINR and yields higher complexity than ZF receiver. In addition, exact performance analysis is not tractable even in the case of perfect CSI [32]. It was shown in [78] that ZF processing scheme can provide a good trade-off between complexity and system. Especially when the number of BS antennas is very large. Therefore, ZF processing scheme is used in this thesis.

3.2.3 Channel estimation in Downlink LS MIMO

In [84], the study considered MIMO configuration with a ZF receiver, where the CSI is assumed to be perfectly known to both transmitter and the receiver. Under such assumptions for the CSI, the expression of the exact performance of the system might be tractable. In practice, however, CSI is not perfect at the transmitter and the receiver. For the BS to acquire the CSI, a simple scheme can be employed where users send pilot signals to the BS, so that the BS can estimate the channel by analysing the received pilot signals in an uplink training phase [32], [82], [17 85], [90], and [92]. The Least-squares (LS) methods is a conventional method that is generally used to estimate the CSI. Unfortunately, this method causes significant degradation in the system performance due to strong inter-cell interference. In contrast, the MMSE estimation method can results in more accurate channel estimation [32]. In the uplink transmission phase, the signals transmitted from the users to BS can be detected by using a linear detector using the estimated CSI.

3.3 Large-Scale MIMO System and Signal Model

The operation of an LS MIMO systems uplink and downlink considered over a bandwidth of B Hz. The BS uses a co-located array with M antennas to communicate with K single-antennas UEs that are selected in round-robin fashion from a large set of UEs within the coverage area. A block flat-fading channels is considered where, B_{C} (in Hz) is the coherence bandwidth and T_{C} (in seconds) is the coherence time. Hence, the channels are static within time-frequency coherence block of $U = B_{\mathrm{C}}T_{\mathrm{C}}$ symbols. The BS and UEs are assumed perfectly synchronised and operate per the time-division duplex (TDD) protocol shown in Figure 3.1. The fixed ratios of uplink and downlink transmission are denoted by $\zeta^{(\mathrm{ul})}$ and $\zeta^{(\mathrm{dl})}$, respectively, with $\zeta^{(\mathrm{ul})} + \zeta^{(\mathrm{dl})} = 1$. As seen from Figure 3.1, uplink transmission takes place first and consists of $U\zeta^{(\mathrm{ul})}$ symbols. The subsequent downlink transmission consists of $U\zeta^{(\mathrm{dl})}$ symbols. The pilot signalling occupies $\tau^{(\mathrm{ul})}K$ symbols in the uplink and $\tau^{(\mathrm{dl})}K$ in the downlink, where $\tau^{(\mathrm{ul})}, \tau^{(\mathrm{dl})} \geq 1$ to enable orthogonal pilot sequences among the UEs [29],[32],[33]. The uplink pilots enable the BS to estimate the UE channels. Since the TDD protocol is matched to the coherence blocks, the uplink and downlink channels are considered reciprocal and the BS can make use of uplink estimates for both reception and downlink transmission. TDD protocols basically require M and K to be the same in the uplink and downlink. The downlink pilots let each UE estimate its effective channel and interference variance with the current precoding.

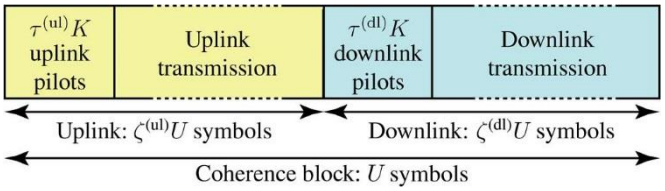

Figure 3.1: Illustration of the TDD protocol [23].

The physical location of UE k is denoted by $x_k \in \mathbb{R}^2$ (in meters) and computed on the BS (assumed to be in origin). First, non-line-of-sight propagation considered for analytic tractability. The function $\iota(.): \mathbb{R}^2 \rightarrow \mathbb{R}$ describes the large-scale channel fading at different user locations; that is, $l(x_k)$ is the average channel attenuation due to path-loss, scattering, and shadowing at location x_k. Since the UEs are selected in a round-robin fashion, the user's location can be treated as random variables from user distribution f (x). Thus, user's location implicitly defining the shape and density of the coverage area; as illustrated in Figure 3.2. The large-scale fading between a UE and BS is assumed to be the same for all BS antennas. This is reasonable since the distances between UEs and the BS are much larger than the distance between the antennas. Since the forthcoming analysis does not depend on a choice of $l(.)$ and user distribution, it is kept generic. The following symmetric example is used for simulations.

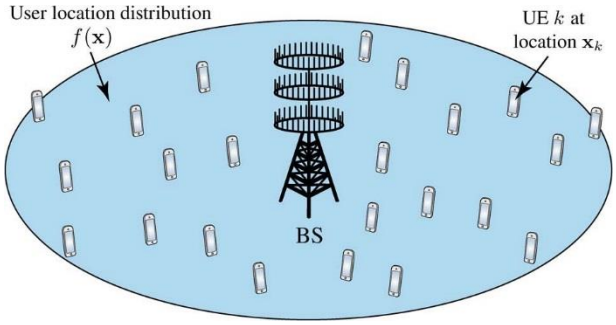

Figure 3.2: Illustration of a generic Multiuser MIMO [23].

The UEs are supposed uniformly distributed in a round cell radius $\mathrm{d_{max}}$ moreover, the minimum distance $\mathrm{d_{min}}$. The density function described this user distribution

$$f(x) = \begin{cases} \frac{\mathbf{1}}{\boldsymbol{\pi}(\boldsymbol{d_{max}^2}-\boldsymbol{d_{min}^2})} & d_{min} \leq \| \mathrm{x} \| \leq d_{max}, \\ \mathbf{0} & \text{otherwise.} \end{cases} \tag{3.1}$$

By allowing the path-loss take-over the large-scale fading, this model as

$$l(x) = \frac{\bar{d}}{\|\mathrm{X}\|^{\kappa}} \qquad for \ \| \mathrm{x} \| \geq d_{min} \tag{3.2}$$

where $\kappa \geq 2$ is the path-loss exponent and the constant $\bar{d} > 0$ regulates the channel attenuation at a distance d_{min} [96]. The average inverse channel attenuation $\mathbb{E}_x\left\{\left(l(x)\right)^{-1}\right\}$ plays a key role in all subsequent discussions. In this example, simple integration (using polar coordinates) shows that

$$\mathbb{E}_x\left\{\left(l(x)\right)^{-1}\right\} = \frac{d_{max}^{\kappa+2} - d_{min}^{\kappa+2}}{\bar{d}\left(1+\frac{\kappa}{2}\right)\left(d_{max}^2 - d_{min}^2\right)} \tag{3.3}$$

3.3.1 Channel Model and Linear Processing LS MIMO System

All *M* antennas at the BS sufficiently are set apart so that the channel components are uncorrelated among the BS antennas and the single-antenna UEs. The channel vector $\mathbf{h}_k = [h_{k,1}, h_{k,2}, \ldots, h_{k,M}]^T \in \mathbb{C}^{M \times 1}$ has entries $\{h_{k,n}\}$ that describe the instantaneous propagation channel between the *n*th antenna at the BS and the *k*th UE. A Rayleigh small scale fading assumed distribution such that $h_k \sim \mathcal{CN}(0_M, \iota(x_k) I_M)$, which is a valid model for both small and large arrays [97]. Linear processing is used for uplink data detection and downlink data precoding. For analytic tractability, the BS can acquire perfect CSI from the uplink pilots.

Besides, the imperfect CSI case is considered in Chapter 4. The uplink linear receive combining matrix denote by $\mathbf{G} = [g_1, g_2, \ldots, g_K] \in \mathbb{C}^{M \times K}$ with the column $\mathbf{g}_k$ being assigned to the *k*th UE. The MRC, ZF, and MMSE processing are considered for uplink detection, which gives

$$\mathbf{G} = \begin{cases} \boldsymbol{H} & \text{For MRC,} \\ \boldsymbol{H}(\boldsymbol{H}^{\boldsymbol{H}}\boldsymbol{H})^{-1} & \text{For ZF,} \\ (\boldsymbol{H}\boldsymbol{P}^{(\boldsymbol{ul})}\boldsymbol{H}^{\boldsymbol{H}} + \boldsymbol{\sigma}^{\boldsymbol{2}}\boldsymbol{I}_{\boldsymbol{M}})^{-\boldsymbol{1}}\boldsymbol{H} & \text{For MMSE,} \end{cases} \tag{3.4}$$

where $H = [h_1, h_2, \ldots, h_K]$ contains all the user channels, σ2 denotes the noise variance (in Joule/symbol), $\boldsymbol{P}^{(\boldsymbol{ul})} = \mathrm{diag}(p_1{}^{(ul)}, p_2{}^{(ul)}, \ldots, p_K{}^{(ul)})$, and the design parameter $p_i{}^{(ul)} \geq 0$ is the transmitted uplink power of UE i (in Joule/symbol) for $i = 1, 2, \ldots, K$. Similarly, MRT, ZF, and MMSE as precoding schemes considered

for downlink transmission [100]. The precoding schemes matrix denoted by $\mathrm{V} = [\mathrm{v}_1, \mathrm{v}_2, \ldots, \mathrm{v}_K] \in \mathbb{C}^{M \times K}$, where

$$\mathbf{V} = \begin{cases} \boldsymbol{H} & \text{For MRC,} \\ \boldsymbol{H(H^H H)^{-1}} & \text{For ZF,} \\ \boldsymbol{(HP^{ul}H^H + \sigma^2 I_M)^{-1}H} & \text{For MMSE,} \end{cases} \quad (3.5)$$

setting $\mathbf{V} = \mathbf{G}$ is normal since it reduces the computational complexity, but it is optional.

The aim is to design the system assuring a uniform *gross* rate $\bar{R}$ (in bit/second) for any active UE, whereof $\zeta^{\mathrm{ul}}\bar{R}$ is the uplink rate and $\zeta^{\mathrm{dl}}\bar{R}$ is the downlink rate, while conventional systems have a significant difference between peak and average rates. As detailed below, this is achieved by combining the linear processing with proper power allocation.

3.3.2 Uplink in LS MIMO System

Under the assumption of Gaussian codebooks, linear processing, and the perfect CSI [32], the achievable uplink rate in (bit/second) of the kth UE is

$$R_k^{(\mathrm{ul})} = \zeta^{(\mathrm{ul})}\left(1 - \frac{\tau^{(\mathrm{ul})}K}{U\zeta^{(\mathrm{ul})}}\right)\bar{R}_K^{(\mathrm{ul})} \quad (3.6)$$

where the pre-log factor $\left(1 - \frac{\tau^{(\mathrm{ul})}K}{U\zeta^{(\mathrm{ul})}}\right)$ accounts for pilot overhead and $\zeta^{(\mathrm{ul})}$ is the the fraction of uplink transmission. Likewise,

$$\bar{R}_k^{(\mathrm{ul})} = B\log\left(1 + \frac{P_k^{(\mathrm{ul})}\left|g_k^H h_k\right|^2}{\sum_{\ell=1,\ell\neq k}^{K} P_\ell^{(\mathrm{ul})}\left|g_k^H h_\ell\right|^2 + \sigma^2\|g_k\|^2}\right) \quad (3.7)$$

is the uplink gross rate (in bit/second) of the transmission from the *k*th UE, where "gross" refers to overhead factors which are excluded. As mentioned above, the aim is to provide the same gross rate $\bar{R}_k^{(\mathrm{ul})} = \bar{R}$ for $k = 1, 2, \ldots, K$. By utilizing a

technique from [98], this equal-rate condition is met if and only if the uplink power allocation vector $\mathbf{p}^{(\mathrm{ul})} = \left[p_1^{(\mathrm{ul})}, p_2^{(\mathrm{ul})}, \ldots, p_k^{(\mathrm{ul})}\right]^T$ is such that

$$\mathbf{p}^{(\mathrm{ul})} = \sigma^2 \left(\mathbf{D}^{(\mathrm{ul})}\right)^{-1} 1_K \tag{3.8}$$

Where the (k, ℓ)th element of $\mathbf{D}^{(\mathrm{ul})} \in \mathbb{C}^{K \times K}$ is

$$\left[\mathbf{D}^{(\mathrm{ul})}\right]_{k\ell} = \begin{cases} \frac{|\boldsymbol{g}_k^{\boldsymbol{H}} \boldsymbol{h}_k|^2}{\left(2^{\bar{R}/B} - \mathbf{1}\right)_2 \|\boldsymbol{g}_k\|^2} \\ \frac{-|\boldsymbol{g}_k^{\boldsymbol{H}} \boldsymbol{h}_\ell|^2}{\|\boldsymbol{g}_k\|^2} \end{cases} \tag{3.9}$$

The power allocation in (3.2) figured precisely for MRC and ZF detection, where for MMSE detection it is a fixed-point equation since also **G** varies on the power allocation [99].The average uplink PA power (in Watt) expressed as the power consumed by the power amplifiers (PAs), which comprises radiated transmit power and PA dissipation. By using (3.8), it is to be

$$\mathrm{P}_{\mathrm{TX}}^{(\mathrm{ul})} = \frac{B\zeta^{(ul)}}{\eta^{(ul)}} \mathbb{E}\left\{\mathbf{1}_K^T \mathbf{p}^{(\mathrm{ul})}\right\} = \sigma^2 \frac{B\zeta^{(ul)}}{\eta^{(ul)}} \mathbb{E}\left\{\mathbf{1}_K^T \left(\mathbf{D}^{(\mathrm{ul})}\right)^{-1}\right\} \mathbf{1}_K \tag{3.10}$$

where $0 < \eta^{(\mathrm{ul})} \leq 1$ is the PA efficiency at the UEs.

Observe that it might happen that $\bar{R}$ cannot be supported for any transmit powers. In such a case, computing $\mathbf{p}^{(\mathrm{ul})}$ in (3.2) would lead to some negative powers. However, this can easily be detected and avoided by computing the spectral radius of $\mathbf{D}^{(\mathrm{ul})}$ [98]. Moreover, it only happens in interference-limited cases; thus, it is not an issue when ZF is employed (under perfect CSI). In these circumstances, $\mathrm{P}_{\mathrm{TX}}^{(\mathrm{ul})}$ in (3.4) can be computed is closed form as stated in the following.

Lemma 1: If a ZF detector engaged with $M \geq K + 1$, with loss of generality the gross rate is parameterize as,

$$\bar{R} = B \log 1 + \rho(\mathrm{M} - \mathrm{K}) \tag{3.11}$$

where ρ is a design parameter that is proportional to the received signal-to-interference-and-noise ratio (SINR). Using this parameterization, the RF power $\mathrm{P}_{\mathrm{TX}}^{(\mathrm{ul-zf})}$ required to guarantee each UE a gross rate in (3.8) is

$$\mathrm{P}_{\mathrm{TX}}^{(\mathrm{ul-ZF})} = \frac{B\zeta^{(ul)}}{\eta^{(ul)}} \sigma^2 \alpha S_{\mathrm{x}} K \tag{3.12}$$

where $S_x = \mathbb{E}_x\left\{\left(1(x)\right)^{-1}\right\}$ account for user distribution and propagation environment. The gross rate in (3.11) is used for ZF processing in the remainder of this thesis since it gives simple PA power expressions. The parameter ρ is later treated as an optimisation variable.

3.3.3 Downlink in LS MIMO System

A normalised precoding vector $\mathrm{v}_k/\|\mathrm{v}_k\|$ and the downlink signal to the *k*th is assigned a transmit power of $p_k^{(\mathrm{dl})}$ (in Joule/symbol). In [j00], assuming Gaussian codebooks and perfect CSI the achievable downlink rate (in bit/second) of the *k*th UE with linear processing is

$$R_k^{(\mathrm{dl})} = \zeta^{(\mathrm{dl})}\left(1 - \frac{\tau^{(\mathrm{dl})}K}{U\zeta^{(\mathrm{dl})}}\right)\bar{R}_K^{(\mathrm{dl})} \tag{3.13}$$

where $\left(1 - \frac{\tau^{(\mathrm{dl})}K}{U\zeta^{(\mathrm{dl})}}\right)$ accounts for downlink pilot overhead and $\bar{R}_K^{(\mathrm{dl})}$ is the gross rate (in bit/second) given by

$$\bar{R}_k^{(\mathrm{dl})} = B \log\left(1 + \frac{P_k^{(\mathrm{dl})}\frac{\left|\mathrm{h}_k^H \mathrm{v}k\right|^2}{\|\mathrm{v}_k\|^2}}{\sum_{\ell=1,\ell\neq k}^{K} P_\ell^{(\mathrm{dl})}\frac{\left|g_k^H h_\ell\right|^2}{\|v_\ell\|^2} + \sigma^2}\right) \tag{3.14}$$

The average PA power defined as

$$\mathrm{P}_{\mathrm{TX}}^{(\mathrm{dl})} = \frac{B\zeta^{(dl)}}{\eta^{(dl)}} \sum_{k=1}^{K} \mathbb{E}\left\{P_\ell^{(\mathrm{dl})}\right\} \tag{3.15}$$

where $0 < \eta^{(\mathrm{dl})} \leq 1$ is the PA efficiency at the BS. Imposing the equal-rate condition $\bar{R}_k^{(\mathrm{dl})} = \bar{R}$ for all *k*, it follows that the power allocation vector $\mathbf{p}^{(\mathrm{dl})} = \left[p_1^{(\mathrm{dl})}, p_2^{(\mathrm{dl})}, \ldots, p_k^{(\mathrm{dl})}\right]^T$ must be computed as $\mathbf{p}^{(\mathrm{dl})} = \sigma^2\left(\mathbf{D}^{(\mathrm{dl})}\right)^{-1} 1_K$[98], where the (k, ℓ)th element of $\mathbf{D}^{(\mathrm{dl})} \in \mathbb{C}^{K \times K}$ is

$$\left[\mathbf{D}^{(\mathrm{ul})}\right]_{k,\ell} = \begin{cases} \frac{\left|\mathbf{h}_k^H \mathbf{v}_k\right|^2}{\left(2^{\bar{R}/B} - 1\right)_2 \|\mathbf{v}_k\|^2} & \text{for } k = \ell, \\ \frac{-\left|\mathbf{h}_k^H \mathbf{v}_\ell\right|^2}{\|\mathbf{v}_\ell\|^2} & \text{for } k \neq \ell. \end{cases} \tag{3.16}$$

Plugging $\boldsymbol{p}^{(dl)} = \sigma^2\left(\boldsymbol{D}^{(dl)}\right)^{-1} 1_K$ into (3.12), the average down-link PA power (in Watt) is

$$\mathrm{P}_{\mathrm{TX}}^{(\mathrm{dl})} = \sigma^2 \frac{B\zeta^{(dl)}}{\eta^{(dl)}} \mathbb{E}\left\{1_K^T \left(\mathbf{D}^{(\mathrm{dl})}\right)^{-1} 1_K\right\} \tag{3.17}$$

Observe that $\mathbf{D}^{(\mathrm{dl})} = \left(\mathbf{D}^{(\mathrm{ul})}\right)^{\mathrm{T}}$ if the same processing scheme is used for transmit precoding and receive combining (i.e., if $\mathrm{G} = \mathrm{V}$). In this case, the user-specific uplink/downlink transmit powers are different, but the total uplink and downlink PA powers in (10) and (17), respectively, are the same (except for the factors $\zeta^{\mathrm{ul}}/\eta^{\mathrm{ul}}$ and $\zeta^{\mathrm{dl}}/\eta^{\mathrm{dl}}$. This is a consequence of the well-known uplink-downlink duality [101]. Like the uplink, the following result can be proved for ZF in the downlink.

Lemma 2: If a ZF precoding devised with $M \geq K + 1$, then the average downlink PA power $\mathrm{P}_{\mathrm{TX}}^{(\mathrm{dl-ZF})}$ required to serve each UE with a gross rate equal to $\bar{R}$ in (3.8) is

$$\mathrm{P}_{\mathrm{TX}}^{(\mathrm{dl-ZF})} = \frac{B\zeta^{(ul)}}{\eta^{(ul)}} \sigma^2 \rho S_{\mathrm{x}} K \tag{3.18}$$

where S_x is the propagation environment parameter defined in Lemma 1 [23].

From Lemmas 1 and 2, that the average uplink and downlink PA powers sum up to

$$\mathrm{P}_{\mathrm{TX}}^{(\mathrm{ZF})} = \mathrm{P}_{\mathrm{TX}}^{(\mathrm{ul-ZF})} + \mathrm{P}_{\mathrm{TX}}^{(\mathrm{dl-ZF})} = \frac{\mathrm{B}\sigma^2 \rho S_{\mathrm{x}}}{\eta} K \tag{3.19}$$

under ZF processing, where $\eta = \left(\frac{\zeta^{ul}}{\eta^{ul}} + \frac{\zeta^{dl}}{\eta^{dl}}\right)^{-1}$.A key assumption in this thesis is that a uniform gross rate $\bar{R}$ is a guarantee to all UEs by means of power allocation. However, the main results are also applicable in cases with in cases with fixed power allocation. Suppose for example that the transmit power is allocated equally under ZF processing. The Jensen's inequality can be used (as is done in [102]) to prove that $\bar{R}$ is a lower bound of the average gross rates $\mathbb{E}\left\{\bar{R}_k^{(\mathrm{ul})}\right\}$ and $\mathbb{E}\left\{\bar{R}_k^{(\mathrm{dl})}\right\}$ (where the expectation is taken with respect to both user locations and channel realizations).

3.4 Existing Power Consumption Model in LS MIMO System

The EE of a wireless communication system measured in bit/Joule. Likewise, the EE calculated as per the ratio between the average sum rate in (bit/second) and the average total power consumption P_{T} (in Watt = Joule/second) [40]. The total EE metric accounting for both uplink and downlink takes the following form, in a multi-user setting, where P_{CP} accounts for the circuit power consumption.

The uplink and downlink total EE is

$$\mathrm{EE} = \frac{\sum_{k=1}^{K}\left(\mathbb{E}\left\{R_k^{(\mathrm{ul})}\right\}+\mathbb{E}\left\{R_k^{(\mathrm{dl})}\right\}\right)}{\mathrm{P}_{\mathrm{TX}}^{(\mathrm{ul})}+\mathrm{P}_{\mathrm{TX}}^{(\mathrm{dl})}+P_{\mathrm{CP}}} \tag{3.20}$$

In most of the existing work, $P_{\mathrm{CP}} = P_{FIX}$ is a constant quantity accounting for fixed power consumption required for site-cooling, control signaling, and load-independent power of backhaul infrastructure and baseband processors [28]. Moreover, this is not an accurate model to design a good system by optimizing a number of antennas (*M*) and number of UEs (*K*).

In fact, Lemmas 1 and 2 shows that the achievable rates with ZF grow logarithmically with *M* (for a fixed PA power). Hence, the simplified model $P_{\mathrm{CP}} = P_{FIX}$ gives the impression that achieved an unbounded EE by adding more and more antennas. This modelling artefact comes from ignoring that each antenna at the BS requires dedicated circuits with non-zero power consumption, and that the signal processing tasks also become increasingly complex. In other words, an accurate modelling of P_{CP} is of paramount importance when dealing with the design of energy-efficient communication systems.

3.5 Energy Efficiency Problem in LS MIMO System

Based on this EE model in (3.20), the main problem formulated:

$$\mathrm{EE} = \frac{\sum_{k=1}^{K}\left(\mathbb{E}\left\{R_k^{(\mathrm{ul})}\right\}+\mathbb{E}\left\{R_k^{(\mathrm{dl})}\right\}\right)}{\mathrm{P}_{\mathrm{TX}}^{(\mathrm{ul})}+\mathrm{P}_{\mathrm{TX}}^{(\mathrm{dl})}+P_{\mathrm{CP}}(M,K,\bar{R})} \tag{3.21}$$

Solution is designed in Chapter 4 to provide an appropriate model for $P_{\mathrm{CP}}(M, K, \bar{R})$as a function of the three main design parameters: the number of BS antennas(M), number of active UEs(K), and the user gross rates$(\bar{R})$.This problem is solved analytically for ZF processing in Chapter 4. In Chapter 5, the problem solved by Monte Carlo Simulation for MMSE and MRT processing schemes. Numerical results for all the processing schemes shown in Chapter 5. Furthermore, prior works on EE optimisation have focused on either uplink or downlink. In contrast, the main problem, is a holistic optimisation where the total EE maximised provided for $\zeta^{(ul)}$ and $\zeta^{(dl)}$ of uplink and downlink transmission. The optimisation of the uplink or downlink is clearly a special case in which $\zeta^{(ul)} = 0$ or $\zeta^{(dl)} = 0$, respectively. Maximising the EE in (3.21) doesn't decrease the total power, but choosing a right power level and use it wisely.

3.6 Summary

There is four main part of the literature review are explained in this chapter. First is the Energy Efficiency in LS MIMO systems, second is the LS MIMO system and model, third is the existing power consumption model in LS MIMO system and finally the problem formulated based first ,second and third part. In the first part, the definition of EE, the design parameters of EE, and the interplay between EE and key system parameters are examined based on the prior works. In the second part, the LS MIMO system model, and the LS MIMO system key design parameters such number of BS antennas, number of users and transmit power are explained. In the third part, the existing power consumption model in LS MIMO system and its drawbacks are explained. Finally, the Energy Efficiency maximisation problem is formulated. The solution is designed to provide an appropriate power consumption model which is scalable with the key design parameters of EE in LS MIMO system. The problem is solved analytically with ZF processing scheme in Chapter 4.

Chapter 4

Energy Efficiency Maximisation in Large-Scale MIMO Systems - Analytical Framework

4.1 Introduction

Most prior work on LS MIMO system either ignores the circuit power consumption on LS MIMO systems either ignores the circuit power consumption at the nodes or the models it as fixed component [20], [21]. This model could be misleading because the total power consumption caries with different system parameters such as the number of antennas, the numbers of users, and the choice of the transmit/receive filters. With this motivation, EE of LS MIMO with a scalable power-consumption model is studied. The interplay between EE and the key parameters are examined.

4.2 Total Power Consumption Model EE in LS MIMO System

Based on this EE model in (3.20), the average total power consumption, P_{T} is sum of P_{TX} and P_{CP}. P_{TX} denotes, the average transmit power consumption (in watts) while P_{CP} denotes the total average circuit [i.e., all hardware except power amplifier (PA)] power consumption (in watts) at the BS. While deploying more antenna at the BS boots the data rate, the additional antennas circuitry leads to increased power consumption. Inspired by [23], the circuit power consumption allowed to scale with the key parameters such as *M* and *K*.

In particular, P_{TX} defines the total RF power, as in Equation (3.19) where η in is the effective power amplifier efficiency, averaged over uplink and downlink. Based on works from [28], [107] on advanced power amplifier technologies like Doherty Power Amplifier, the uplink power amplifier efficiency, $\eta^{(ul)}$ set to be 30%, and the downlink power amplifier efficiency, $\eta^{(dl)}$set to be 39%.

4.3 Realistic Circuit Power Consumption Model in LS MIMO System

The total power utilised by different analogue components and digital signal processing is the circuit consumption P_{CP} in [28]. Based from prior works of [28],[27],[34],[93][103] and[104], a new refined circuit power consumption model for multi-user MIMO systems is proposed:

$$P_{CP} = P_{FIX} + P_{TC} + P_{CE} + P_{C/D} + P_{BH} + P_{LP} \tag{4.1}$$

where the fixed power P_{FIX} was defined in Chapter 3, P_{TC} accounts for the power consumption of the transceiver chains, P_{CE} of the channel estimation process (performed once per coherence block), $P_{\mathrm{C/D}}$ of the channel coding and decoding units, P_{BH} of the load-dependent backhaul, and P_{LP} of the linear processing at the BS. In the following, simple and realistic models provided for how each term in Equation (4.1) depends, linearly or non-linearly, on the main system parameters$(M, K, \bar{R})$. This is achieved by characterizing the hardware setup using a variety of fixed coefficients, which are kept generic in the analysis; typical values are given later in Table 2. The proposed model is inspired by [28] [27], [34], [30], [93], and [106-109] but goes beyond these prior works by modelling all the terms with realistic, and sometimes non-linear, expressions.

4.3.1 Transceiver Circuit Power

For standard transmitters and receivers, power consumption P_{TC} can be computed as

$$P_{\mathrm{TC}} = MP_{\mathrm{BS}} + P_{\mathrm{SYN}} + KP_{\mathrm{UE}} \tag{4.2}$$

where P_{BS} is the power required to run the circuit components (such as converters, mixers, and filters) attached to each antenna at the BS and P_{SYN} is the power consumed by the local oscillator. The last term P_{UE} accounts for the power required by all circuit components (such as amplifiers, mixer, oscillator, and filters) of each single-antenna UE.

4.3.2 Channel Estimation Circuit Power

All channel estimation process is carried out at the BS and UEs, whose computational efficiency are L_{BS} and L_{UE} . In addition, computational efficiency is measured as arithmetic complex-valued operations per Joule also known as flops/Watt. There are $\frac{B}{U}$ coherence blocks per second and, the pilot-based CSI estimation is performed once per block. In the uplink, the BS receives the pilot signal as a $\mathrm{M} \times \tau^{(\mathrm{ul})}K$ matrix and estimates each UE's channel by multiplying with the corresponding pilot sequence of length $\tau^{(\mathrm{ul})}K$ [17]. This standard linear algebra operation [105] and requires $\mathrm{P}_{\mathrm{CE}}^{(\mathrm{ul})} = \frac{B}{U}\frac{2\tau^{\mathrm{ul}}MK^2}{L_{\mathrm{BS}}}$ Watt. In the downlink, each active UE receives a pilot sequence of length $\tau^{(\mathrm{dl})}K$ and processes it to acquire its effective precoded channel gain (one inner product). From [105], $\mathrm{P}_{\mathrm{CE}}^{(\mathrm{dl})} = \frac{B}{U}\frac{4\tau^{\mathrm{ul}}K^2}{L_{UE}}$ Watt is obtained. Therefore, the total power consumption $P_{\mathrm{CE}} = \mathrm{P}_{\mathrm{CE}}^{(\mathrm{ul})} + \mathrm{P}_{\mathrm{CE}}^{(\mathrm{dl})}$ of the channel estimation process becomes

$$\mathrm{P}_{\mathrm{CE}} = \frac{B}{U}\frac{2\tau^{\mathrm{ul}}MK^2}{L_{BS}} + \frac{B}{U}\frac{4\tau^{\mathrm{ul}}K^2}{L_{UE}} \quad \text{Watt} \tag{4.3}$$

4.3.3 Coding and Decoding Circuit Power

In the downlink, the BS applies channel coding and modulation to K sequences of information symbols. Similarly, each UE applies some suboptimal fixed-complexity algorithm for decoding its own sequence. The opposite is done in the uplink. The power consumption $P_{\mathrm{C/D}}$ accounting for these processes is proportional to the number of bits [104] can thus be quantized as

$$P_{\mathrm{C/D}} = \sum_{K=1}^{K} \left(\mathbb{E}\left\{ R_k^{(\mathrm{ul})} + R_k^{(\mathrm{dl})} \right\} \right) (P_{\mathrm{COD}} + P_{\mathrm{DEC}}) \quad \text{Watt} \tag{4.4}$$

where P_{COD} and P_{DEC} are the coding and decoding powers (in Watt per bit/sec), respectively. For simplicity, P_{COD} and P_{DEC} are assumed the same in the uplink and downlink, but it is straightforward to assign them different values.

4.3.4 Backhaul Circuit Power

The backhaul circuit power is used to transfer uplink/downlink data between the BS and the core network. The power consumption of the backhaul is modelled as the sum of two parts [104]: one load-independent and one load-dependent. The first part comprised in P_{FIX}, while the load-dependent part is proportional to the average sum rate. Looking jointly at the downlink and uplink, the load-dependent term P_{BH} can be computed as [104]

$$\mathrm{P_{BH}} = \sum_{K=1}^{K} \left(\mathbb{E}\left\{ R_k^{(\mathrm{ul})} + R_k^{(\mathrm{dl})} \right\} \right) P_{\mathrm{BT}} \quad \text{Watt} \tag{4.5}$$

where P_{BT} is the backhaul traffic power (in Watt per bit/s).

4.3.5 Linear Processing Circuit Power

The transmitted and received vectors of information symbols at the BS are generated by transmit precoding and processed by receive combining, respectively. From [105];

$$\mathrm{P_{LP}} = B\left(1 - \frac{(\tau^{\mathrm{ul}}+\tau^{\mathrm{dl}})K}{U}\right)\frac{2MK}{L_{\mathrm{BS}}} + P_{\mathrm{LP-C}}\mathrm{Watt} \tag{4.6}$$

where the power consumed describes the first term by making one matrix-vector multiplication per data symbol. The second term $P_{\mathrm{LP-C}}$, accounts for the power required for the uplink linear receive combining matrix **G**; and the linear precoding schemes matrix **V**; as described in Chapter 3. The precoding and linear receive combining matrices are computed once per coherence block and the complexity depends strongly on the choice of processing scheme. Since **G** = **V** is a natural choice (except when the uplink and downlink are designed very differently, only one need to be computed and thereby reduce the computational complexity. If MRT/MRC is used, only each column of **H** need to normalize. This requires approximately

$$P_{\mathrm{LP-C}}^{(\mathrm{MRT/MRC})} = \frac{B}{U}\,\frac{3MK}{L_{\mathrm{BS}}}\ \ \mathrm{Watt} \tag{4.7}$$

which was calculated using the arithmetic operations for standard linear algebra operations in [105]. On the other hand, if ZF processing is selected, then approximately

$$P_{\mathrm{LP-C}}^{(\mathrm{ZF})} = \frac{B}{U}\left(\frac{K^3}{3L_{\mathrm{BS}}} + \frac{3MK^2+MK}{L_{\mathrm{BS}}}\right) \text{ Watt} \qquad (4.8)$$

consumed, if the channel matrix inversion implementation based on standard Cholesky factorization and back-substitution [105]. The computational of optimal MMSE processing is more complex since the power allocation in Equation (3.8) is a fixed-point equation that needed iteration until convergence. Such fixed-point iterations usually converge very quickly, but for simplicity, the number of iterations to some predefined number Q is fixed. This $P_{\mathrm{LP-C}}^{(\mathrm{MMSE})} = QP_{\mathrm{LP-C}}^{(\mathrm{ZF})}$ Watt since the operations in each iteration are approximately the as in ZF.

4.4 Energy Efficiency Maximisation with ZF Processing in LS MIMO System

A theoretical solution for the Energy Efficiency problem is explained here under the assumption of employing ZF linear processing in LS MIMO system. The Energy Efficiency problem is solved analytically by utilising ZF processing scheme in the uplink and downlink. The is solution motivated by analytic convenience and likewise the numerical results, which are close to optimal.

For ZF processing, Energy Efficiency problem reduces to

$$\mathrm{EE}^{(\mathrm{ZF})} = \frac{K\left(1-\frac{\tau_{\mathrm{sum}}K}{U}\right)\bar{R}}{\frac{B\sigma^2\rho S_{\mathrm{x}}}{\eta}K+P_{\mathrm{CP}}^{(\mathrm{ZF})}} \tag{4.9}$$

where the notation

$$\tau_{\mathrm{sum}} = \tau^{(\mathrm{ul})} + \tau^{(\mathrm{dl})} \tag{4.10}$$

used the expression in (3.19), and the fact that

$$\mathbb{E}\left\{R_k^{(\mathrm{dl})}\right\} + \mathbb{E}\left\{R_k^{(\mathrm{ul})}\right\} = R_k^{(\mathrm{dl})} + R_k^{(\mathrm{ul})} = \left(1 - \frac{\tau_{\mathrm{sum}}K}{U}\right)\bar{R} \tag{4.11}$$

and

$$P_{\mathrm{CP}}^{(\mathrm{ZF})} = P_{\mathrm{FIX}} + P_{\mathrm{TC}} + P_{\mathrm{CE}} + P_{\mathrm{C/D}} + P_{\mathrm{BH}} + P_{\mathrm{LP}}^{(\mathrm{ZF})} \tag{4.12}$$

with $P_{\mathrm{LP}}^{(\mathrm{ZF})}$ being given by (27) after replacing $P_{\mathrm{LP-C}}$ with $P_{\mathrm{LP-C}}^{(\mathrm{ZF})}$ from (4.8). For notational convenience, the constant coefficient $\mathcal{A}, \{\mathcal{C}_i\}$, and $\{\mathcal{D}_i\}$ introduced in Table I. These, coefficients collect all the different terms in (4.2) – (4.6) and allow us to rewrite $P_{\mathrm{LP}}^{(\mathrm{ZF})}$ in (4.12) in the more compact form

$$P_{\mathrm{CP}}^{(\mathrm{ZF})} = \sum_{\mathrm{i}=0}^{3} \mathcal{C}_i K^i + M \sum_{\mathrm{i}=0}^{2} \mathcal{D}_i K^i + \mathcal{A}K\left(1 - \frac{\tau_{\mathrm{sum}}\mathrm{K}}{U}\right)\bar{R} \tag{4.13}$$

where recalling that $\bar{R}$ is given by (3.11) and, thus, is also a function of (M, K, ρ). Plugging (34) into (30) yields

$$\mathrm{EE}^{(\mathrm{ZF})} = \frac{K\left(1-\frac{\tau_{\mathrm{sum}}K}{U}\right)\bar{R}}{\frac{B\sigma^2\rho S_{\mathrm{x}}}{\eta}K+\sum_{\mathrm{i}=0}^{3}\mathcal{C}_i K^i+M\sum_{\mathrm{i}=0}^{2}\mathcal{D}_i K^i+\mathcal{A}K\left(1-\frac{\tau_{\mathrm{sum}}\mathrm{K}}{U}\right)\bar{R}} \tag{4.14}$$

In the following, the aim is to solve Equation (4.9) for $\mathcal{A}$,$\{\mathcal{C}_i\}$ and $\{\mathcal{D}_i\}$. Firstly, derive a closed-form expression for the EE-optimal value of either *M*, *K*, or ρ, when the other two are fixed. This does not bring indispensable insights on the interplay between these parameters and the coefficients $\mathcal{A}$,$\{\mathcal{C}_i\}$ and $\{\mathcal{D}_i\}$, but provides the means to solve the problem by an alternating optimization algorithm. Observe that the subsequent analysis is generic with respect to the coefficient $\mathcal{A}$, $\{\mathcal{C}_i\}$ and $\{\mathcal{D}_i\}$, while the hardware characterization
given in Table I for used simulations setup.

Preliminary Definition of Energy Efficiency Maximisation

Definition *2:* Denoting The Lambert W function by $W(x)$ and defined by the equation $x = W(x)e^{W(x)}$ for any $x \in \mathbb{C}$.

TABLE 1
Circuits Power Coefficients for ZF Processing

Coefficients $\{\mathcal{C}_i\}$	Coefficients $\{\mathcal{C}_i\}$ and $\{\mathcal{D}_i\}$
$\mathcal{C}_0 = P_{\text{FIX}} + P_{\text{SYN}}$	$\mathcal{A} = P_{\text{COD}} + P_{\text{DEC}} + P_{\text{BT}}$
$\mathcal{C}_1 = P_{\text{UE}}$	$\mathcal{D}_0 = P_{\text{BS}}$
$\mathcal{C}_0 = \frac{4B_\tau^{(\text{dl})}}{UL_{\text{UE}}}$	$\mathcal{D}_1 = \frac{B}{L_{\text{BS}}}\left(2 + \frac{1}{U}\right)$
$\mathcal{C}_0 = \frac{\text{B}}{3L_{\text{BS}}}$	$\mathcal{D}_2 = \frac{\text{B}}{UL_{\text{BS}}}\left(3 - 2\tau^{(\text{dl})}\right)$

Lemma 3: Consider the optimisation problem

$$\underset{z \geq \frac{a}{b}}{\text{maximise}} \quad \frac{g \log a + bz}{c + dz + h \log a + bz} \tag{4.15}$$

with constant coefficients $a \in \mathbb{R}$, c, $h \geq 0$, and b, d, $g > 0$. The unique solution to (36) is

$$z^* = \frac{e^{W\left(\frac{bc}{ae}+\frac{a}{e}\right)+1}-a}{b} \tag{4.16}$$

Lemma 4: The Lambert W function $W(x)$ is an increasing function for $x \geq 0$ and satisfies the inequalities

$$\text{for } x \geq e. \qquad e\frac{x}{\ln(x)} \leq e^{W(x)+1} \leq (1+e)\frac{x}{\ln(x)} \tag{4.17}$$

The above lemma follows the results and inequalities in and implies that $e^{W(x)+1}$ is approximately equal to e for small x (i.e., when $\ln x \approx x$) whereas it increases almost linearly with x when x takes large values. In other words,

$$\text{for small values} \qquad e^{W(x)+1} \approx e \tag{4.18}$$

$$\text{for small values of } x \qquad e^{W(x)+1} \approx x \tag{4.19}$$

Lemma 3 is used to optimise the EE, while (4.18) and (4.19) are useful in the subsequent discussion to bring insights on how solutions in the form of z^* in (4.16) behave.

4.4.1 Optimal Number of Users for Energy Efficiency Maximisation

When *M* and ρ are given, the EE-optimal value of *K* is considered. For analytic tractability, the sum SINR ρK(and thereby the PA power) assumed and the number of BS antennas per UE, $\frac{M}{K}$ are kept constant and equal to $\rho K = \bar{\rho}$ and $\frac{M}{K} = \bar{\beta}$ with $\bar{\rho} > 0$ and $\bar{\beta} > 1$. The gross rate is then fixed at $\bar{c} = \mathrm{B}\log\left(1 + \bar{\rho}\left(\bar{\beta} - 1\right)\right)$. The following is the result;

Theorem 1: Suppose $\mathcal{A}$,$\{\mathcal{C}_i\}$ and $\{\mathcal{D}_i\}$ are non-negative and constant. For given values of $\bar{\rho}$ and $\bar{\beta}$, the number of UEs that maximize the EE metric is

$$\mathrm{K}^* = \max_{\ell} \left\lceil \mathrm{K}_{\ell}^{(\mathrm{o})} \right\rfloor \tag{4.20}$$

Where the quantities $\left\{K_{\ell}^{(o)}\right\}$ denote the real positive roots of the quartic equation

$$K^4 - \frac{2U}{\tau_{\mathrm{sum}}} K^3 - \mu_1 K^2 - 2\mu_0 K + \frac{U\mu_0}{\tau_{sum}} = 0 \tag{4.21}$$

where $\mu_1 = \frac{\frac{U}{\tau_{sum}}(\mathcal{C}_2+\bar{\beta}\,\mathcal{D}_1)+\mathcal{C}_1+\bar{\beta}\,\mathcal{D}_0}{\mathcal{C}_2+\bar{\beta}\,\mathcal{D}_2}$ and $\mu_1 = \frac{\frac{U}{\tau_{sum}}(\mathcal{C}_2+\bar{\beta}\,\mathcal{D}_1)+\mathcal{C}_1+\bar{\beta}\,\mathcal{D}_0}{\mathcal{C}_2+\bar{\beta}\,\mathcal{D}_2}$

The optimal *K* is root to the quartic polynomial given in (4.21) shown in this theorem. The notation $\lceil\cdot\rfloor$ in (4.20) says that the optimal value K^* is either the closest smaller or closest larger integer to $K_{\ell}^{(o)}$, which is easily determined by comparing the corresponding EE. A basic property in linear algebra is that quartic polynomials have exactly 4 roots (some can be complex-valued) and there are generic closed-form root expressions (4.11). However, these expressions are very lengthy and not given here for a brevity infact, the closed-form expressions are seldom used because there are simple algorithms to find the roots with higher numerical accuracy [106].

To gain insights on K^* is affected by the different parameters, assume that the power consumption required for linear processing and channel estimation are both negligible (i.e., $P_{\mathrm{CE}} = \mathrm{P}_{\mathrm{LP}}^{(\mathrm{ZF})} \approx 0$). This case is particularly relevant as P_{CE} and $\mathrm{P}_{\mathrm{LP}}^{(\mathrm{ZF})}$ essentially decrease with the computational efficiencies L_{BS} and L_{UE}, which are expected to increase rapidly in the future. Then, the following result is of interest.

Corollary 1: If P_{CE} and $\mathrm{P}_{\mathrm{LP}}^{(\mathrm{ZF})}$ are both negligible, then K^* in (41) can be approximated as

$$K^* \approx \left\lfloor \mu \left(\sqrt{1 + \frac{U}{\tau_{\mathrm{sum}} \mu}} - 1 \right) \right\rfloor \tag{4.22}$$

with

$$\mu = \frac{\mathcal{C}_0 + \frac{B\sigma^2 S_{\mathrm{X}} \bar{\rho}}{\eta}}{\mathcal{C}_1 + \bar{\beta} \mathcal{B}_0} = \frac{P_{\mathrm{FIX}} + P_{\mathrm{SYN}} + \frac{B\sigma^2 S_{\mathrm{X}} \bar{\rho}}{\eta}}{P_{\mathrm{UE}} + \bar{\beta} P_{\mathrm{BS}}} \tag{4.23}$$

From (4.22) and (4,23), it is seen that K^* is a decreasing function of the terms in (4.1) that are independent of *K* and *M*. This amounts to saying that the number of UEs is increases with $\{P_{\mathrm{FIX}}, P_{\mathrm{SYN}}\}$ and S_{X}, as well as with the PA power (proportional to ρ) and the noise power σ^2. Looking at the Example 1, S_{X} increases proportionally to d_{max}^k which means that a larger number of UEs must be served as the cell radius d_{max} increases. Moreover, K^* is unaffected by the terms $\{P_{\mathrm{COD}}, P_{\mathrm{DEC}}, P_{\mathrm{BT}}\}$, which are the ones that are multiplied with the average sum rate. The above results are summarized on the following corollaries.

Corollary 2: If the power consumptions for linear processing and channel estimation are both negligible, then the optimal K^* decreases UE and BS antenna $\{P_{\mathrm{UE}}, P_{\mathrm{BS}}\}$, is unaffected by the rate-dependent power $\{P_{\mathrm{COD}}, P_{\mathrm{DEC}}, P_{\mathrm{BT}}\}$, and increase with the fixed power $\{P_{\mathrm{FIX}}, P_{\mathrm{SYN}}\}$.

Corollary 3: A larger number of UEs must be served when the coverage area increases.

4.4.2 Optimal Number of BS Antennas for Energy Efficiency Maximisation

The $M \geq K+1$ that maximizes the EE in (4.14) is found and yielded the following result.

Theorem 2: for given values of K and ρ, the number of BS antennas maximising the EE metric can be computed as $M^* = \lfloor M^{(o)} \rceil$, where

$$M^{(o)} = \frac{e^{W\left(\frac{\rho\left(\frac{\beta\sigma^2 S_X}{\eta}\rho+\mathcal{C}'\right)}{\mathcal{D}'e}+\rho\frac{K-1}{e}\right)+1}+\rho K-1}{\rho} \tag{4.24}$$

M^* is an optimal integer-value and $\lfloor M^{(o)} \rceil$ is an optimal real value; where the notation $\lceil \cdot \rfloor$ represents, the optimal value M^* is either the closest smaller or closest larger integer to $M^{(o)}$.

$\mathcal{C}' > 0$ and $\mathcal{D}' > 0$ are defined as

$$\mathcal{C}' = \frac{\sum_{i=0}^{3} \mathcal{C}_i K^i}{K} \quad \text{and} \quad \mathcal{D}' = \frac{\sum_{i=0}^{3} \mathcal{D}_i K^i}{K} \tag{4.25}$$

Theorem 2 provides explicit guidelines on how to select M in a multi-user MIMO system to maximize EE. It provides the following fundamental insights.

Corollary 4: The optimal M^* does not depend on the rate-dependent power$\{P_{\text{COD}}, P_{\text{DEC}}, P_{\text{BT}}\}$ whereas it decreases with the power per BS antenna P_{BS} and increases with the fixed power and UE-dependent power $\{P_{\text{FIX}}, P_{\text{SYN}}, P_{\text{UE}}\}$.

Corollary 5: The optimal M^* is lower bounded as

$$M^* \geq K + \frac{\frac{\beta\sigma^2 S_{\mathrm{x}}}{\eta\mathcal{D}'}\rho + \frac{\mathcal{C}'}{\mathcal{D}'} + K - \frac{1}{\rho}}{\ln(\rho) + \ln\left(\frac{\beta\sigma^2 S_{\mathrm{x}}}{\eta\mathcal{D}'}\rho + \frac{\mathcal{C}'}{\mathcal{D}'} + K - \frac{1}{\rho}\right) - 1} - \frac{1}{\rho} \tag{4.26}$$

for moderately large values of ρ (a condition is given in the proof). When ρ grows large, then

$$M^* \approx \frac{\beta\sigma^2 S_{\mathrm{x}}}{2\eta\mathcal{D}'} \frac{\rho}{\ln(\rho)} \tag{4.27}$$

which is an almost linear scaling law.

Corollary 6: A larger number of antennas are needed as the size of the coverage area increases.

The above corollary follows from the observation that M^* increases almost linearly with S_{x}, which is a parameter that increases with the cell radius $d_{\max}^{K}$ expressed as Equation (3.1).

4.4.3 Optimal Transmit Power for Energy Efficiency Maximisation

Recollecting that ρ is proportional to the SINR, which is directly proportional to the PA/transmit power under ZF processing. Finding the EE-optimal total PA power amounts to looking for the value of ρ in (3.19) that maximizes (4.14). The solution is given by the following theorem.

Theorem 3: For given values of M and K, the EE-optimal $\rho \geq 0$ can be computed as

$$\rho^* \approx \frac{e^{W\left(\frac{\eta}{\beta\sigma^2 S_{\mathrm{x}}} \frac{(M-K)(\mathcal{C}' + M\mathcal{D}')}{e} - \frac{1}{e}\right) + 1}}{M-K} - 1 \tag{4.28}$$

with $\mathcal{C}' > 0$ and $\mathcal{D}' > 0$ given by (4.25).

Using Lemma 4, it turns out that the optimal ρ^* increases with $\mathcal{C}'$ and $\mathcal{D}'$, which were defined in (4.25), and thus with the coefficients in the circuit power model. Since the maximizing total PA power with ZF processing is $P_{\mathrm{TX}}^{(\mathrm{ZF})} = \frac{\beta\sigma^2 S_{\mathrm{X}}}{\eta} K\rho^*$, the following result is found.

Corollary 7: The optimal transmit power does not depend on the rate-dependent power $\{P_{\mathrm{COD}}, P_{\mathrm{DEC}}, P_{\mathrm{BT}}\}$ whereas it increases with fixed power and the power per UE and BS antenna $\{P_{\mathrm{BS}}, P_{\mathrm{FIX}}, P_{\mathrm{SYN}}, P_{\mathrm{UE}}\}$.

The fact that the optimal PA/transmit power *increases* with $\{P_{\mathrm{BS}}, P_{\mathrm{FIX}}, P_{\mathrm{SYN}}, P_{\mathrm{UE}}\}$ might seem a bit counter intuitive at first, but it makes much sense and can be explained as follows.

If the fixed circuit powers are large, then higher PA power $P_{\mathrm{TX}}^{(\mathrm{ZF})}$(and thus higher average rates) can be afforded in the system since $P_{\mathrm{TX}}^{(\mathrm{ZF})}$ has a small impact on the total power consumption.

It has recently been shown in [29], [17], and [18] that TDD systems permit a power reduction proportional to $1/M$ (or $1/\sqrt{M}$ with imperfect CSI) while maintaining non-zero rates as $M \to \infty$. Despite being a remarkable result and a key motivation for massive MIMO systems, Theorem 3 proves that this is *not* the most energy-efficient strategy. In fact, the EE metric is maximized by the opposite strategy of increasing the power with M.

Corollary 8: the optimal ρ^* is lower bounded as

$$\rho^* \geq \frac{\frac{\eta(\mathcal{C}'+M\mathcal{D}')}{\beta\sigma^2 S_{\mathrm{X}}} - \frac{\ln\left(\frac{\eta(M-K)(\mathcal{C}'+M\mathcal{D}')}{\beta\sigma^2 S_{\mathrm{X}}} - 1\right)}{M-K}}{\ln\left(\frac{\eta(M-K)(\mathcal{C}'+M\mathcal{D}')}{\beta\sigma^2 S_{\mathrm{X}}} - 1\right) - 1} \tag{4.29}$$

for moderate and large values of M (a condition is given in the proof) whereas

$$\rho^* \approx \frac{\eta \mathcal{D}'}{2\beta\sigma^2 S_{\mathrm{X}}} \frac{M}{\ln M} \tag{4.30}$$

when M grows large.

The above corollary states that the total PA power $P_{\mathrm{TX}}^{(\mathrm{ZF})}$ required maximizing the EE metric increases approximately as $M/\ln(M)$, which is an almost linear scaling. The explanation is the same as for Corollary 7; the circuit power consumption grows with M, thus using more transmit power to improve the rates is practical before it becomes the limiting factor for the EE. Although the total transmit power increases with M, the average transmit power emitted per BS antenna (and per UE if K is let scale linearly with M) decays as$1/\ln(M)$. Hence, the RF amplifiers can be gradually simplified with M. The EE-maximizing per-antenna transmit power reduction is, nevertheless, much slower than the linear to quadratic scaling laws observed in [17], [18] for the unrealistic case of no circuit power consumption.

4.4.4 Alternating optimisation

Theorem 1-3 provide simple closed-form expressions that enable EE-maximization by optimising K, M, or ρ separately when the other two parameters are fixed. However, the goal for a system designer is to find the joint global optimum. Since K and M are integers, the global optimum can be obtained by an exhaustive search over all reasonable combinations of the pair (K, M) and computing the optimal power allocation for each pair using Theorem 3. Since Theorem 1 shows that EE metric is quasi-concave when K and M are increased jointly which is a fixed ratio, K and M can be increased step-by-step and can be stopped when the EE starts to decrease. Hence, there is no need to consider all integers.

Although feasible and utilised for simulations in Chapter 5, the brute-force joint optimisation is of practical interest only for off-line cell planning, while in low-complexity approach is required to take into account changes in the system settings eventually (e.g., the user distribution or the path-loss model as specified by S_{x}). A practical solution in this direction is to optimize the system parameters sequentially per a standard alternating optimization:

1) Assume that an initial set (K, M, ρ) is given;
2) Update the number of UEs K (and implicitly M and ρ) per Theorem 1;
3) Replace M with the optimal value from Theorem 2;
4) Optimise the PA power through ρ by using Theorem 3;
5) Repeat 2) – 5) until convergence is achieved.

Observe that the EE metric has a finite upper bound (for $\mathcal{C}' > 0$ and $\mathcal{D}' > 0$). Therefore, the alternating algorithm illustrated above monotonically converges to a local optimum for any initial set (K, M, ρ) because the alternating updates of K, M, and ρ may either increase or maintain (but not decrease) the objective function. Convergence is declared when the integers M and K are left unchanged in the iteration.

4.5 Imperfect CSI and Multi-Cell Deployment

The EE-optimal parameter values were derived in the previous section for a single-cell scenario with perfect CSI. In this section, to what extent the analysis can be extended to single-cell scenarios with imperfect CSI investigated. A newly achievable rate for symmetric multi-cell scenarios with ZF forcing processing is derived. The analysis is protracted to single-cell scenarios with imperfect CSI. A new achievable rate is derived for symmetric multi-cell scenarios with ZF forcing processing.

The following lemma gives achievable user rates in single-cell scenarios with imperfect CSI.

Lemma 5: approximately if ZF detection/precoding is applied under imperfect CSI, the average gross rate

$$\bar{\mathcal{R}} = B \log 1 + \frac{\rho(M-K)}{1+\frac{1}{\tau^{(\mathrm{ul})}}+\frac{1}{\rho K \tau^{(\mathrm{ul})}}} \tag{4.31}$$

is achievable using the same average PA power $\frac{\beta\sigma^2 S_{\mathrm{X}}}{\eta} K$ as in (3.19), where $\rho \geq 0$ is a parameter.

The rate expression in (4.31) is different from (3.11) due to the imperfect CSI which causes unavoidable interference between the UEs. The design parameters K and ρ appear in both the numerator and denominator of the SINRs, while in both the numerator and denominator of the SINRs, while these only appeared in the numerator. Consequently, the EE-optimal K and ρ in closed form under imperfect CSI not found. This optimal number of BS antennas can, however, be derived similarly to Theorem 2, (4.32). Despite the analytic difficulties, Chapter 5 shows numerically that the single-cell behaviours that were proved in Section 4.2 are applicable also under imperfect CSI.

$$M^* = \left\lceil \left(1 + \frac{1}{\tau^{(\mathrm{ul})}} + \frac{1}{\rho K \tau^{(\mathrm{ul})}}\right) \frac{e^{w\left(\frac{\rho\left(\frac{\beta\sigma^2 S_{\mathrm{X}}}{\eta}\rho + \mathcal{C}'\right)}{e\left(1+\frac{1}{\tau^{(\mathrm{ul})}}+\frac{1}{\rho K \tau^{(\mathrm{ul})}}\right)} + \frac{\rho K - 1}{e\left(1+\frac{1}{\tau^{(\mathrm{ul})}}+\frac{1}{\rho K \tau^{(\mathrm{ul})}}\right)}\right)+1}}{\rho} + \rho K - 1 \right\rceil \tag{4.32}$$

The analytic framework and observations of this thesis can also be applied in multi-cell scenarios. To illustrate this, a complete symmetric scenario is considered where the system parameters M, K, and $\bar{\mathcal{R}}$ are the same in all cells and optimized jointly. The symmetry implies that the cell shapes, user distributions, and propagation conditions are the same in all cells. There are $\mathcal{J}$ cells in the system assumed. Let x_{jk} denote the position of the kth UE in cell j and call $l_j(\mathrm{x})$ the average channel attenuation between a certain position $\mathrm{x} \in \mathbb{R}^2$ and the jth BS. The symmetry implies that the average inverse attenuation to the serving BS, $S_{\mathrm{x}} = \mathbb{E}\left\{\left(l_j\left(\mathrm{x}_{jk}\right)\right)^{-1}\right\}$, is independent of the cell index j. Moreover, defined as

$$I_{j\ell} = \mathbb{E}_{x_{\ell k}}\left\{\frac{l_j(x_{\ell k})}{l_\ell(x_{\ell k})}\right\} \tag{4.33}$$

as the average ratio between the channel attenuation to another BS and the serving BS. This parameter describes the average interference that leaks from a UE in cell ℓ to the BS in cell k in the uplink, and in the inverse direction in the downlink. The symmetry implies $I_{j\ell} = I_{\ell j}$.

The necessity of reusing pilot resources across cells causes pilot contamination (PC) [11]. To investigate its impact on the EE, different pilot reuse patterns by defining $\mathcal{Q}_j \subset\{1, 2, ..., J\}$ as the set of cells (including cell j) that use the same pilot sequences as cell j are considered. For symmetry reasons, the cardinality $\left|\mathcal{Q}_j\right|$ allowed to be the same for all j. The uplink pilot sequence length is $K_\tau^{(\mathrm{ul})}$ where $\tau^{(\mathrm{ul})} \geq J \,/\, \left|\mathcal{Q}_j\right|$ to account for the pilot reuse factor is recorded. The average relative power from PC is $I_{\mathrm{PC}} = \sum_{\ell \in \mathcal{Q}_j \setminus \{j\}} I_{j\ell}$, while $I = \sum_{\ell=1}^{J} I_{jl}$ is the relative interference from all cells and $I_{\mathrm{PC}^2} = \sum_{\ell \in \mathcal{Q}_j \setminus \{j\}} I_{j\ell}^2$ is defined for later use defined for later use. Note that these parameters are also independent of j for symmetry reasons.

Lemma 6: If ZF detection/precoding are applied by treating channel uncertainty as

noise, the average total PA power $\frac{\beta\sigma^2 S_{\mathrm{x}}}{\eta} K$ as in (19) achieves the average gross rate

$$\bar{\mathcal{R}} = B \times \log\left(1 + \frac{1}{I_{\mathrm{PC}} + \left(1 + I_{\mathrm{PC}} + \frac{1}{\rho K \tau(\mathrm{ul})}\right)\frac{(1+K\rho I)}{\rho(M-K)} - \frac{K\left(I_{\mathrm{PC}}{}^2\right)}{M-K}}\right) \quad (4.34)$$

in each cell, where $\rho \geq 0$ is a design parameter.

The rate expression is (4.34) for symmetric multi-cell scenarios (with imperfect CSI) are even more complicated than single-cell imperfect CSI case considered in Lemma 5. All the design parameters M, K, and ρ appear in both the numerator and denominator of the SINRs, which generally makes it inflexibly to find a closed-form expression for the EE-optimal parameter values. Indeed, this is the reason Section 4.2 given for an analytically practicable in the single-cell scenario. However, in the Chapter 5 that symmetric multi-cell scenarios perform similarly to the ingle-cell scenario, by utilizing the rate expression in Equation (4.34) for simulations.

4.6 Total Power Requirement in Single-cell and Multi-Cell scenario with Perfect CSI and Imperfect CSI

For perfect CSI scenario in single-cell deployment, CSI is assumed to be perfectly known to both the BS and UEs for analytic tractability. In practice, however, CSI is not perfect. For imperfect CSI scenario in single-cell and multi-cell deployment, for the BS to acquire the CSI, a simple scheme employed where UEs send pilots signals to the BS.

Then the BS can estimate the channel by analysing the received pilot signals in an uplink training phase. This is acquired from pilot signalling and MMSE channel estimation method, where it results in more accurate channel estimation [32].

The average sum rate in Equation (4.31) for imperfect CSI in single-cell deployment and in Equation (4.44) for imperfect CSI in Multi-cell deployment are obtained using the same average PA power from Equation (3.19). However, the average sum rates are different from perfect CSI average sum rate in Equation (3.11). This is due to the imperfect CSI which causes unavoidable interference between in the UEs in single-cell deployment. As per the multi-cell deployment, the necessity of reusing pilot resources across cells causes pilot contamination [11] among the cells.

As for the total power consumed to achieve the EE, these analytical expressions are found to be in an agreement with numerical results provided in Chapter 5 in Figure 5.5. In single-cell deployment, increasing the number of BS antennas increases the total power consumption, where it also increases the hardware-consumed power (different processing schemes are consuming a different amount of power in the digital baseband processing.). Likewise, in multi-cell deployment, however, the numbers are smaller due to inter-cell interference. These analyses are confirmed with numerical results over simulation in Chapter 5 in Figure 5.6. This is in line with Corollary 8 but stands in contrast to the results in [17] and 18], which indicated that the total power consumption should be decreased with a number of BS antennas.

Corollary 8 states that the circuit power consumption grows with M, thus using more total power to improve the rates is practical before it becomes the limiting factor for the EE. Although the total power increases with M, the average transmit power emitted per BS antenna (and per UE if K is let scale linearly with M) decays as $1/\ln(M)$.

Hence, the RF amplifiers can be gradually simplified with M. The EE-maximizing per-antenna transmit power reduction is, nevertheless, much slower than the linear to quadratic scaling laws observed in [17] and [18], for the unrealistic case of no circuit power consumption.

From [17] and [18], the energy efficiency in LS MIMO can be increased by decreasing the total radiated power by increasing the number of the transmit antennas per user. This is a straightforward consequence of beamforming and the concentration of the transmitted power in a much smaller radiation angle targeting a specific user. Since the number of transmit antennas increase per user, the number of the processing blocks increases, which consumes additional energy which is called the processing energy for precoding. If the precoding is accomplished in digital processors, it will consume appreciable additional energy since it increases as the number of antennas increases.

To reduce such precoding energy, the precoding to be divided into the analogue functions at high frequency and the digital functions at baseband frequencies. It is found that in such hybrid precoding the processing energy can be fundamentally reduced. The analogue precoding is dedicated to the so-called beam forming steering the radiation to specific users. Hence, finding the right balance between these is important. Nevertheless, LS MIMO can be energy efficient, despite the additional hardware consumed power.

4.7 Summary

In this chapter, the realistic power consumption model is explained and derived as the first contribution to Energy Efficiency maximisation in LS MIMO systems. Following the first contribution, the second contribution is computing the closed-form analytical expressions using ZF for the optimal number of UEs, the number of BS antennas, and transmit power under the assumption of ZF processing. This analysis is extended to imperfect CSI case and symmetric multi-cell scenarios as the third contribution in Energy Maximisation in Large-Scale MIMO systems. The expressions derived here then confirmed with numerical results in Chapter 5 through simulation along MRT/MRC and MMSE processing schemes.

Chapter 5

Simulation and Numerical Results

5.1 Introduction

MATLAB based simulations executed in this chapter to validate the system design guidelines under analytical ZF processing scheme and to make a comparison with other processing schemes such as MRT and MMSE. Numerical results are provided under both perfect and imperfect CSI, in the single cell and multi-cell deployment for analytical ZF processing schemes. Analytical closed-form equations for the EE-maximising parameters from Chapter 4 are computed to simulate ZF processing scheme. Furthermore, the optimal EE for ZF processing with Monte Carlo simulation is numerically compared with the optimal EE obtained under ZF analytical closed-form equations. Meanwhile, numerical results are provided for single-cell deployment with perfect CSI for both MRT and MMSE processing scheme. Whilst for MRT and MMSE processing schemes, Monte Carlo simulations are executed; both under random user locations and small-scale fading to maximise EE.

5.2 Simulation Setting

Simulations are performed using two key system designs from Chapter 4. The first key design is; the scalable realistic power consumption model which scales non-linearly with design parameters; the number of BS antennas M ranges from 1 to 220 , and number of users K ranges from 1 to 150 and gross rate $\bar{\mathcal{R}}$.

The second key design is; the closed-form analytical EE-maximising parameters; the number of BS antennas M, number of active UEs K, and transmit power ρ (per UE) which were under derived under ZF processing with perfect CSI and imperfect CSI , for both single-cell and multi-cell scenario to maximise the EE in Chapter 4. Moreover, as explained in Lemma 1 ZF processing operates only when $M > K + 1$. Otherwise it i,s not possible to operate ZF and EE is unobtainable in both single-cell and multi-cell scenarios. Meanwhile, due to analytical complexity closed-form EE -maximising parameters were not derived under MMSE and MRT/MRC processing scheme in Chapter 4. Thus, Monte Carlo simulation with random user locations and small-scale were performed to optimise EE with MMSE and MRT/MRC processing schemes for single-cell scenario with perfect CSI.

Moreover, for single -cell scenario, a symmetric circular cell considered with radius 250 m, as shown in Figure 3.2. For the symmetric multi-cell scenario, 24 identical clustered cell is considered, as shown in Figure 5.8. Each cell is a 500×500 meters square with uniformly distributed UEs, with the same minimum distance as in the single-cell scenario. The cell *under study* is in middle and respective for another cell in the system. The interference that arrives from the two closest cells in each direction only considered. Thus the cell under study is the representative for any cell in the system. Motivated by the single-cell deployment from Chapter 4, only ZF processing is considered and focused to compare different pilot reuse patterns. As depicted in Figure 5.8, the cells are divided into four clusters. Three different pilot reuse patterns are considered, where the same pilots in all cells $\left(\tau^{(\mathrm{ul})} = 1\right)$, two orthogonal sets of pilots of $\left(\tau^{(\mathrm{ul})} = 2\right)$ in Cluster 1 and Cluster 4 and finally all clusters have different orthogonal pilots $\left(\tau^{(\mathrm{ul})} = 4\right)$.

The corresponding simulation parameters are given in Table 2 and are inspired by a variety of prior works: the 3GPP propagation environment defined in [96], RF and baseband power modeling from [28], [104], [93], [107], backhaul power according to [108], and the computational efficieny are from [34], [109] and power amplifier efficiency are from [34], ,[93], [107], [103],[104].

TABLE 2
Simulation Parameters

Parameter	Value
Carrier frequency: f_{c}	2 GHz
Cell radius (single-cell): d_{max}	250 m
Channel coherence bandwidth: B_{C}	180 kHz
Channel coherence time: T_{C}	10ms
Coherence block (symbols): U	1800
Computational efficiency at BSs: L_{BS}	12.8 Gflops/W
Computational efficiency at UEs: L_{UE}	5 Gflops/W
Fixed power consumption (control signals, backhaul): P_{FIX}	18 W
Fraction of downlink transmission: $\zeta^{(\mathrm{dl})}$	0.6
Fraction of uplink transmission: $\zeta^{(\mathrm{dl})}$	0.4
Inter-site distance for multi-cell	500 m
Large-scale fading model: $l(x)$	$10^{-3.53}$ /‖ x ‖$^{3.76}$
Minimum distance: d_{min}	35 m
Network Deployment for multi-cell	25-cell clustered grid
Network Deployment for single-cell	circular
Power Amplifier efficiency at the UEs: $\eta^{(\mathrm{ul})}$	0.3
Power Amplifier efficiency at the BSs: $\eta^{(\mathrm{dl})}$	0.39
Power consumed by local oscillator at BSs: P_{SYN}	2 W
Power required for backhaul traffic: P_{BT}	0.25 W/(Gbit/s)
Power required for coding of data signals: P_{COD}	0.1 W/(Gbit/s)
Power required for decoding of data signals: P_{DEC}	0.8 W/(Gbit/s)
Power required to run the circuit components at a BS: P_{BS}	1 W
Power required to run the circuit components at a UE: P_{UE}	0.1 W
Propagation environment	3GPP [48]
Relative pilot lengths: $\tau^{(\mathrm{ul})}$, $\tau^{(\mathrm{dl})}$	1
Total noise power: $B\sigma^2$	96 dBm
Transmission bandwidth: B	20 MHz

5.3 Simulation Method

There are two methods primarily carried out to achieve objectives of this thesis; first is obtaining the EE maximising parameters under analytical ZF Processing Scheme and second is obtaining the EE maximising parameters under Monte Carlo Simulation for MMSE and MRT/MRC Scheme. The EE maximising parameters such as; the number of BS antennas M, number of active UEs K, and transmit power ρ (per UE) were derived under closed-form analytical ZF processing scheme and new refined total power consumption model P_{T} from Chapter 4, for both single-cell and multi-cell with perfect CSI and imperfect CSI.

However, due to analytic complexity,the EE maximising parameters above were obtained under Monte Carlo simulation based on power allocation from Equation (3.8), Equation (3.9) and Equation (3.16) in Chapter 3 and the new circuit power consumption model P_{CP} from Equation (4.1) in Chapter 4 for; MMSE and MRT/MRC processing for single-cell scenario with perfect CSI .

The optimal number of (BS) antennas M, the optimal number of active (UEs) K, and the optimal transmit power ρ were obtained by implementing the standard alternating optimisation algorithm from Chapter 4 for all the processing schemes. The standard alternating optimising algorithm enable EE maximisation by optimising the number of (BS) antennas M, numba er of active (UEs) K, and the transmit power ρ separately when the other two are fixed.

Since the goal of the system design is to find the joint global optimum, thus the global optimum can be obtained by an exhaustive search over all reasonable combinations of the pair (K, M) and computing the optimal power allocation ρ for each pair using Theorem 3 in Chapter 4. Since Theorem 1 shows that EE metric is quasi-concave when K and M are increased jointly which is a fixed ratio, K and M can be increased step-by-step and can be stopped when the EE starts to decrease. Hence, there is no need to consider all integers.

Achievable global optimum Energy Efficiency values for all the processing schemes are computed for different values of M and K where a number of BS antennas ranges from 1 to 220 and number of users ranges from 1 to 150 are considered based on EE maximising parameters. The EE maximising parameters are likewise utilised to compute other system parameters such as; Energy Efficiency, Area throughput, Total Transmit Power and Radiated Power per BS antenna where a number of BS antennas M ranges between 1 to 220 and the optimal number of users K is fixed.

5.4 Optimal Energy Efficiency in Single Cell with Existing Power Consumption Model with Analytical ZF processing

In the following plot, an analytical expression derived for EE optimal with ZF processing scheme from Equation (3.20) used to compute existing circuit power consumption, P_{CP} where P_{CP} is a constant quantity accounting for fixed power consumption. For this purpose, the EE-optimal transmit power, the EE-optimal number of BS antennas (*M*) and the EE-optimal number of users (*K*) derived from Equation (4.28), Equation (4.26) and Equation (4.22), respectively are utilised. In the Figure 5.1, the maximum EE is plotted against nua mber of BS antennas ranges from 1 to 220 and number of users ranges from 1 to 150. The plot confirms the simplified model $P_{\mathrm{CP}} = P_{FIX}$ gives the impression that achieved an unbounded EE by adding more and more antennas, where maximum BS antennas which is 220 accounts for optimal EE. Thus, this is not an accurate model to design a good system by optimizing number a of antennas (*M*) and number of UEs (*K*).

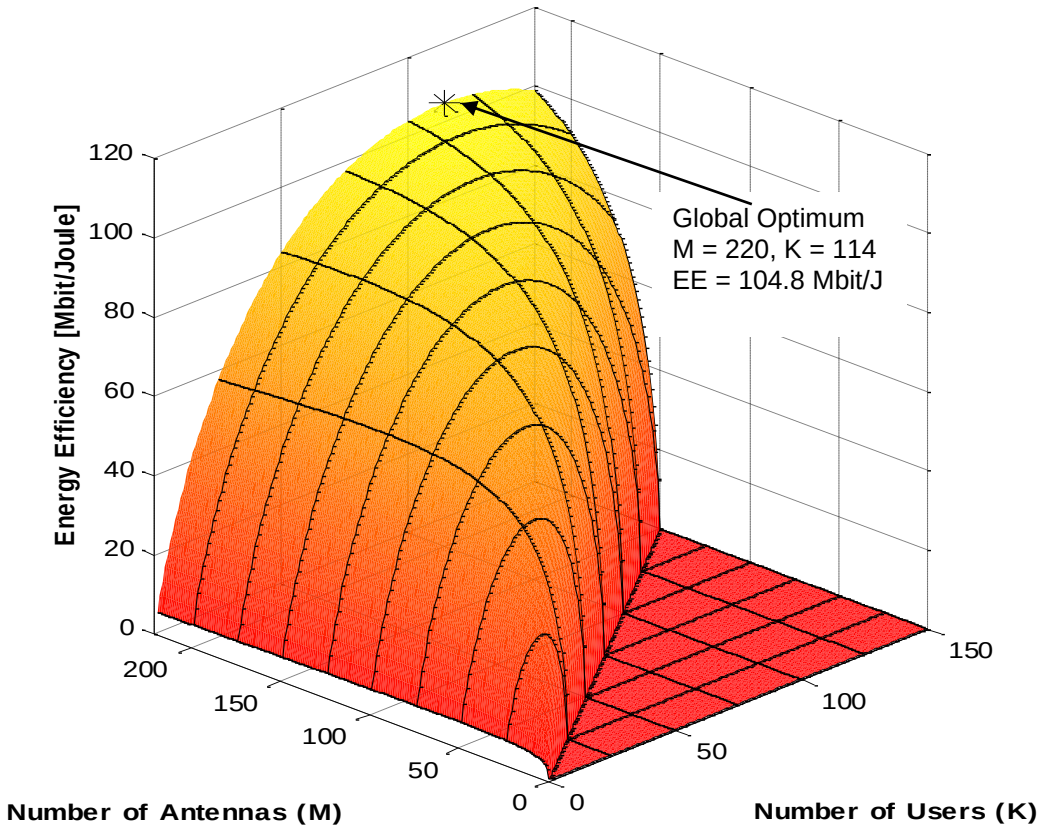

Figure 5.1: Energy Efficiency in the single-cell scenario for ZF processing with Existing Power Consumption Model.

5.4.1 Comparison of EE Optimal for Existing Energy Model and Realistic Power Model with Analytical ZF Processing

Figure 5.2 shows the comparison of EE optimal for existing energy model and realistic energy model. The results are compared for a fixed 100 number of users when the number of BS antennas ranges from 1 to 220. The plot in Figure 5.2 shows that the existing energy model gives unbounded EE as the number of BS antennas. The EE is optimal when the BS antennas are maximum, which is 220.

However, for realistic energy model, the EE optimal is obtained when the BS antennas are 160. The numerical result for existing energy model is obtained from analytical expression derived in Equation (3.20).

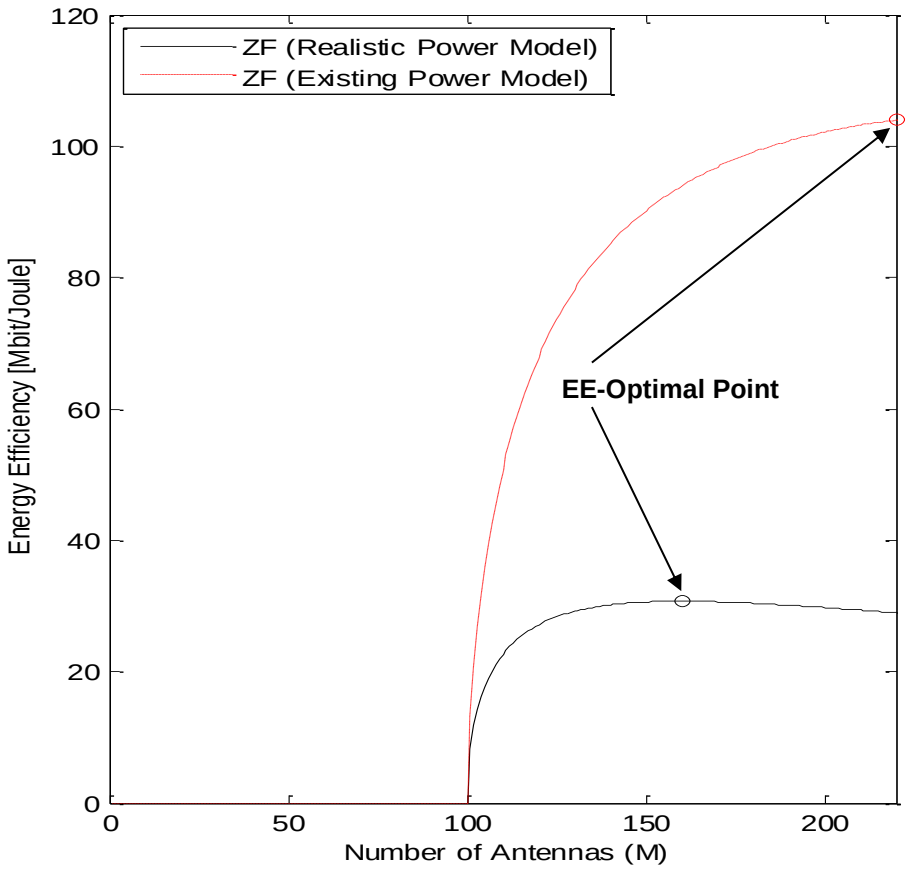

Figure 5.2: Comparison of Energy Efficiency in the single-cell scenario with perfect CSI for ZF processing with Existing Power Consumption Model and Realistic Power Consumption Model.

5.5 Optimal Energy Efficiency in Single Cell Deployment for ZF Processing scheme with Monte Carlo Simulation

In Figure 5.3, the EE is plotted against a number of BS antennas and number of users for Single-cell deployment with perfect CSI. In the plot, Monte Carlo simulation is utilised to compute EE optimal with ZF processing where a number of BS antennas ranges from 1 to 220 and number of users ranges from 1 to 150 are considered.

For this purpose, the power allocation is computed from Equation (3.8) and Equation (3.16) for ZF processing scheme. The EE optimal is obtained by optimising the power allocation to each UE for a given processing scheme and system dimension. The optimal EE = 30.8 Mbit/Joule is obtained when a number of BS antennas, *M* = 162 and numbers of users, K = 133. The plot confirms the Monte Carlo simulation results in Figure 5.2 and the analytical result from Equation (4.14) in Figure 5.5 are found to be in an agreement.

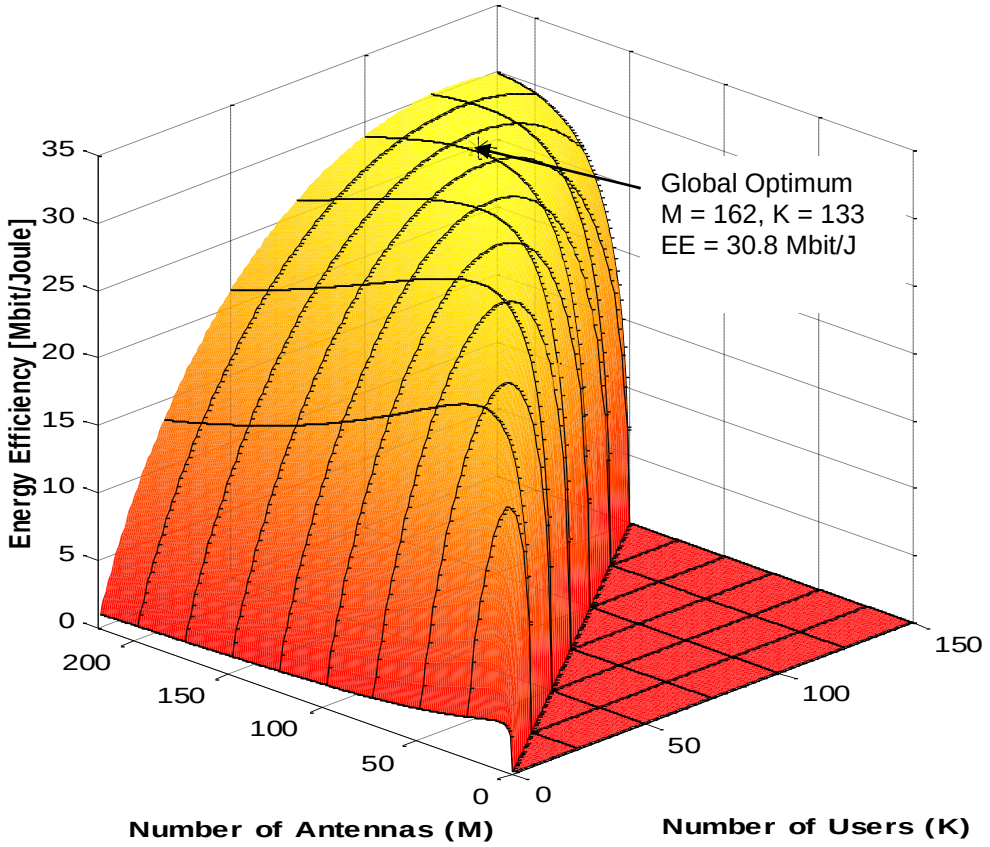

Figure 5.3: Energy Efficiency with Monte Carlo ZF simulation in the single-cell scenario with perfect CSI.

5.5.1 Comparison of EE Optimal obtained under Analytical ZF processing and ZF Processing under Monte Carlo simulation

Figure 5.4 shows the comparison of EE optimal obtained under Analytical ZF processing and ZF processing under Monte Carlo Simulation. The results are compared for a fixed 100 number of users when the number of BS antennas ranges from 1 to 220. The plot shows that EE optimal obtained under analytical ZF processing from Equation (3.21) is in an agreement with the EE optimal obtained under Monte Carlo ZF processing simulation. For example, in the Single-cell scenario with perfect CSI, the EE is optimal when BS antennas are 160 in both analytical ZF processing and Monte Carlo ZF processing simulation.

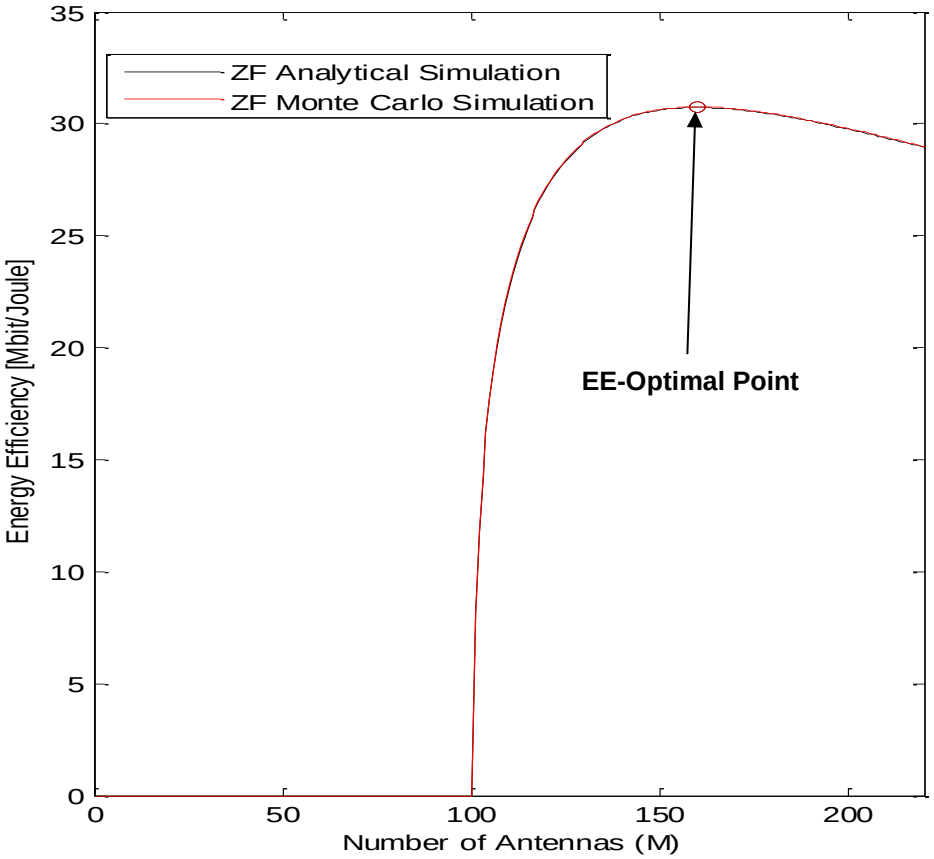

Figure 5.4: Comparison of Energy Efficiency in the single-cell scenario with perfect CSI for ZF processing with Analytical Simulation and Monte Carlo Simulation.

5.6 Total Power Consumption in Single-cell and Multi-cell with perfect and Imperfect CSI with Analytical ZF processing

In Figure 5.5, the total power consumption is plotted against a number of Base Station antennas, *M* utilising an EE-optimal number of users, *K* = 133 with perfect CSI and *K* = 127 with imperfect CSI in single-cell deployment, where BS antennas from 1 to 220 are considered in the simulation. The EE-optimal total power consumption is 342 Watt. As the number of BS antennas increases, the transmit power increases, where it also increases the total power consumption and the hardware-consumed power. The total power consumption with imperfect CSI is smaller due to unavoidable interference between in the UEs in single-cell deployment, where the EE-optimal total power consumption is 38.62 Watt.

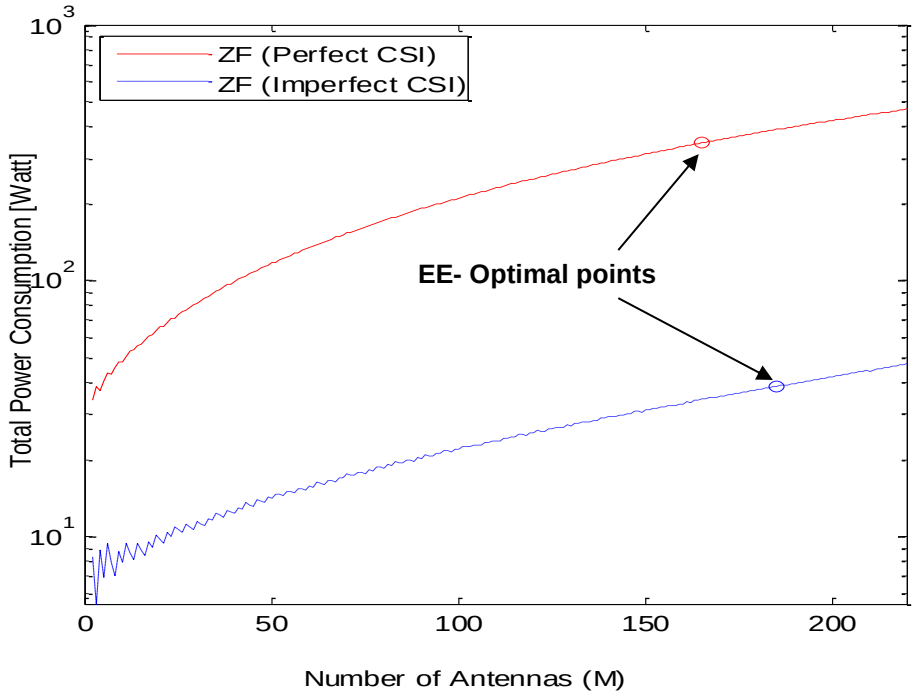

Figure 5.5: Total power consumption in the single-cell scenario under analytical ZF simulation with an EE-optimal number of users, *K* = 133 with perfect CSI and *K* = 127 with imperfect CSI.

In multi-cell deployment shown in Figure 5.6, however, the total power consumption is smaller compared to single-cell, due inter-cell interference. The EE-optimal number of users, K = 77, 70, and 60 for pilot reuse, $\tau^{(\mathrm{ul})} = 1,\ 2, \mathrm{and}\ 4$, respectively, and BS antennas from 1 to 220 are considered in the simulation. The optimal total power consumption are 2.82 watt, 1.71 watt and 0.6857 respectively.

These plots confirmed the numerical results through simulation to agree with analytical results in Chapter 4. This result is in line with Corollary 8 but stands in contrast to the results in [31] and [33], which indicated that the transmit power should be decreased with a number of BS antennas.

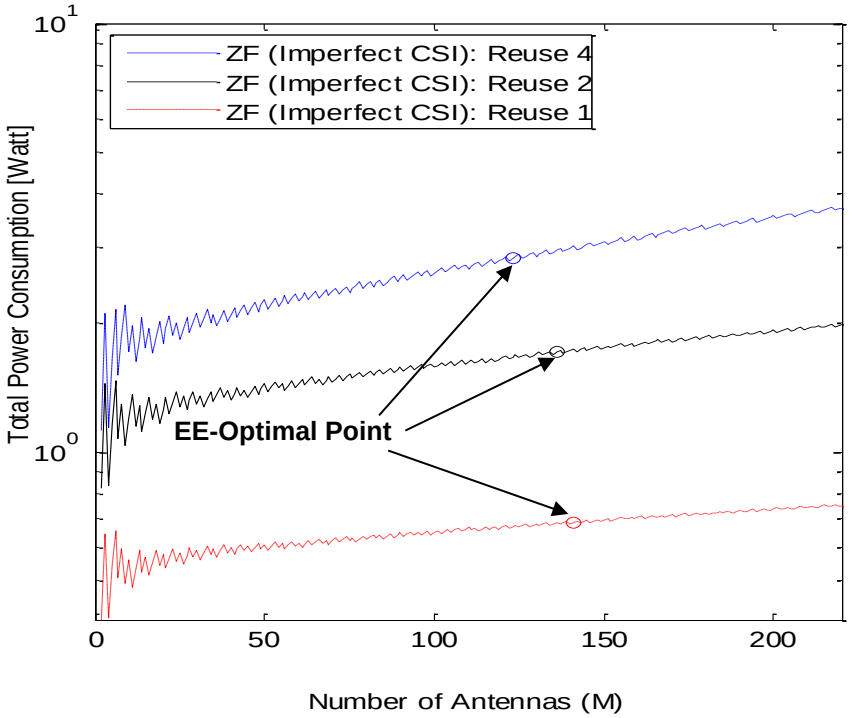

Figure 5.6: Total power consumption in the multi-cell scenario under analytical ZF processing with an EE-optimal number of user K = 77, 70, and 60 with pilot reuse 1, 2, and 4 for imperfect CSI.

5.7 Single-Cell Deployment

The single-cell deployment model validated in Figure 5.7 shows the set of achievable EE values with perfect CSI, under analytical ZF processing from Equation (3.21), and for different values of M and K where a number of BS antennas ranges from 1 to 220 and number of users ranges from 1 to 150 are considered. ZF processing operates when $M > K + 1$, otherwise it is not possible to operate ZF. Each point uses the EE-maximizing value of transmit power ρ from Theorem 3. The plot shows that there is a global EE-optimum at $M = 165$ and $K = 104$, which is achieved by $\rho = 0.8747$ and the practically reasonable spectral efficiency 5.7644 bit/symbol (per UE). The optimum is clearly a massive MIMO setup, which is notable since it is the output of an optimization problem where the system dimension is not restricted. The surface in Figure 5.7 is concave and quite smooth. Thus, there is a variety of system parameters that provides close-to-optimal EE and the results appear to be robust to small changes in the circuit coefficients. The alternating optimization algorithm from Chapter 4 is applied with a starting point of (K,M,ρ)=(3,1,1). The iterative progression is shown in Figure 5.7 and the algorithm converged after 7 iterations to the global optimum.

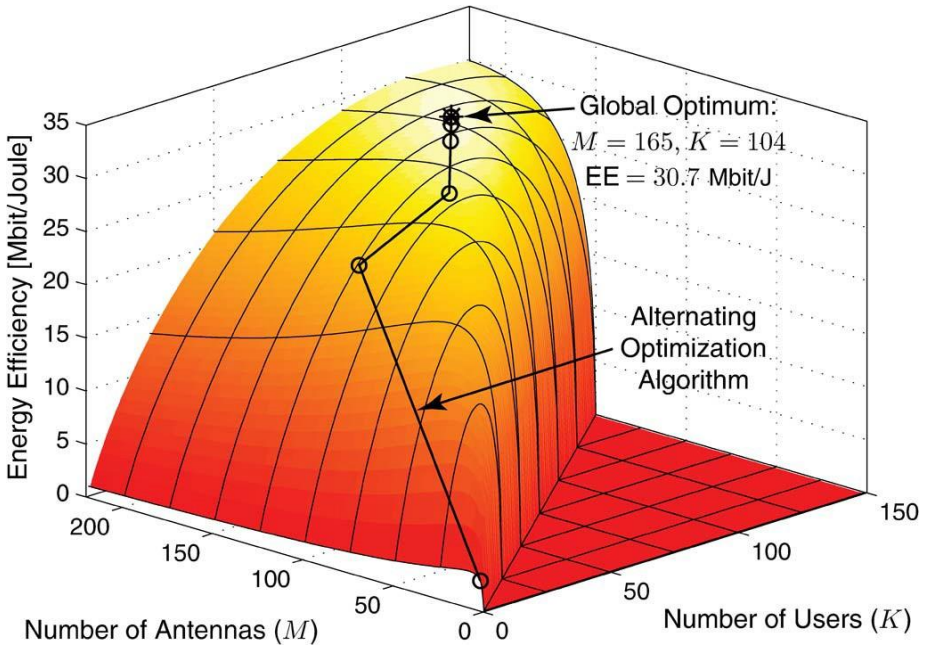

Figure 5.7: Energy Efficiency with analytical ZF simulation in the single-cell scenario with perfect CSI.

For comparisons, Figure 5.8 shows the corresponding set of achievable EE values under MMSE processing ($Q = 3$) Figure 5.9 illustrates the results for MRT/MRC processing with, and Figure 5.10 considers analytical ZF processing under imperfect CSI where number of BS antennas from 1 to 220 and number of users and from 1 to 150 are considered. The MMSE and MRT/MRC results were generated by Monte Carlo simulations, while the ZF results were computed using the expression in Lemma 5. Although MMSE processing is optimal from a throughput perspective, however ,ZF processing yielded higher EE. This is due to the higher computational complexity of MMSE otherwise, the difference in throughput is quite small.

MMSE also has the unnecessary benefit of handling $M < K$ in LS MIMO setting. ZF processing with imperfect CSI has the similar behaviour as ZF processing and MMSE processing with perfect CSI. Therefore, this analysis has bearing on realistic single-cell systems.

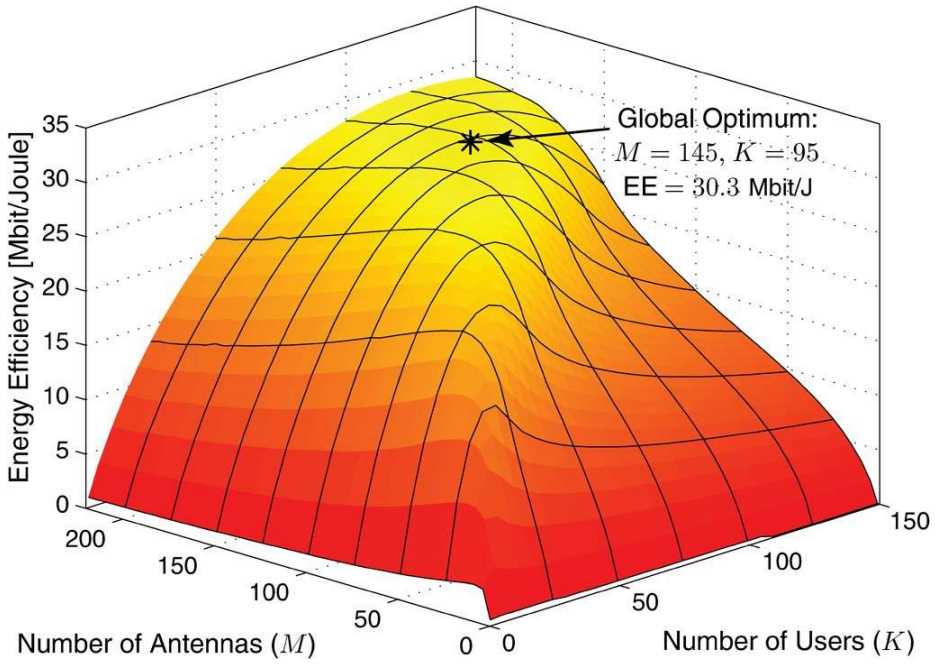

Figure 5.8: Energy Efficiency with MMSE processing in the single-cell scenario with Monte Carlo simulation.

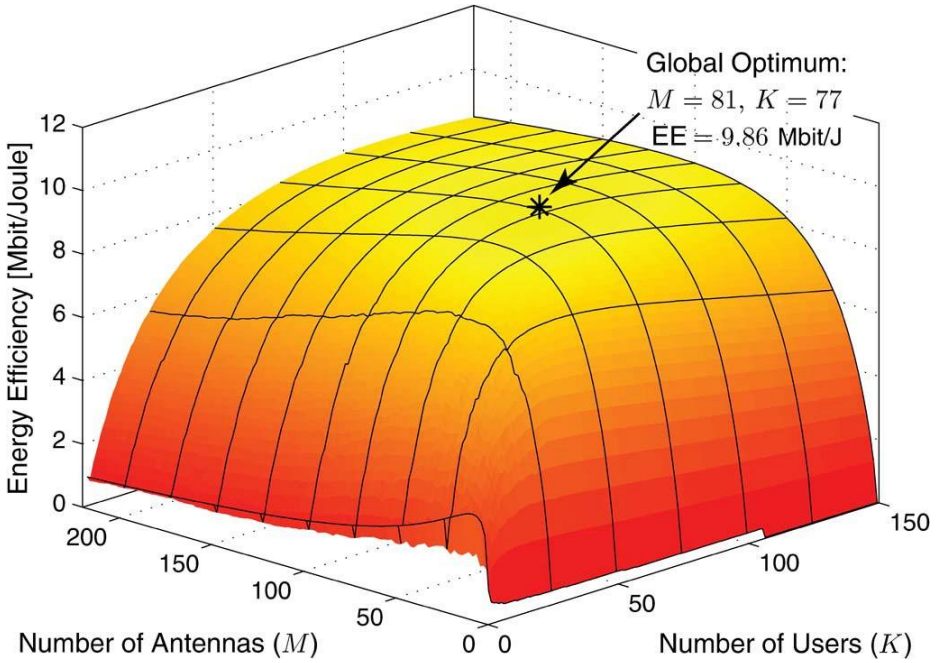

Figure 5.9: Energy Efficiency with MRT/MRC processing in the single-cell scenario with Monte Carlo simulation.

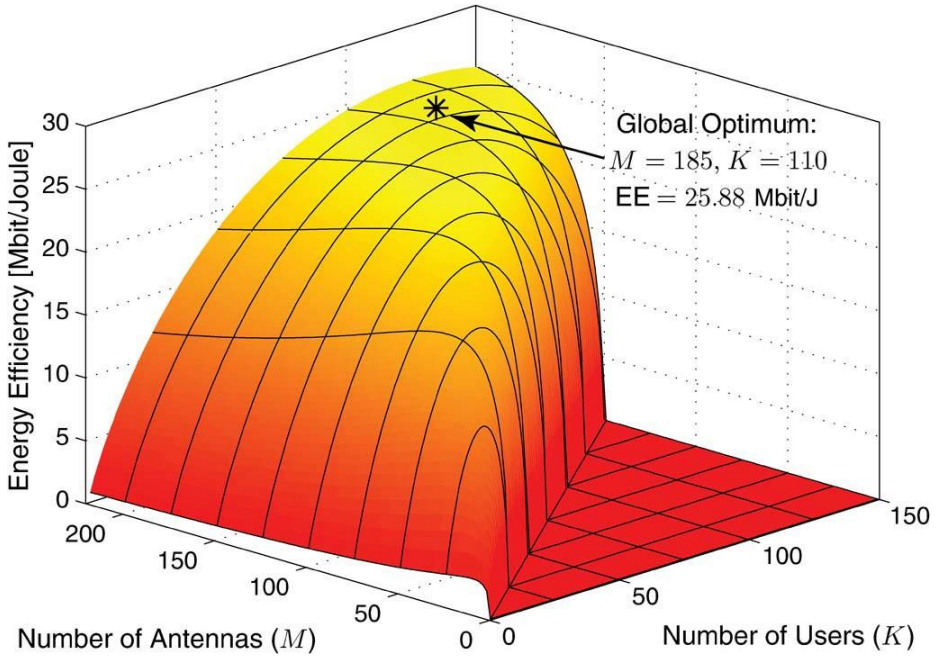

Figure 5.10: Energy Efficiency in the single-cell scenario with imperfect CSI with analytical ZF simulation.

Remarkably, MRT/MRC processing gives a very different behaviour. The EE optimum is much smaller than with ZF and MMSE and achieved when $M = 81$ and $K = 77$. This can still be called a Large-Scale MIMO setting since there are a large number of BS antennas. However, it is a degenerative case where M and K are almost equal. Thus, the typical asymptotic LS MIMO properties from [11], [18] will not hold. The cause for $M \approx K$,is that MRT/MRC operates under strong inter-user interference. Thus, the rate per UE is small and it make sense to schedule as many UEs as possible to wind up the sum rate. The signal processing complexity is lower compare to ZF processing for the same number of M and K. However, the power savings are not big enough to compensate for the lower rates. To achieve the same rates as ZF, MRT/MRC requires $M \gg K$. This setting would drastically increase the computational complexity and circuit power, however not improving the EE.

Looking at the respective EE-optimal operating points, the formulas in Chapter 4 can be used to compute the total complexity of channel estimation, the precoding/combining matrices, and performing precoding and receive combining. The complexity becomes 710 Gflops with ZF processing, 239 Gflop with MRT/MRC processing, and 664 Gflops with MMSE processing. These numbers are all within a realistic range, and a clear majority of the computations can be parallelised for each antenna. This is due to the total complexity is dominated by performing precoding and receive combining on every vector of data symbols in MRT/MRC. Despite its larger number of BS antennas and UEs, ZF processing only requires 3 times more operations than MRT/MRC processing. However, the computation of the precoding matrix which scales as $\mathcal{O}\,(K^3 + MK^2)$ in ZF only occurs once per coherence block.

Furthermore, to compare the different processing schemes, Figure 5.11 shows the maximum EE as a function of the number of BS antennas where a number of users are fixed and BS antennas from 1 to 220 are considered in the simulation. Undoubtedly, the similarity between MMSE and ZF processing shows an optimality of operating at high SNRs where these precoding schemes are almost equal in EE.

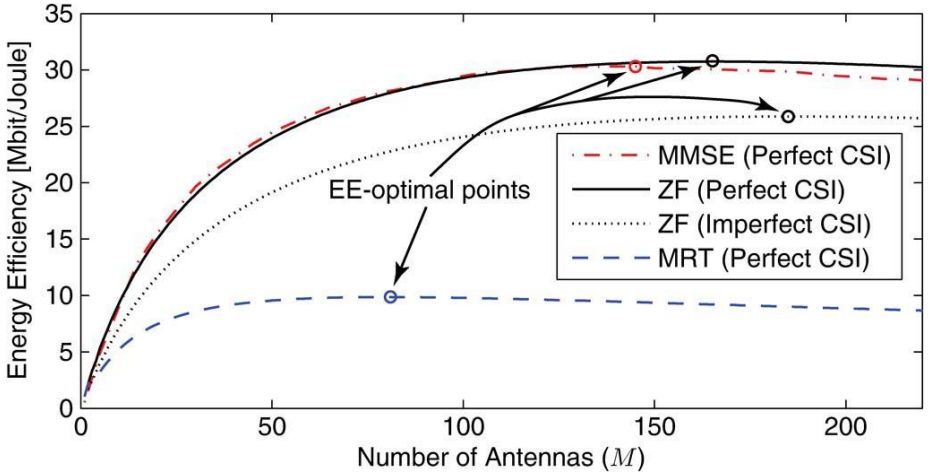

Figure 5.11: Maximum EE of BS antennas for different processing schemes in the single-cell scenario at EE-optimal number of user K (K_{ZF} = 133, K_{MMSE} = 134 and K_{MRT} = 81).

Subsequently, Figure 5.12, shows the total Power Amplifier power that maximizes the EE for different M ranges from 1 to 220 using the corresponding optimal K. For all the considered processing schemes, the most energy-efficient strategy is to increase the transmit power with M. This is in line with Corollary 8 but stands in contrast to the results in [17] and [18], which indicated that the transmit power should be decreased with M. However, Figure 5.12 likewise shows that the transmit power with ZF precoding and MMSE precoding is about 100mW/antenna. Mean,while it drops to 23 mW/antenna with MRT, as it gives higher interference and thus makes the system interference-limited at lower power.

These numbers are much smaller than conventional macro BSs which operate at around 40×10^3 mW/antenna [96] and reveals that the EE-optimal solution can be deployed with low-power UE-like RF amplifiers.

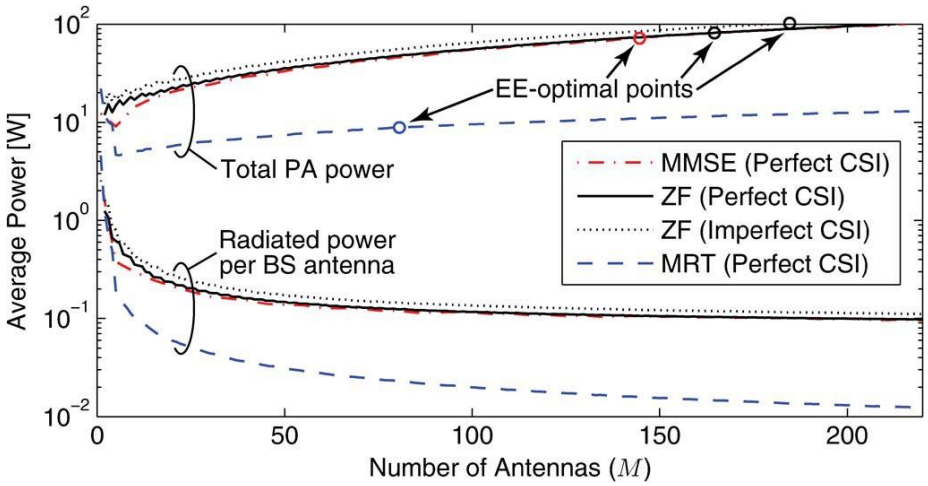

Figure 5.12: Total PA Power of BS antennas for different processing schemes in the single-cell scenario and the radiated power per BS antenna at EE-optimal number of user (K_{ZF} = 133, KMMSE = 134 and K_{MRT} = 81).

Finally, Figure 5.13 shows the area throughput (in Gbit/s/Km$^{2)}$ that maximizes the EE for different Base station antennas M ranges from 1 to 220 for all the processing schemes as in Figure 5.11 and 5.12. By referring to Figure 5.11, there are a 3-fold improvement in optimal EE for ZF and MMSE processing as compared to MRT/MRC. Figure 5.13 shows, that there is simultaneously 8-fold improvement in area throughput. Mostly, this gain also is achieved under imperfect CSI with ZF processing scheme, which shows that LS MIMO with proper interference-suppressing precoding can achieve both great energy efficiency and unprecedented area throughput. In contrast, it is inefficient to deploy many BS antennas and then co-process them using a MRT/MRC processing scheme. This is because MRT/MRC severely limiting both the energy efficiency and area throughput.

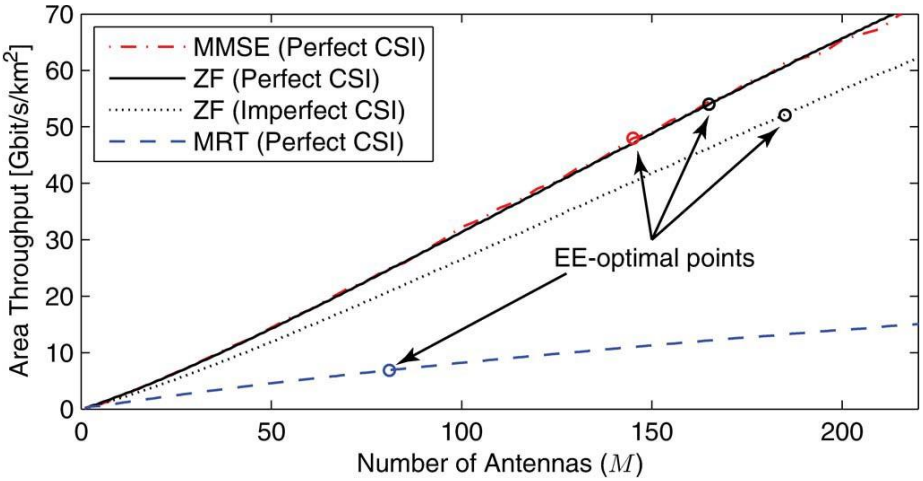

Figure 5.13: Area throughput of BS antennas for different processing schemes in the single-cell scenario at EE-optimal number of user (K_{ZF} = 133, KMMSE = 134 and K_{MRT} = 81).

5.8 Multi-Cell Deployment

A lot of studies have been carried out on the symmetric multi-cell scenario. The symmetric multi-cell scenario illustrated in Figure 5.14 is considered and concentrated on the cell in the middle. Each cell is a 500×500 meters square with uniformly distributed UEs, with the same minimum distance as in the single-cell scenario. The interference that arrives from the two closest cells in each direction only considered. Thus the cell *under study* in Figure 5.14 is respective for another cell in the system. Motivated by the single-cell deployment results, only ZF processing is considered and focused to compare different pilot reuse patterns. As depicted in Figure 5.14, the cells are divided into four clusters. Three different pilot reuse patterns are considered, where the same pilots in all cells $\left(\tau^{(\mathrm{ul})} = 1\right)$, two orthogonal sets of pilots of $\left(\tau^{(\mathrm{ul})} = 2\right)$, in Cluster 1 and Cluster 4 and finally all clusters have different orthogonal pilots $\left(\tau^{(\mathrm{ul})} = 4\right)$.

Numerical computations of the relative inter-cell interference give $I_{\mathrm{PC}} \in \{0.5288, 0.1163, 0.0214\}$ and $I_{\mathrm{PC}^2} \in \{0.0405, 0.0023, 7.82 \cdot 10^{-5}\}$, where the values reduce with increasing reuse factor $\tau^{(\mathrm{ul})}$. Moreover, $I = 1.5288$ and $\frac{B\sigma^2 \rho S_{\mathrm{X}}}{\eta} = 1.6022$ in this multi-cell scenario.

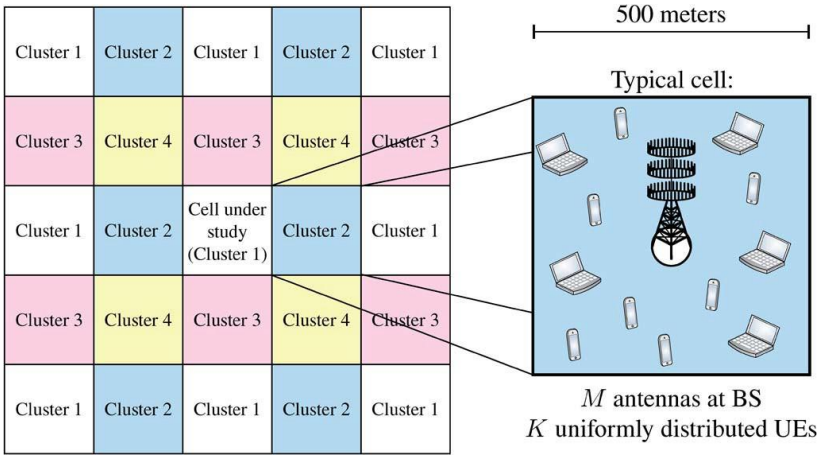

Figure 5.14: a Multi-cell scenario where cells are clustered (25 identical cells) to enable different pilot reuse factor.

The maximal EE for a different number of antennas is shown in Figure 5.15. Meanwhile, Figure 5.16 shows the corresponding PA power and power per BS antenna, whereby 5.17 shows the area throughout. A number of BS antennas *M* ranges from 1 to 200, and EE-optimal number of users *K* is fixed in the simulations. These figures are very similar to the single-cell counterparts in Figure 5.11, Figure 5.12 and Figure 5.13. However, the main difference is, all the values are smaller. Hence, the inter-cell interference affects the system by reducing the throughput, reducing the transmit power consumption, and thereby the EE likewise. Interestingly, the largest pilot reuse factor $\left(\tau^{(\mathrm{ul})} = 4\right)$ gives the highest EE and area throughput. This shows the requirement of mitigating pilot contamination in multi-cell deployment. EE-optimal is nevertheless increasing the transmit power with M as proved in Corollary 8 in the single-cell scenario, but a pace where the power per antenna reduces with M.

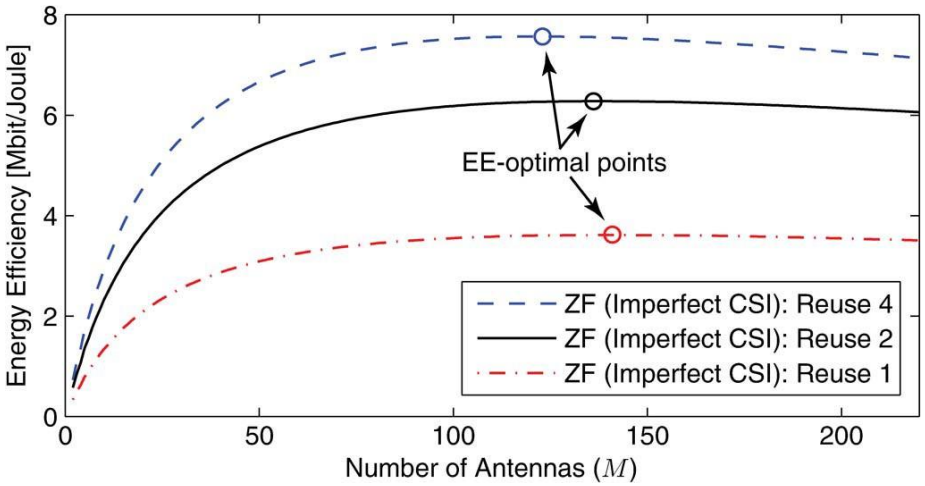

Figure 5.15: Maximum EE for different BS antennas and different pilot reuse factors in the multi-cell scenario at EE-optimal number of user *K* = 77, 70, and 60 with pilot reuse 1, 2, and 4.

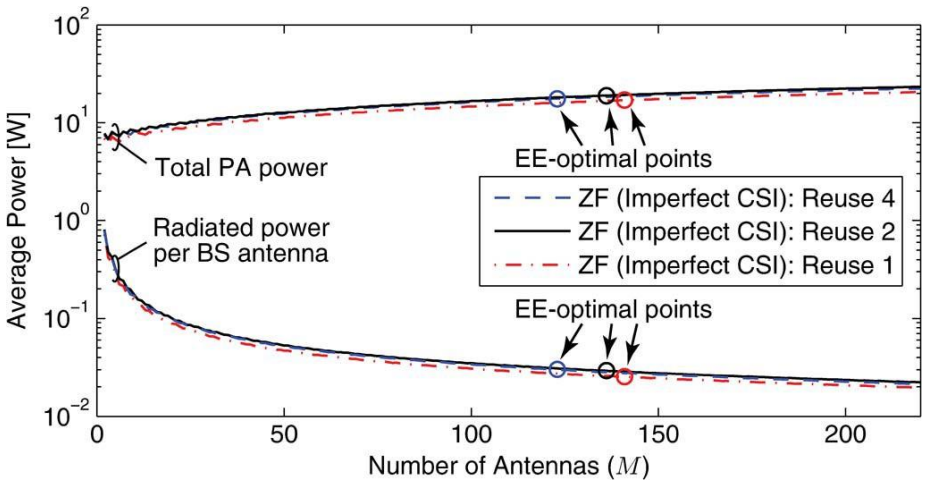

Figure 5.16: Total PA for different BS antennas and different pilot reuse factors in the multi-cell scenario at an EE-optimal number of user *K* = 77, 70, and 60 with pilot reuse 1, 2, and 4.

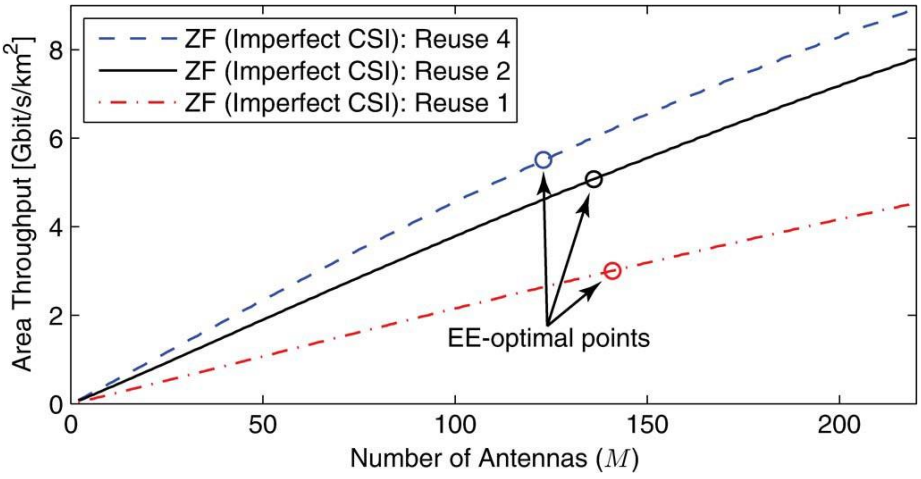

Figure 5.17: Area Throughput for different BS antennas and different pilot reuse factors in the multi-cell scenario at an EE-optimal number of user *K* = 77, 70, and 60 with pilot reuse 1, 2, and 4.

Finally, the set of achievable EE values for ZF precoding deployed multi-cell scenario shown in Figure 5.18, where a number of BS antennas from 1 to 220 and number of users and from 1 to 150 are considered. This simulation setup devised a pilot reuse of $\tau^{(\mathrm{ul})} = 4$. This gives the highest EE as the shape of the concave is like the single-cell counterpart is observed in Figure 5.9, but the optimal EE value is smaller since it occurs at the smaller system dimensions of M =123 and K =40. This is mainly due to inter-cell interference, which forces each cell to sacrifice some degrees-of-freedom. The pilot over-head is almost the same as in the single-cell scenarios, but the pilot reuse factor gives room for fewer UEs. Nevertheless, the conclusion drawn is that Large -Scale MIMO is the EE-optimal architecture.

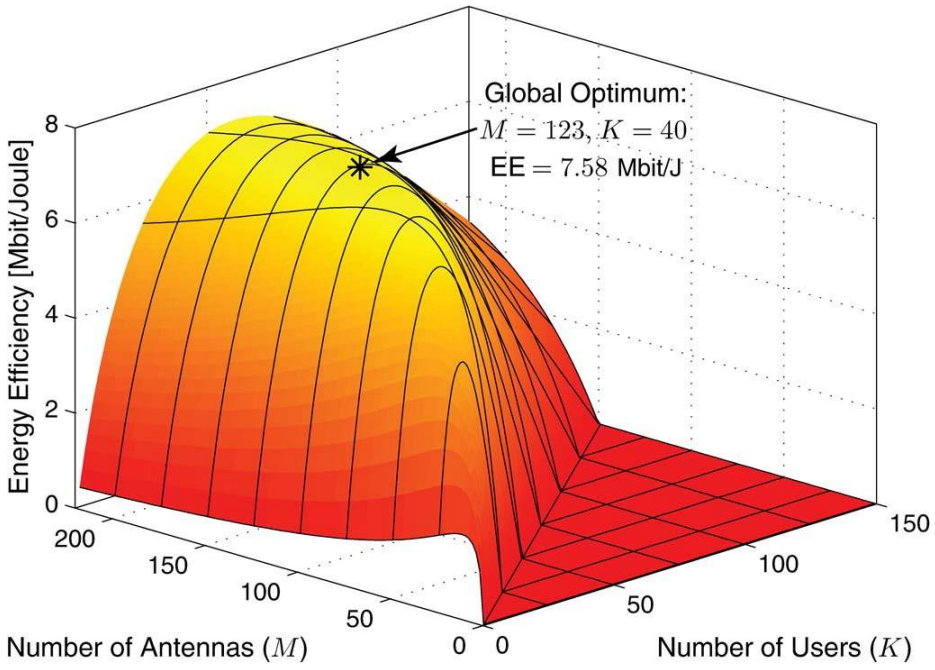

Figure 5.18: Energy efficiency with ZF processing in the multi-cell scenario with pilot reuse 4

5.9 Summary

This chapter gives numerical results for an analytical framework based on ZF processing scheme and Monte Carlo simulation for MRT and MMSE processing scheme. Moreover, this chapter proved the studies in Chapter 4, that Energy Efficiency can be maximised by the interplay between different key system parameters such as the number of Base Station antennas, the number of users and the choice of the transmit power in LS MIMO systems including propagation and different components of the power consumption model. Furthermore, a realistic power consumption model which scalable key system parameters for Large-Scale MIMO is validated in this chapter.

The results reveal that (a) an LS MIMO with 100 – 200 BS antennas are the correct number of antennas for energy efficiency maximisation; (b) these number of BS antennas should serve number of active UEs of the same size; (c) since the circuit power increases the transmit power should increase with number of BS antennas since the circuit power increases; (d) the radiated power antenna is in the range of 10-100 mW and decreases with number of BS antennas; (e) ZF processing provides the highest EE in all the scenarios due to active interference-suppression at affordable complexity. Therefore, these highly relevant numerical results prove that it is energy efficient to operate the next generation cellular networks in the LS MIMO regime.

Chapter 6

Conclusions and Future Research

6.1 Introduction

This chapter presents the main conclusion and a summary of research done in each chapter with some contributions to the knowledge. Since the research in LS MIMO is a continuous work, then this chapter also highlights a possible further investigation as a guide to the next research direction.

6.2 Conclusions

This thesis focuses on the energy maximisation improvement of the LS MIMO systems to cope with energy maximisation problem. The thesis has three main contributions; all the three contributions elaborated in detail.

This thesis analysed how to select the number of BS antennas M, number of active UEs K, and transmit power ρ (per UE) to maximise the EE in Large-Scale MIMO systems. Contrary to most prior works, a realistic power consumption model is deployed that explicitly described how the total power consumption depends non-linearly on M, K, and $\bar{\mathcal{R}}$. Simple-closed-form expressions for the EE-optimising parameter values and their scaling behaviours were derived under ZF processing with perfect CSI and verified by simulations for other processing schemes, under imperfect CSI, and in symmetric multi-cell scenarios.

The applicability in general multi-cell scenarios is an important open problem for future work.

The EE (in bit/Joule) is a quasi-concave function of M and K, thus it has a finite global optimum. The numerical results show that deploying 100-200 antennas to serve a relatively large number of UEs is the EE-optimal solution using today's circuit technology. This is interpreted as Large-Scale MIMO setups, but stress that M and K are at the same order of magnitude in contrast to the $\frac{M}{K} \gg 1$ assumption in the seminal paper of [30]. Contrary to common belief, the transmit power should increase with M (to compensate for the increasing circuit power) and not decrease. Energy-efficient systems are therefore not operating in the low SNR regime, but in a regime where proper interference-suppressing processing (e.g., ZF or MMSE) is highly preferably over interference-ignoring MRT/MRC processing. The radiated power per antenna is, however, decreasing with M and the numerical results show that it is in the range of 10-100 mW. This indicates that massive MIMO can be built using low-power consume-grade transceiver equipment at the BSs instead of conventional industry-grade high-power equipment.

6.2 Future Research

Several recommendations, which may guide to the future research directions on LS MIMO systems. The analysis was based on spatially uncorrelated fading, while each user might have unique non-identity channel covariance matrices in practice (e.g., due to limited angular spread and variations in the shadow fading over the array). The statistical information carried in these matrices can be utilised in the scheduler to find statistically compatible users that are likely to interfere less with each other [113].

This makes the results with imperfect CSI and with MRT/MRC processing behaves more like ZF processing with perfect CSI does.

The numerical results are stable to small changes in the circuit power coefficients, but can otherwise change drastically. The simulation code is available for download, to enable simple testing of other coefficients. the circuit power coefficients are predicted to decrease over time, implying that the EE-optimal operating point will get a larger value and be achieved using fewer UEs, fewer BS antennas, less transmit power and more advanced processing. The system model of this thesis assumes that any number of UEs can be served with any data rate. The problem formulation can be extended to take specific traffic patterns and constraints into account; delay can, for example, be used as an additional dimension to optimise [112]. This is outside the scope of this thesis, but the closed-form expressions in Theorem 1-3 regardless used to optimise a subset of the parameters while traffic constraints select the others. Another extension is to consider *N*-antenna UEs, where $N > 1$. If one stream is sent per UE, one can approximate the end performance by treating each UE as *N* separate UEs in the framework. In both cases, the exact analysis would require a revised and more complicated system model.

Appendix A

Proofs for Chapter 3

A.1 Proof of Lemma 1 and 2

ZF is employed for this purpose, $\mathbf{D}^{(\mathrm{ul})}$ in (3.8) is reduces to a diagonal matrix where the kth diagonal entry is $\frac{1}{p(M-K)\|g_k\|^2}$ since $|g_k^H h_k|^2 = 1$ with ZF detection.

$$p_k^{(\mathrm{ul-ZF})} = p(M-K)\sigma^2\|g_k\|^2$$

$$= p(M-K)\sigma^2[(\boldsymbol{H^H H})^{-1}]_{\boldsymbol{k,k}} \quad (1)$$

since g_k is the kth column of $\boldsymbol{G} = \boldsymbol{H}(\boldsymbol{H^H H})^{-1}$. Therefore, (3.10) reduces to

$$P_{\mathrm{TX}}^{(\mathrm{ul-ZF})} = \frac{B\zeta^{(ul)}}{\eta^{(ul)}} p(M-K)\sigma^2 \mathbb{E}_{\{h_k, \mathrm{x}_k\}}\{\mathrm{tr}((\boldsymbol{H^H H})^{-1})\} \quad (2)$$

where the expectation is computed with respect to both the channel realization $\{h_k\}$ and the user locations $\{\mathrm{x}_k\}$. For fixed user locations, $\boldsymbol{H^H H} \in \mathbb{C}^{\boldsymbol{K}\times\boldsymbol{K}}$ has a complex Wishart distribution with M degrees of freedom and parameter matrix $\boldsymbol{\Lambda} = \mathrm{diag}(l(\mathrm{x}_1), l(\mathrm{x}_1), l(\mathrm{x}_1), \ldots, l(\mathrm{x}_K))$. By using [113, Eq. (50)], the inverse first-order moment is

$$\mathbb{E}_{\{h_k, \mathrm{x}_k\}}\{\mathrm{tr}((\boldsymbol{H}^{\boldsymbol{H}}\boldsymbol{H})^{-1})\} = \mathbb{E}_{\{h_k\}}\left\{\frac{tr(\boldsymbol{\Lambda}^{-1})}{M-K}\right\}$$

$$= \sum_{k=1}^{K} \frac{\mathbb{E}_{x_k}\left\{\left(l(x_k)\right)^{-1}\right\}}{M-K} \quad (3)$$

The average uplink PA power in (3.12) is obtained and expected same for all the k with respect to x_k. The same step as described above followed to proof Lemma 2 by referring to [110] for details.

Appendix B

Proofs for Chapter 4

B.1 Proof of Lemma 3

The objective function is denoted by $\varphi(z) = \frac{g \log a + bz}{c + dz + h \log a + bz}$. This function is proven quasi concave by allowing the level sets $S_\kappa = \{z : \varphi(z) \geq \kappa\}$ to be concave for any $\kappa \in \mathbb{R}$ [114, Section 3.4]. The set is empty for $\kappa > \frac{g}{h}$ since $\varphi(z) \leq \frac{g}{h}$. When the set is non-empty, the second-order derivative of $\varphi(z)$ should be negative, which holds for $z \geq -\frac{a}{b}$ since $\frac{\partial^2 \varphi(z)}{\varphi z^2} = \frac{h\kappa - g}{\ln(2)} \frac{b^2}{(a+bz)^2} \leq 0$ for $\kappa \leq \frac{g}{h}$. Hence, $\varphi(z)$ is a quasi-concave function.

If there $z^* \geq -\frac{a}{b}$ such that $\varphi'(z^*) = 0$, then the quasi-concavity implies that z^* is the global maximiser and that $\varphi(z)$ is increasing for $z < z^*$ and decreasing for $z > z^*$. The existence of z^* is proven, when $\varphi'(z) = 0$ if and only if $\frac{1}{\ln(2)} \frac{b(c+dz)}{a+bz} - d \log(a + bz) = 0$ or, equivalently,

$$\frac{bc+ad}{a+bz} = d(\ln a + bz) - 1 \qquad (1)$$

Plugging $\ln(a + bz) - 1$ into (B.1) yields $\frac{bc}{de} - \frac{a}{e} = xe^x$ whose is eventually found to be $x^* = W\left(\frac{bc}{de} - \frac{a}{e}\right)$ where $W(\cdot)$ is defined in Definition 2. Finally obtaining $z^* = \frac{e^{(x^*+1)} - a}{b}$.

B.2 Proof of Theorem 1

Plugging $\bar{\rho}$, $\bar{\beta}$ and $\bar{c}$ into Equation (4.14) leads to the optimisation problem

$$\begin{aligned} &\text{maximise } \phi(K) \\ &K \in \mathbb{Z}_+ \end{aligned} \tag{2}$$

where

$$\phi(K) = \frac{K\left(1-\frac{\tau \mathrm{sum}^K}{U}\right)\bar{c}}{\frac{B\sigma^2 S_{\mathrm{X}}}{\eta}\bar{\rho} + \sum_{\mathrm{i}=0}^{3} \mathcal{C}_i K^i + \bar{\beta} \sum_{\mathrm{i}=0}^{2} \mathcal{D}_i K^i + \mathcal{A}K\left(1-\frac{\tau \mathrm{sum}^{\mathrm{K}}}{U}\right)\bar{c}} \tag{3}$$

The function $\phi(K)$ is quasi-concave for $K \in \mathbb{R}$ if the level sets $S_\kappa = \{K: \varphi(z) \geq \kappa\}$ are convex for any $\kappa \in \mathbb{R}$ [114, Section 3.4]. This condition is easily verified by differentiation when the coefficients $\mathcal{A}$,$\{\mathcal{C}_i\}$ and $\{\mathcal{D}_i\}$ are non-negative (note that S_κ is an empty set for $\kappa > \frac{1}{\mathcal{A}}$). The quasi-concavity implies that the global maximiser of $\phi(K)$ for $K \in \mathbb{R}$ satisfies the stationary condition $\frac{\partial \phi}{\partial K}(K) = 0$, which is equivalent to finding the roots of the quartic polynomial given in (4.21) and $\left\{K_\ell^{(o)}\right\}$ is noted as the real roots. The quasi-concavity of $\phi(K)$ is observed where it implies K^* is either the closest smaller or the closest larger integer.

B.3 Proof of Corollary 1

This follows from the same line of reasoning used for proving Theorem 1. Observe that if $P_{\mathrm{CE}} = P_{\mathrm{LP}}^{(\mathrm{ZF})} = 0$ then $\mathcal{C}_2 = \mathcal{C}_3 = \mathcal{D}_1 = \mathcal{D}_2 = 0$ so that K^* is obtained as one of the two roots to a quadratic polynomial, for which there are well-known expressions.

B.4 Proof of Theorem 2

To find the integer value $M^* \geq K + 1$ that maximises

$$\mathrm{EE}^{(\mathrm{ZF})} = \frac{K\left(1-\frac{\tau_{\mathrm{sum}}K}{U}\right)\bar{R}}{\frac{B\sigma^2\rho S_{\mathrm{x}}}{\eta}+\mathcal{C}'+M\mathcal{D}'+\mathcal{A}\left(1-\frac{\tau_{\mathrm{sum}}\mathrm{K}}{U}\right)\bar{R}} \tag{4}$$

where $\mathcal{C}'$ and $\mathcal{D}'$ are defined in (4.25). By relaxing M to be real-valued, the maximisation of (4) is solved by Lemma 3 by setting $a = 1 - \rho K, b = \rho, c = \frac{B\sigma^2\rho S_{\mathrm{x}}}{\eta} + \mathcal{C}^{'}, d = \mathcal{D}^{'}, g = B\left(1 - \frac{\tau_{\mathrm{sum}}K}{U}\right)$ and $h = \mathcal{A}g$. This lemma proves that $\mathrm{EE}^{(\mathrm{ZF})}$ is a quasi-concave function, thus the optimal real value solution $M^{(o)}$ in (4.16) can be transformed into an optimal integer-valued solution as $M^* = \lfloor M^o \rceil$. Finally, the condition $M^* \geq K + 1$ is always satisfied since $\mathrm{EE}^{(\mathrm{ZF})}$ is quasi-concave and goes to zero for $M = K$ and when $M \to \infty$.

B.5 Proof of Corollary 4

The independence from $\{P_{\mathrm{COD}}, P_{\mathrm{DEC}}, P_{\mathrm{BT}}\}$ follows from that M^* is independent of $\mathcal{A}$. From Lemma 4, the function $e^{W(x)}$ is monotonically increasing with x. Applying this result to (4.24), it turns out that M^* is monotonically increasing with $\mathcal{C}'$ and monotonically decreasing with $\mathcal{D}'$. Recalling (4.25), this means that M^* increases with $\mathcal{C}_i$ and decreases with $\mathcal{D}_i$. Based on these results, the second part follows from Table 1.

B.6 Proof of Corollary 5

The first statement comes direct application of Lemma 4 to (4.24), which requires $\frac{\beta\sigma^2 S_{\mathrm{x}}}{\eta\mathcal{D}'}\rho^2 + \frac{\mathcal{C}'}{\mathcal{D}'}\rho + K\rho - 1 \geq e^2$, this is satisfied for the moderately large value of ρ. The scaling law for a large value of ρ follows directly from (4.26).

B.7 Proof of Theorem 3

From (4), the optimal ρ maximises

$$\frac{B\left(1-\frac{\tau_{\mathrm{sum}}K}{U}\right)\log(1+\rho(M-K))}{\frac{B\sigma^2 S_{\mathrm{x}}}{\eta}\rho+\mathcal{C}'+M\mathcal{D}'+\mathcal{A}\left(1-\frac{\tau_{\mathrm{sum}}K}{U}\right)\log(1+\rho(M-K))} \tag{5}$$

whose solution follows from Lemma 3 by setting $a = 1, b = M - K, c = \mathcal{C}^{'} + M\mathcal{D}^{'}, d = \frac{B\sigma^2 S_{\mathrm{x}}}{\eta}, g = B\left(1 - \frac{\tau_{\mathrm{sum}}K}{U}\right)$ and $h = \mathcal{A}g$. The value ρ^* in (4.28) is always positive since the objective function is quasi-concave and is equal to zero at $\rho = 0$ and when $\rho \to \infty$.

B.8 Proof of Corollary 8

The lower bound follows from the direct application of Lemma 4 to (4.24) under the condition $\frac{\eta(M-K)(\mathcal{C}'+M\mathcal{D}')}{\beta\sigma^2 S_{\mathrm{x}}} - 1 \geq e^2$ which is satisfied for moderately large values of M. The approximation for large M is achieved from (4.29) by simple algebra.

B.9 Proof of Lemma 5

Uplink pilot power of the kth UE is $\frac{\rho\sigma^2}{l(\mathrm{x}_k)}$and length of orthogonal pilot sequences is $K\tau^{(\mathrm{ul})}$. By using MMSE estimation [115], a channel estimate $\hat{h}_k \sim \mathcal{CN}\left(\mathrm{O}_N, \frac{l(\mathrm{x}_k)}{1+\frac{1}{\rho K\tau^{(\mathrm{ul})}}}\mathrm{I}_k\right)$ obtained with estimation error covariance matrix

$$l(\mathrm{x}_k)\left(1-\frac{1}{1+\frac{1}{\rho K\tau^{(\mathrm{ul})}}}\right)\mathrm{I}_N \tag{6}$$

Approximated ZF applied in uplink and downlink by treating the channel estimates as the true channels. By treating the estimation errors as noise with a variance that is averaged over the channel realisation, the kth achieves the average gross rate

$$\bar{\mathcal{R}} = B\log\left(1+\frac{p_k^{(\mathrm{ul})}}{\|g_k\|^2\left(\sigma^2+\left(1-\frac{1}{1+\frac{1}{\rho K\tau^{(\mathrm{ul})}}}\right)K\rho\sigma^2\right)}\right) \tag{7}$$

which is equivalent to (4.31) for the uplink transmit powers $p_k^{(\mathrm{ul})} = \frac{\rho\sigma^2(M-K)\|g_k\|^2}{1+\frac{1}{\rho K\tau^{(\mathrm{ul})}}}$.

The downlink rate is derived analogously and it is straightforward to compute the average PA power.

B.10 Proof of Lemma 6

During data transmission where g_{jk} is the receive filter, the uplink power for UE k in cell j is

$$p_{jk}^{(\mathrm{ul})} = \frac{\sigma^2 \rho (M-K) \|g_k\|^2}{1+I_{\mathrm{PC}}+\frac{1}{\rho K \tau^{(\mathrm{ul})}}} \tag{8}$$

Under approximate ZF, after averaging over the channel realisation, the average UE power is

$$\mathbb{E}\{\|g_k\|^2\} = \frac{1+I_{\mathrm{PC}}+\frac{1}{\rho K \tau^{(\mathrm{ul})}}}{(M-K) l_j(\mathrm{x}_{jk})} \tag{9}$$

which is same as in Lemma 1. The channel-averaged value $p_{jk}^{(\mathrm{ul-pilot})} = \frac{\sigma^2 \rho}{l_j(\mathrm{x}_{jk})}$ is used for pilot transmission, since it can only depend on channel statistic s. If the BS applies MMSE estimation [115] and is unaware of the UE position s in other cells, the average interference from cells with orthogonal pilots is $\|g_k\|^2 \rho K \tau^{(\mathrm{ul})} \sum_{\ell \notin Q_j} I_{j\ell}$. The average interference from the cells using the same pilots is

$$\rho(M-K)\|g_k\|^2 \frac{\mathrm{I}^{(PC)}}{1+\mathrm{I}^{(PC)}+\frac{1}{\rho K \tau^{(\mathrm{ul})}}} + \|g_k\|^2 \rho K \tau^{(\mathrm{ul})} \left(\sum_{\ell \in Q_j} I_{j\ell} - \frac{\sum_{\ell \in Q_j} {I_{j\ell}}^2}{\rho K \tau^{(\mathrm{ul})}} \right) \tag{10}$$

where the first term is due to PC and the second is due to channel uncertainty. Combining this together, the gross rate in the uplink in (4.44) is achieved. The same expression is achieved in the downlink by treating channel uncertainty as noise and exploiting the cell symmetry.

Bibliography

[1] K. Zheng, L. Zhao, J. Mei, B. Shao, W. Xiang and L. Hanzo, "Survey of Large-Scale MIMO Systems," in *IEEE Communications Surveys & Tutorials*, vol.17, no.3, pp. 1738-1760, third quarter 2015.

[2] Global Mobile Data Traffic Forecast Update, 2012–2017, Cisco Visual Networking, May 2013.

[3] Z. Hasan, H. Boostanimehr, and V. K. Bhargava, "Green cellular networks: A survey, some research issues and challenges," *IEEE Commun. Surveys Tuts.*, vol. 13, no. 4, pp. 524–540, 4th Quart. 2011.

[4] D. Feng *et al.*, "A survey of energy-efficient wireless communications," *IEEE Commun. Surveys Tuts.*, vol. 15, no. 1, pp. 167–168, 1st Quart. 2012.

[5] Y. Chen, S. Zhang, S. Xu, and G. Y. Li, "Fundamental trade-offs on green wireless networks," IEEE *Commun. Mag.*, vol. 49, no. 6, pp. 30–37, Jun. 2011.

[6] G. Y. Li *et al.*, "Energy-efficient wireless communications: Tutorial, survey, and open issues," *IEEE Wireless Commun.*, vol. 18, no. 6, pp. 28–35, Dec. 2011.

[7] G. Auer *et al.*, "How much energy is needed to run a wireless network?" *IEEE Wireless Commun.*, vol. 18, no. 5, pp. 40–49, Oct. 2011.

[8] T. Kailath and A. J. Paulraj, “Increasing capacity in wireless broadcast systems using Distributed Transmission/Directional Reception (DTDR),” U.S. Patent 5 345 599, Sep. 6, 1994.

[9] G. Golden, C. Foschini, R. Valenzuela, and P. Wolniansky, “Detection algorithm and initial laboratory results using V-BLAST space-time communication architecture,” *Electron. Lett.*, vol. 35, no. 1, pp. 14–16, Jan. 1999.

[10] A. Ghrayeb and T. M. Duman, *Coding for MIMO Communication System*. Hoboken, NJ, USA: Wiley, 2007.

[11] T. Marzetta, “Noncooperative cellular wireless with unlimited numbers of base station antennas,” *IEEE Trans. Wireless Commun.*, vol. 9, no. 11, pp. 3590–3600, Nov. 2010.

[12] E. G. Larsson, F. Tufvesson, O. Edfors, and T. L. Marzetta, “Massive MIMO for next-generation wireless systems,” *IEEE Commun. Mag.*, vol. 52, no. 2, pp. 186–195, Feb. 2014.

[13] F. Rusek *et al.*, “Scaling up MIMO: Opportunities and challenges with very large arrays,” *IEEE Signal Process. Mag.*, vol. 30, no. 1, pp. 40–60, Jan. 2013.

[14] R e q u i r e m e n t s, Candidate Solutions & Technology Roadmap for LTE R12 Onward, 3GPP RWS-120010, DoCoMo, Jun. 2012.

[15] Technologies for Rel-12 and Onward, 3GPP RWS-120021, Samsung, Nov. 2013.

[16] Views *on Rel-12 and Onwards for LTE and UMTS*, 3GPP RWS-120006, HUAWEI and HiSilicon, 2013.

[17] J. Hoydis, S. ten Brink, and M. Debbah, "Massive MIMO in the UL/DL of cellular networks: How many antennas do we need?," *IEEE J. Sel. Areas Commun.*, vol. 31, no. 2, pp. 160–171, Feb. 2013.

[18] H. Q. Ngo, E. Larsson, and T. Marzetta, "Energy and spectral efficiency of very large multiuser MIMO systems," *IEEE Trans. Commun.*, vol. 61, no. 4, pp. 1436–1449, Jul. 2013.

[19] L. Zhao, K. Zheng, H. Long, and H. Zhao, "Performance analysis for downlink massive MIMO system with ZF precoding," *Trans. Emerging Telecommun. Technol.*, vol. 25, no. 12, pp. 1219–1230, Dec. 2014.

[20] G. Yang, et al., "Throughput optimization for massive MIMO systems powered by wireless energy transfer," *IEEE J. Sel. Areas Commun.* vol. 33, no. 8, pp. 1640–1650, Aug. 2015.

[21] Y. Chen, S. Zhang, S. Xu, and G. Li, "Fundamental trade-offs on green wireless networks," *IEEE Commun. Mag.*, vol. 49, no. 6, pp. 30–37, Jun. 2011.

[22] H. Q. Ngo, et al., “Energy and spectral efficiency of very large multiuser MIMO systems,” *IEEE Trans. Commun.*, vol. 61, no. 4, pp. 436–1449, Apr. 2013.

[23] E. Bjornson, et al., “Optimal design of energy-efficient multiuser MIMO systems: Is massive MIMO the answer?,” *IEEE Trans. Wireless Commun.*, vol. 14, no. 6, pp. 3059–3075, June 2015.

[24] W. Liu, S. Han, and C. Yang, (2015). “Is massive MIMO energy efficient?,” *arXiv Preprint*, arXiv:1505.07187.

[25] T. A. Khan, A. Y. Panah, Y. Maguire, and R. W. Heath, “Energy efficiency of wireless information and power transfer with massive MIMO,” in *Proc. 2017 IEEE Vehicular Technology Conf.*, Mar. 2017, pp. 1–6.

[26] J. Constine (2013). Facebook and 6 phone companies launch Internet. org to bring affordable access to everyone. Internet.org. [Online]. Available: https://info.internet.org/en/

[27] S. Tombaz, A. Västberg, and J. Zander, “Energy- and cost-efficient ultra-high-capacity wireless access,” *IEEE Wireless Commun. Mag.*, vol. 18, no. 5, pp. 18–24, Oct. 2011.

[28] G . Auer *et al.*, “D2.3: Energy efficiency analysis of the reference systems, areas of improvements and target breakdown,” Energy Aware Radio and Network Technologies (EARTH), INFSO-ICT-247733, ver. 2.0. [Online]. Available: http://www.ict-earth.eu/

[29] E. Björnson, J. Hoydis, M. Kountouris, and M. Debbah, “Massive MIMO systems with non-ideal hardware: Energy efficiency, estimation, capacity limits,” *IEEE Trans. Inf. Theory*, vol. 60, no. 11, pp. 7112–7139, Nov. 2014.

[30] G. Miao, “Energy-efficient uplink multi-user MIMO,” *IEEE Trans. Wireless Commun.*, vol. 12, no. 5, pp. 2302–2313, May 2013.

[31] Y. Hu, B. Ji, Y. Huang, F. Yu, and L. Yang, “Energy-efficiency resource allocation of very large multi-user MIMO systems,” *Wireless Netw.*, vol. 20, no. 6, pp. 1421–1430, Aug. 2014.

[32] E. Björnson, M. Kountouris, and M. Debbah, “Massive MIMO and small cells: Improving energy efficiency by optimal soft-cell coordination,” in *Proc. ICT*, 2013, pp. 1–5.

[33] D. Ha, K. Lee, and J. Kang, “Energy efficiency analysis with circuit power consumption in massive MIMO systems,” in *Proc. IEEE PIMRC*, 2013, pp. 938–942.

[34] H. Yang and T. Marzetta, “Total energy efficiency of cellular large scale antenna system multiple access mobile networks,” in *Proc. IEEE Online-GreenComm*, 2013, pp. 27–32.

[35] S. K. Mohammed, "Impact of Transceiver Power Consumption on the Energy Efficiency of Zero-Forcing Detector in Massive MIMO Systems," in *IEEE Transactions on Communications*, vol. 62, no. 11, pp. 3874-3890, Nov. 2014.

[36] Y. Chen, S. Zhang, S. Xu, and G. Li, “Fundamental trade-offs on green wireless networks,” *IEEE Commun. Mag.*, vol. 49, no. 6, pp. 30–37, Jun. 2011.

[37] “Smart 2020: Enabling the low carbon economy in the information age,” The Climate Group and Global e-Sustainability Initiative (GeSI), Brussels, Belgium, 2008, Tech. Rep.

[38] Green Touch Consortium, Tech. Rep. [Online].Available: http://www.greentouch.org

[39] Cisco, \Cisco visual networking index: global mobile data tra_c forecast update,2013-2018," White Paper, Feb. 2014. [Online]. Available: http://www.cisco.com.

[40] WWRF, L. Sorensen and K. E. Skouby, \User scenarios 2020,"Report, July 2009. [Online]. Available: http://www.wireless-world-research.org.

[41] 3GPP, TS 36.201 V8.3.0, \Evolved universal terrestrial radio access (E-\UTRA); LTE physical layer - general description," Rel. 8, Mar. 2009.

[42] A. Hashimoto, H. Yorshino, and H. Atarashi, \Roadmap of IMT-Advanced development," IEEE Microw. Mag., vol. 9, no. 4, pp. 80-88, Aug. 2008.

[43] 3GPP, TS 36.104 V10.0.0, \Evolved universal terrestrial radio access (EUTRA) base station (BS) radio transmission and reception," Rel. 10, Oct. 2010.

[44] M. Agiwal, A. Roy, and N. Saxena, \Next generation 5G wireless networks: a comprehensive survey," IEEE Commun. Surveys Tuts., early access, Feb.2016.

[45] “Multi-user MIMO Wireless System-From Theory to Chip Design”, class note for Kyutech Lab, Department of Electrical and Computer Engineering, Kyushu Institute of Technology, Japan, 2006.

[46] A. Goldsmith, \Wireless communications", Cambridge University Press, 2005.

[47] D. Tse and P. Viswanath, \Fundamentals of Wireless Communications", Cambridge University Press, 2005.

[48] Farhad E. Mahmood (2012). Mobile Radio Propagation Prediction for Two Different Districts in Mosul-City, MATLAB - A Fundamental Tool for Scientific Computing and Engineering Applications - Volume 2, Prof. Vasilios Katsikis (Ed.), InTech, DOI: 10.5772/46469.

[49] G. Caire, N. Jindal, M. Kobayashi, and N. Ravindran, \Multiuser MIMO achievable rates with downlink training and channel state feedback," IEEE Trans. Inf. Theory., vol. 56, no.6, pp. 2845-2866, Jun. 2010

[50] E. Björnson, E. G. Larsson and T. L. Marzetta, "Massive MIMO: ten myths and One critical question," in *IEEE Communications Magazine*, vol. 54, no. 2, pp.114-123, February 2016.

[51] J. Vieira *et al*., "A flexible 100-antenna testbed for Massive MIMO," *2014 IEEE Globes Workshops (GC Wkshps)*, Austin, TX, 2014, pp. 287-293.

[52] H. Yin, D. Gesbert, M. Filippou and Y. Liu, "A Coordinated Approach to Channel Estimation in Large-Scale Multiple-Antenna Systems," in *IEEE Journal on Selected Areas in Communications*, vol. 31, no. 2, pp. 264-273, February 2013.

[53] E. Björnson, E. G. Larsson and M. Debbah, "Massive MIMO for Maximal Spectral Efficiency: How Many Users and Pilots Should Be Allocated?," in *IEEE Transactions on Wireless Communications*, vol. 15, no. 2, pp. 1293-1308, Feb. 2016.

[54] C-RAN: The Road Towards Green Radio Access Network, China Mobile Research Institute, Beijing, China, Oct. 2012.

[55] Y. Wu, R. Zhou, and W. Zhang, “Active antenna system: Utilizing the full potential of radio sources in the spatial domain,” Huawei, Shenzhen, China, 2012.

[56] C.-L. I *et al.*, “Toward green and soft: A 5G perspective,” *IEEE Commun.Mag.*, vol. 52, no. 2, pp. 66–73, Feb. 2014.

[57] A. Khan and A. Brown, “Null steering in irregularly spaced sparse antenna arrays using aperture distributed subarrays and hybrid optimiser,” *IET Microw., Antennas Propag.*, vol. 8, no. 2, pp. 86–92, Jan. 2014.

[58] D. S. Weile, “Orthogonal methods for array synthesis: Theory and the ORAMA computer tool,” *IEEE Antennas Propag. Mag.*, vol. 49, no. 6, pp. 131–132, Dec. 2007.

[59] A. Antonis, A. G. Kanatas, and C. B. Constantinos, *Parasitic Antenna Arrays for Wireless MIMO Systems*. New York, NY, USA: Springer- Verlag, 2014.

[60] S. Payami and F. Tufvesson, “Channel measurements and analysis for very large array systems at 2.6 GHz,” in *Proc. 6th EUCAP*, Prague, Czech Republic, Mar. 2012, pp. 433–437.

[61] X. Gao, F. Tufvesson, O. Edfors, and F. Rusek, “Measured propagation characteristics for very-large MIMO at 2.6 GHz,” in *Proc. 46th ASILOMA Conf. Signals, Syst. Comput.*, Pacific Grove, CA, USA, Nov. 2012, pp. 295-299.

[62] C.X. Wang, X. Hong, H. Wu, and W. Xu, “Spatial-temporal correlation properties of the 3GPP spatial channel model and the Kronecker MIMO channel model,” *EURASIP J. Wireless Commu. Netw.*, vol. 2007, no. 1, Feb. 2007, Art. ID. 39871.

[63] J. Hoydis, C. Hoek, T. Wild, and S. ten Brink, “Channel measurements for large antenna arrays,” in *Proc. ISWCS*, Paris, France, Aug. 2012, pp. 811–815.

[64] C.X. Wang, X. Hong, H. Wu, and W. Xu, “Spatial-temporal correlation properties of the 3GPP spatial channel model and the Kronecker MIMO channel model,” *EURASIP J.Wireless Commu. Netw.*, vol. 2007, no. 1, Feb.2007, Art. ID. 39871.

[65] L. Schumacher, L. T. Berger, and J. Ramiro-Moreno, “Recent advances in propagation characterisation and multiple antenna processing in the 3GPP framework,” in *Proc.XXVIth URSI Gen. Assem.*, Prague, Czech Republic, Aug. 2002, pp. 1–9.

[66] H. Yin, D. Gesbert, M. Filippou, and Y. Liu, “A coordinated approach to channel estimation in large-scale multiple-antenna systems,” *IEEE J. Sel. Areas Commun.*, vol. 31, no. 2, pp. 264-273, Feb. 2013.

[67] J. Jose, A. Ashikhmin, T. L. Marzetta, and S. Vishwanath, “Pilot Contamination and precoding in multi-cell TDD systems,” IEEE Trans. Wireless Commun., vol. 10, no. 8, pp. 2640-2651, Aug. 2011.

[68] H. Q. Ngo and E. G. Larsson, “EVD-based channel estimations for multicell multiuser MIMO with very large antenna arrays,” in Proc. IEEE International Conference on Acoustics, Speech and Signal Processing (ICASSP), Kyoto, Japan, 2012.

[69] R. Müeller, L. Cottatellucci, and M. Vehkaperä, “Blind pilot decontamination, IEEE J. Sel. Sig. Process.,” vol. 8, no. 5, pp. 773_786, Oct. 2014.

[70] A. Ashikhmin and T. L. Marzetta, “Pilot contamination precoding in multicell large-scale antenna systems,” in Proc. IEEE International Symposium on Information Theory (ISIT), Cambridge, MA, Jul. 2012.

[71] H. Yin, D. Gesbert, M. Filippou, and Y. Liu, “A coordinated approach to channel estimation in large-scale multiple-antenna systems,” IEEE J. Sel. Areas Commun., vol. 31, no. 2, pp. 264_273, Feb. 2013.

[72] H. Q. Ngo and E. G. Larsson, “Blind estimation of elective downlink Channel gains in Massive MIMO,” in Proc. IEEE International Conference on Acoustics, Speed and Signal Processing (ICASSP), Brisbane, Australia, April 2015.

[73] D. Gesbert, M. Kountouris, R. W. Heath Jr., C.B. Chae, and T. Sälzer, “Shifting the MIMO paradigm,” IEEE Signal Process. Mag., vol. 24, no. 5, pp. 36-46, Sep. 2007.

[74] S. Buzzi I. Chih-Lin T. E. Klein H. V. Poor C. Yang A. Zappone "A survey of energy-efficient techniques for 5G networks and challenges ahead," IEEE J. Sel. Areas Commun. vol. 34 no. 4 pp. 697-709, 2016.

[75] M. Ismail W. Zhuang "Network cooperation for energy saving in green radio communications," IEEE Wireless Commun. Mag.vol. 18 no. 5 pp. 76-81, 2011.

[76] I. Chih-Lin C. Rowell S. Han Z. Xu G. Li Z. Pan "Toward green and soft: A 5G perspective," IEEE Commun. Mag.vol. 52 no. 2 pp.66-73, 2014.

[77] Yang, H., & Marzetta," Performance of conjugate and zero-forcing beamforming in large-scale antenna systems," IEEE Journal on Selected Areas in Communications, 31(2), 172–179, 2013.

[78] Hanif, M.-F., Tran, L.-N., Tölli, A., & Juntti, "Computationally efficient robust beamforming for SINR balancing in the multicell downlink with applications to large antenna array systems," IEEE Transactions on Communications, 62(6), 1908–1920, 2014.

[79] Huh, H. Caire, G., Papadopoulos, H. C., & Ramprashad, S. A., "Achieving massive MIMO spectral efficiency with a not-so-large number of Antennas," IEEE Transactions on Wireless Communication, 11(9), 3226 – 3239, 2012.

[80] Ozgur, A., Leveque, O., & Tse, D., "Spatial degrees of freedom of Large distributed MIMO systems and wireless ad hoc networks," IEEE Journal on Selected Areas in Communications, 31(2), 202–214, 2013.

[81] Pitarokoilis, A., Mohammed, S. K., & Larsson, E. G., "On the optimality of single-carrier transmission in large-scale antenna systems," IEEE Communications Letters, 1(4), 276–279, 2012.

[82] Jose, J., Ashikhmin, A., & Marzetta, T. L., "Pilot contamination and precoding in multi-cell TDD systems," IEEE Transactions on Wireless Communications, 10(8), 2640–2651, 2011.

[83] Cramer, H. (1970). Random variables and probability distributions. Cambridge: Cambridge University Press.

[84] Ngo, H. Q., Matthaiou, M., Duong, T. Q., & Larsson, E. G., “Uplink performance analysis of multicell MU-SIMO systems with ZF receivers”, IEEE Transactions on Vehicular Technology, 62(9), 4471–4483, 2013.

[85] Yin, H., Gesbert, D., Filippou, M., & Liu, Y.,” A coordinated approach to channel estimation in large-scale multiple-antenna systems”, IEEE Journal on Selected Areas in Communications, 31(2), 264–273, 2013.

[86] Fehske, A., Fettweis, G., Malmodin, J., & Biczok, G., “The global footprint of mobile communications: The ecological and economic perspective”, IEEE Communications Magazine, 49(8), 55–62, 2011.

[87] Brevis, P. G., Gondzio, J., Fan, Y., Poor, H. V., Thompson, J., Krikidis, I., et al., ”Base station location optimization for minimal energy consumption in wireless networks”, In Proceedings of the 2nd green wireless communications & networks workshop (GreeNet 2011) (pp. 15–18), 2011, Hungary: Budapest.

[88] Larsson, E. G., Tufvesson, F., Edfors, O., & Marzetta, T. L.,” Massive MIMO for next-generation wireless systems”, IEEE Communications Magazine, 52(2), 186–195, 2014.

[89] Rusek, F., Persson, D., Lau, B. K., Larsson, E. G., Marzetta, T. L., Edfors, O., et al.,” Scaling up MIMO: Opportunities and challenges with very large arrays”, IEEE Communication Magazine, 30(1), 40–46, 2013.

[90] Ngo, H. Q., Larsson, E. G., & Marzetta, T. L, “The multicell multiuser MIMO uplink with very large antenna and a finite-dimensional channel”, IEEE Transactions on Communications, 61(6), 2350–2361, 2013.

[91] Tse, D. N. C., & Viswanath, P. (2005). Fundamentals of wireless communications. Cambridge: Cambridge University Press.

[92] Gopalakrishnan, B., & Jindal, N. (2011). An analysis of pilot contamination on multi-user MIMO cellular systems with many antennas. In Proceedings of the IEEE, international workshop signal process. Advances in wireless communications (SPAWC 2011), San Francisco, CA USA, pp. 381–385.

[93] R. Kumar and J. Gurugubelli, “How green the LTE technology can be?”in *Proc. Wireless VITAE*, 2011, pp. 1–5.

[94] D. K. Jaeho Lee, J. Burm, and J. S. Park, “Integratable micro-doherty transmitter,” Communications Magazine, IEEE, vol. 48, no. 11, pp. 66–72, 2010.

[95] N. Srirattana, A. Raghavan, D. Heo, P. Allen, and J. Laskar, “Analysis and design of a high-efficiency multistage Doherty power amplifier for wireless communications,” Microwave Theory and Techniques, IEEE Transactions on, vol. 53, no. 3, pp. 852 – 860, 2005.

[96] *Further Advancements for E-UTRA Physical Layer Aspects (Release 9)*,3GPPTS 36.814, Mar. 2010.

[97] X. Gao, O. Edfors, F. Rusek, and F. Tufvesson, "Massive MIMO in real Propagation environments," *IEEE Trans. Wireless Commun.*, 2014. [Online]. Available: http://arxiv.org/abs/1403.3376.

[98] S. Pillai, T. Suel, and S. Cha, "The Perron-Frobenius theorem: Some of its applications," *IEEE Signal Process. Mag.*, vol. 22, no. 2, pp. 62–75, Mar. 2005.

[99] A.Wiesel, Y. Eldar, and S. Shamai, "Linear precoding via conic optimization for fixed MIMO receivers," *IEEE Trans. Signal Process.*, vol.54, no. 1, pp.161–176, Jan.2006.

[100] E. Björnson and E. Jorswieck, "Optimal resource allocation in Coordinated multi-cell systems," *Found. Trends Commun. Inf. Theory*, vol. 9, no. 2/3, pp. 113–381, 2013.

[101] H. Boche and M. Schubert, "A general duality theory for uplink and downlink beamforming," in *Proc. IEEE VTC-Fall*, 2002, pp. 87–91.

[102] Y.-G. Lim, C.-B. Chae, and G. Caire, "Performance analysis of massive MIMO for cell-boundary users," *IEEE J. Sel. Topics Signal Process.*, 2013. [Online]. Available: http://arxiv.org/abs/1309.7817

[103] S. Cui, A. Goldsmith, and A. Bahai, "Energy-efficiency of MIMO and cooperative MIMO techniques in sensor networks," *IEEE J. Sel. Areas Commun.*, vol. 22, no. 6, pp. 1089–1098, Aug. 2004.

[104] A. Mezghani and J. A. Nossek, “Power efficiency in communication systems from a circuit perspective,” in *Proc. IEEE ISCAS*, 2011, pp.1896-1899.

[105] S. Boyd and L. Vandenberghe, Numerical Linear Algebra Background. [Online]. Available: www.ee.ucla.edu/ee236b/lectures/num-lin-alg.pdf

[106] F. Shmakov, “A universal method of solving quartic equations,” *Int. J.Pure Appl. Math.*, vol. 71, no. 2, pp. 251–259, 2011.

[107] D. Kang *et al.*, “1.6–2.1 GHz broadband Doherty power amplifiers for LTE handset applications,” in *Proc. IEEE MTT-S Int. Microw. Symp. Dig.*, 2011, pp. 1–4.

[108] S. Tombaz, K. Sung, and J. Zander, “Impact of densification on energy efficiency in wireless access networks,” in *Proc. IEEE GLOBECOM*, 2012, pp. 57–62.

[109] M. Parker, “High-performance floating-point implementation using FPGAs,” in *Proc. IEEE MILCOM*, 2009, pp. 1–5.

[110] E. Björnson, L. Sanguinetti, J. Hoydis, and M. Debbah, “Designing Multiuser MIMO for energy efficiency: When is massive MIMO the answer? “in *Proc. IEEE WCNC*, 2014.

[111] H. Huh, G. Caire, H. Papadopoulos, and S. Ramprashad, “Achieving ‘massive MIMO’ spectral efficiency with a not-so-large number of antennas,” *IEEE Trans. Wireless Commun.*, vol. 11, no. 9, pp. 3226–3239, Sep. 2012.

[112] H. Kim, C.-B. Chae, G. de Veciana, and R. Heath, “A cross-layer approach to energy efficiency for adaptive MIMO systems exploiting spare capacity,” *IEEE Trans. Wireless Commun.*, vol. 8, no. 8, pp. 4264–4275, Aug. 2009.

[113] D. Maiwald and D. Kraus, “Calculation of moments of complex Wishart and complex inverse Wishart distributed matrices,” *IEE Proc. Radar Sonar Navig.*, vol. 147, no. 4, pp. 162–168, Aug. 2000.

[114] S. Boyd and L. Vandenberghe, *Convex Optimization*. Cambridge, U.K.: Cambridge Univ. Press, 2004.

[115] E. Björnson and B. Ottersten, “A framework for training-based estimation in arbitrarily correlated Rician MIMO channels with Rician disturbance,” *IEEE Trans. Signal Process.*, vol. 58, no. 3, pp. 1807–1820, Mar. 2010.

[116] E. Björnson, L. Sanguinetti, J. Hoydis and M. Debbah, "Optimal Design of Energy-Efficient Multi-User MIMO Systems: Is Massive MIMO the Answer?," in *IEEE Transactions on Wireless Communications*, vol. 14 no. 6, pp. 3059-3075, June 2015.

List of Publications

Published Papers

[1] **V. P. Selvan**, M. S. Iqbal**,** and H. S. Al-Raweshidy, "Performance analysis of linear precoding schemes for very large multi-user MIMO downlink system", in Proceeding the 4th International Conference on Innovative Computing Technology (INTECH 2014), Luton-UK, pp.219-224, 13th - 15th August 2014. DOI:10.1109/INTECH.2014.6927765.